Algerian Democratic and Popular Republic
Ministry of Higher Education and Scientific Research
University of El Oued

Order Number:…

Serial Number:…..

Faculty of Exact Sciences

Chemistry Department

Thesis Submitted in Fulfillment of the requirements for Professional Master's Degree in Chemistry
Specialty: Analytical Chemistry
Prepared by students:
Lachheb Khaoula and Mekideche Chahra Zed

Titled

New biocomposite of cross-linked chitosan beads for the removal of anionic dyes: Optimization process using Box-Behnken Design

Defended on: 27 / 05 / 2025

Before the jury composed of:

Dr. Zouari Ahmed Rachida	President	El Oued University
Pr. Atia Djamal	Examiner	El Oued University
Pr. Zobeidi Ammar	Supervisor	El Oued University

Academic Year : 2024/2025

Acknowledgements

First and foremost, we thank and praise Allah for granting us success and support throughout the completion of this work. His mercy and guidance were a source of strength in overcoming challenges and accomplishing this academic effort. We pray for continued ease and success in our future endeavors.

Throughout the course of this thesis, we had the opportunity to encounter and learn from many individuals whose support was invaluable. We are especially grateful to our supervisor, ***Pr.ZOBEIDI Ammar,*** *for his patience, insightful guidance, and unwavering support, all of which played a crucial role in the successful completion of this work.*

We would like to thank ***Dr.Zouari Ahmed Rachida*** *for accepting to chair the jury, and* ***Pr.Atia Djamal*** *for honoring us by examining this work.*

We highly value the efforts of the defense committee members for their interest and constructive remarks, which contributed significantly to the development of this research.

We would also like to express our sincere gratitude to all the professors of the Chemistry Department for their continuous support and cooperation.

Thank you very much to everyone we could not mention.

In conclusion, we pray that Allah accepts this work and makes it sincerely for His sake. All praise is due to Him, at the beginning and the end.

Dedication

I dedicate this work to the One who deserves all gratitude, To Allah, the Almighty, by whose grace good deeds are accomplished, and by whose favor steps are made easy. All praise is due to Him, in a manner befitting His Majesty and Greatness.

*To my dear **parents**, my mother and father the source of my strength and perseverance thank you for your boundless love, patience, and countless sacrifices.*

*To my **brothers** and **sisters**, who have always been a source of support, surrounding me with love and reassurance.*

*To my esteemed supervisor, **Professor** Ammar Zobeidi, who generously shared his knowledge and guidance, and stood by me with sincere support may Allah reward him abundantly.*

*To my **friends** who accompanied and supported me through every stage of this work and the laboratory experiments.*

And to those who could not be with me, yet whose support was always felt in my heart.

To you all, I extend my deepest gratitude and appreciation.

L. Khaoula

Dedication

To the light of my life, the source of my strength, and the reason behind every step of success I've taken.

*To my beloved **mother**, whose prayers accompanied me, who embraced my weakness, and who has always been proud of me throughout my journey.To my dear **father**, who taught me patience, instilled in me the values of perseverance and hard work, and has always been a role model I look up to.*

*To my wonderful **siblings**, companions of my childhood and silent supporters, who never failed to offer encouragement and care. And to my amazing **friends**: Mysou, with her graceful charm; Chaima, with her ever-listening ear; Imma, with her quiet wisdom; Djohine, with her kind soul; and Serine, with her radiant presence—who made the road easier, the difficult moments bearable, and the victories sweeter.*

*To my dear **classmates**, Khaoula, Assia, Maria, Safa, and Asma you were an invaluable source of support and encouragement throughout my academic journey.*

To all of you, thank you for standing by me through every tough moment and every joyful success.

M. Chahra Zed

Abstract

In this study, a novel hybrid adsorbent composed of chitosan crosslinked with epichlorohydrin and loaded with illite–kaolinite clay (CTS-ECH/IKaol) was developed for the removal of the anionic dyes Orange G (OG) and Reactive Orange 16 (RO16) from aqueous media. The Box- Behnken Design (BBD) was applied to determine the crucial factors affecting adsorption performance. These included an adsorbent dose of 0.04 g for OG and 0.06 for RO16, contact times of 25 min, a temperature of 60°C for OG and 45 °C for RO16, and solution pH set at 4. The adsorption data exhibited better agreement with the pseudo- second- order (PSO) kinetic and Freundlich models. The Langmuir model estimated the monolayer capacity to be 416.67mg/ g for OG and 357.14 mg/ g for RO16 at a temperature of 45 ° C. The OG and RO16 dye adsorption mechanism was attributed to various interactions such as electrostatic, n-π, H-bonding. This study's pivotal finding underscores the promising potential of CTS-ECH/IKaol as an effective adsorbent for treating wastewater contaminated with organic dyes.

Keywords:

Adsorption; Chitosan; Dye removal; Epichlorohydrin; Illite–Kaolinite clay; Response surface Methodology.

الملخص

في هذه الدراسة، طُوِّرَ مُمتزٌّ هجينٌ جديدٌ مُكوَّنٌ من الشيتوزان المُتشابك مع الإبيكلوروهيدرين والمُحمَّل بطين الإليت-الكاولينيت (CTS-ECH/IKaol) لإزالة الصبغتين الأنيونيتين Orange G (OG) و Reactive Orange 16 (RO16) من الأوساط المائية. طُبِّقَ تصميم بوكس-بهينكن (BBD) لتحديد العوامل الحاسمة التي تُؤثِّر على أداء الامتزاز. وبينت النتائج أن أعلى كفاءة لإزالة الصبغة، 92.14% لصبغة OG و96.52% لصبغة RO16، تحققت باستخدام المادة الماصة CTS-ECH/IKaol في ظل ظروف مثالية التالية: جرعةً من المُمتزّ قدرها 0.04g لـ OG و 0.06g لـ RO16 ، وأوقات تلامسٍ قدرها 25 min، ودرجة حرارة 60°C لـ OG و 45°C لـRO16 ، ودرجة حموضة عند 4. أظهرت بيانات الامتزاز توافقًا أفضل مع نموذجي الحركية شبه الثاني (PSO) و Freundlich. قدّر نموذج لانجمويير سعة الطبقة الأحادية بـ 416.67 mg/g لـ OG و 357.14 mg/g لـRO16 . وتُعزى آلية امتزاز صبغتي OG و RO16إلى تفاعلات مختلفة، مثل التفاعل الكهروستاتيكي، وπ-n، والروابط الهيدروجينية. وتُبرز هذه النتيجة المحورية في هذه الدراسة الإمكانات الواعدة لـ CTS-ECH/IKaol كممتز فعال لمعالجة مياه الصرف الصحي الملوثة بالأصباغ العضوية.

الكلمات المفتاحية:

الامتزاز؛ الشيتوزان؛إزالة الصبغة؛ الإبيكلوروهيدرين؛ طين الإليت-الكاولينيت؛ منهجية سطح الاستجابة

List of Symbols and Abbreviations

q_e	Adsorption capacity at equilibrium (mg/g)
q_{max}	The maximum capacity for adsorption (mg/g)
PFO	Pseudo-first-order
PSO	Pseudo-second-order
RSM	Response Surface Methodology
BBD	Box Behnken design
FTIR	Fourier Transform Infrared
XRD	X-Ray Diffraction
SEM	Scanning Electron Microscope
ANOVA	Analysis of variance
CCD	Central Composite Design
C_0	Initial Concentration
C_e	Equilibrium concentration
CTS	Chitosan
IKaol	Illite Kaolinite clay
OG	Orange G
RO16	Reactive Orange 16
CTS-ECH/IKaol	Chitosan Epichlorohydrin/Illite Kaolinite
ECH	Epichlorohydrin
MW	Molecular Weight
DD	Deacetylation Degree
f_B	Response Function
K	Number of factors
K_f	Frandlich constant
K_t	Equilibrium link constant
K_L	Langmuir Constant
PFO	Pseudo First Order
PSO	Pseudo Second Order
q_t	Absorbation capacity at t (mg/g)
R	Perfect gaz constant

R^2	Linearity factor
t	time of contact
T	Temperature
V	Solution Volume
pH	Hydrogen Potentiel
ε	Polani factor
Y	continuous response
ΔH°	Change in enthalpie
ΔG°	Change in free energy
ΔS°	Change in entropy

Liste of Tabels

Liste Of Figures

Chapter III: Materials and Methods

Chapter IV: Results and Dicussion

Table of Contents

General Introduction

The environment is the cradle of life, making its preservation from pollution a foremost priority—one of the greatest challenges facing living organisms and ecosystems. Water, a fundamental component of life, constitutes a vital part of every living cell and is indispensable for survival [1]. With the advancement of modern life, environmental pollution particularly water pollution has emerged as one of the most pressing issues, caused by both human activities and natural phenomena. Water pollution is among the most hazardous types of environmental contamination due to water's critical role in both daily life and industrial processes. Many industries require large quantities of high-quality water, making industrial effluents a major source of environmental pollutants [2]. Among the most significant contributors to this pollution are synthetic dyes, which pose a severe challenge for environmental researchers. Industries worldwide use organic dyes to color products such as textiles, paper, leather, cosmetics, and plastics [3]. When discharged into aquatic systems, these dyes harm ecosystems and human health, necessitating their removal from wastewater before release into natural water bodies [4]. Based on their basic structure, dyes are categorized into non-ionic (disperse) dyes, anionic dyes such as Methyl Orange, Reactive Orange 16, Reactive Red 180, Orange G, and Acid Red 18, and cationic dyes [5].

There are several methods that can be applied to remove organic dyes from wastewater prior to discharge. Various treatment methods have been developed for removing color pollutants from contaminated water, including Fenton oxidation, photodegradation, coagulation–flocculation, adsorption, and nanofiltration [6, 7]. The adsorption is considered the most practical and adaptable due to its operational simplicity, insensitivity to contaminants, reusability, high efficiency, low initial cost, and limited waste generation [8].

Chitosan (CTS) is a linear biopolymer composed of 2-amino-2-deoxy-β-D-glucopyranose units [9]. It is the second most abundant polymer in nature, obtained primarily from marine organisms such as shrimp and crabs [10]. Chitosan exhibits several valuable properties, including non-toxicity, biodegradability, antimicrobial activity, and biocompatibility. Its chemical structure features reactive amino and hydroxyl groups, which serve as active sites for adsorption in industrial wastewater treatment [11]. However, the use of unmodified chitosan as an adsorbent remains limited due to its solubility in acidic media and high swelling ratio [12]. Consequently, researchers have focused on modifying chitosan to enhance its adsorption capacity,

surface area, and chemical stability. Chitosan can be improved as a stable and efficient adsorbent material through various modification strategies, such as crosslinking [13], grafting [14], and composite formation with nanomaterials [15].

Crosslinking reaction is one of the successful alternatives for modifying Chi and enhancing its chemical and structural properties. Moreover, crosslinking reaction is a convenient and feasible pathway to reduce CTS solubility in acidic medium and to minimize the hydrophobicity and swelling index in aqueous solution [16]. Several crosslinking agents such as glutaraldehyde, glyoxal, and ethylene glycol diglycidyl ether (EGDE) have been commonly used to prepare crosslinked chitosan [17]. However, the primary limitation of these agents lies in their tendency to block the functional amino groups (NH_2) of the chitosan chain, which are essential adsorption sites. To overcome this limitation, epichlorohydrin (ECH) a mono-functional crosslinking agent is considered a promising alternative, as it does not react with the amino groups of the chitosan polymer, allowing these groups to remain available for adsorption, particularly of anionic dyes [18].

In recent years, composite bio-materials based on chitosan crosslinked with epichlorohydrin (CTS-ECH) and its derivatives have been synthesized and applied for wastewater treatment to remove synthetic dyes and heavy metals [19]. The surface properties and adsorption capacity of chitosan have been further improved by combining it with certain inorganic materials such as fly ash [20], illite–kaolinite clay [21], and titanium dioxide (TiO_2) [22]. Illite–kaolinite clay is one of the most common naturally occurring inorganic clays, available abundantly in crystalline form. This clay possesses unique characteristics that make it suitable as an independent adsorbent or as a component in chitosan-based composites for wastewater treatment. These characteristics include a high surface area, excellent adsorption efficiency, thermal stability, natural abundance, surface modifiability, and its non-toxic and environmentally friendly nature [23].

This study aims to investigate the adsorption of Orange G (OG) and Reactive Orange 16 (RO16) dyes using a composite of chitosan–illite-kaolinite modified with epichlorohydrin (CTS-ECH/IKaol). The composite was prepared by physically incorporating the inorganic illite–kaolinite clay into chitosan, followed by chemical crosslinking using epichlorohydrin as a crosslinking agent. The properties of the composite were characterized using various techniques including XRD, FTIR, SEM,

and pH_{pzc}, to examine its surface structure, elemental composition, crystallinity, functional groups, and surface charge. The adsorption performance of the CTS-ECH/IKOL composite for dye removal from aqueous solutions was evaluated using statistical methods. The Response Surface Methodology (RSM) combined with Box–Behnken Design (BBD) was applied to optimize the adsorption process. Key parameters affecting adsorption—such as adsorbent dose, pH, temperature, and contact time—were studied and optimized. Additionally, adsorption kinetics, isotherm models, and thermodynamic parameters were investigated to assess the environmental performance of the composite. Finally, the adsorption mechanisms of OG and RO16 dyes on the CTS-ECH/IKaol surface were discussed.

This research comprises four chapters:

- Literature Review - Examines recent 15-year studies on chitosan extraction, modification, and its application in pollutant (particularly dye) removal.

- Theoretical Background - Covers water pollution, dye classification, adsorption models/mechanisms, chitosan properties, and response surface methodology.

- Methodology - Details materials, instruments, and batch adsorption experiments using the CTS-ECH/IKaol composite.

- Results & Discussion - Presents findings with comparative analysis and concludes with key outcomes and future research directions.

- The work concludes with a general summary of key outcomes and recommendations for future work.

References

[1] S. L. Postel, "Securing water for people, crops, and ecosystems: new mindset and new priorities," in *Natural Resources Forum*, vol. 27, pp. 89-98, 2003.

[2] A. Omidvar, B. Jaleh, and M. Nasrollahzadeh, "Preparation of the GO/Pd nanocomposite and its application for the degradation of organic dyes in water," *Journal of colloid and interface science*, vol. 496, pp. 44-50, 2017.

[3] V. Selvaraj, T. S. Karthika, C. Mansiya, and M. Alagar, "An over review on recently developed techniques, mechanisms and intermediate involved in the advanced azo dye degradation for industrial applications," *Journal of molecular structure*, vol. 1224, p. 129195, 2021.

[4] B. Padhi, "Pollution due to synthetic dyes toxicity & carcinogenicity studies and remediation," *International journal of environmental sciences*, vol. 3, p. 940, 2012.

[5] S. Benkhaya, S. M'rabet, and A. El Harfi, "A review on classifications, recent synthesis and applications of textile dyes," *Inorganic Chemistry Communications*, vol. 115, p. 107891, 2020.

[6] K. Santhy and P. Selvapathy, "Removal of reactive dyes from wastewater by adsorption on coir pith activated carbon," *Bioresource technology*, vol. 97, pp. 1329-1336, 2006.

[7] W. Wang and A. Wang, "Perspectives on green fabrication and sustainable utilization of adsorption materials for wastewater treatment," *Chemical Engineering Research and Design*, vol. 187, pp. 541-548, 2022.

[8] A. Shajahan, S. Shankar, A. Sathiyaseelan, K. S. Narayan, V. Narayanan, V. Kaviyarasan, *et al.*, "Comparative studies of chitosan and its nanoparticles for the adsorption efficiency of various dyes," *International Journal of Biological Macromolecules*, vol. 104, pp. 1449-1458, 2017.

[9] I. Aranaz, A. R. Alcántara, M. C. Civera, C. Arias, B. Elorza, A. Heras Caballero, *et al.*, "Chitosan: An overview of its properties and applications," *Polymers*, vol. 13, p. 3256, 2021.

[10] I. O. Saheed, W. Da Oh, and F. B. M. Suah, "Chitosan modifications for adsorption of pollutants–A review," *Journal of hazardous materials*, vol. 408, p. 124889, 2021.

[11] A. H. Jawad and M. Nawi, "Characterizations of the photocatalytically-oxidized cross-linked chitosan-glutaraldehyde and its application as a sub-layer in the TiO 2/CS-GLA bilayer photocatalyst system," *Journal of Polymers and the Environment*, vol. 20, pp. 817-829, 2012.

[12] M. Nawi, A. H. Jawad, S. Sabar, and W. W. Ngah, "Photocatalytic-oxidation of solid state chitosan by immobilized bilayer assembly of TiO2–chitosan under a compact household fluorescent lamp irradiation," *Carbohydrate Polymers*, vol. 83, pp. 1146-1152, 2011.

[13] C. Pan, J. Qian, C. Zhao, H. Yang, X. Zhao, and H. Guo, "Study on the relationship between crosslinking degree and properties of TPP crosslinked chitosan nanoparticles," *Carbohydrate Polymers,* vol. 241, p. 116349, 2020.

[14] D. Kumar, S. Gihar, M. K. Shrivash, P. Kumar, and P. P. Kundu, "A review on the synthesis of graft copolymers of chitosan and their potential applications," *International Journal of Biological Macromolecules,* vol. 163, pp. 2097-2112, 2020.

[15] R. C. Choudhary, S. Kumari, R. Kumaraswamy, A. Pal, R. Raliya, P. Biswas, *et al.*, "Characterization methods for chitosan-based nanomaterials," *Plant Nanobionics: Volume 1, Advances in the Understanding of Nanomaterials Research and Applications,* pp. 103-116, 2019.

[16] G. Crini and P.-M. Badot, "Application of chitosan, a natural aminopolysaccharide, for dye removal from aqueous solutions by adsorption processes using batch studies: A review of recent literature," *Progress in polymer science,* vol. 33, pp. 399-447, 2008.

[17] B. Li, C.-L. Shan, Q. Zhou, Y. Fang, Y.-L. Wang, F. Xu, *et al.*, "Synthesis, characterization, and antibacterial activity of cross-linked chitosan-glutaraldehyde," *Marine drugs,* vol. 11, pp. 1534-1552, 2013.

[18] X. Yu, J. Zhang, and Y. Zheng, "Perchlorate adsorption onto epichlorohydrin crosslinked chitosan hydrogel beads," *Science of the total environment,* vol. 761, p. 143236, 2021.

[19] W. Wang, Q. Lu, X. Ren, C. Liu, J. Jin, S. Yin, *et al.*, "Synthesis of novel ECH crosslinked chitosan schiff base-sodium alginate for adsorption of Cd (II) ion from aqueous solution," *Desalination and Water Treatment,* vol. 145, pp. 169-178, 2019.

[20] A. H. Jawad, I. A. Mohammed, and A. S. Abdulhameed, "Tuning of fly ash loading into chitosan-ethylene glycol diglycidyl ether composite for enhanced removal of reactive red 120 dye: optimization using the Box–Behnken design," *Journal of Polymers and the Environment,* vol. 28, pp. 2720-2733, 2020.

[21] E. Eddarai, M. El Mouzahim, R. Boussen, A. Bellaouchou, A. Guenbour, and A. Zarrouk, "Chitosan-kaolinite clay composite as durable coating material for slow release NPK fertilizer," *International Journal of Biological Macromolecules,* vol. 195, pp. 424-432, 2022.

[22] L. M. Anaya-Esparza, J. M. Ruvalcaba-Gómez, C. I. Maytorena-Verdugo, N. González-Silva, R. Romero-Toledo, S. Aguilera-Aguirre, *et al.*, "Chitosan-TiO2: A versatile hybrid composite," *Materials,* vol. 13, p. 811, 2020.

[23] A. H. Jawad and A. S. Abdulhameed, "Facile synthesis of crosslinked chitosan-tripolyphosphate/kaolin clay composite for decolourization and COD reduction of remazol brilliant blue R dye: optimization by using response surface methodology," *Colloids and Surfaces A: Physicochemical and Engineering Aspects,* vol. 605, p. 125329, 2020.

Chapter I:

Literature Review

I.1. Background

The water demand doubles globally every 21 years due to the rapid increase in the population and the industrial activities [1]. With the rapid acceleration of industrial development over recent decades, industrial, agricultural, and urban activities have significantly increased, leading to the release of vast amounts of pollutants into aquatic environments. Furthermore, 5-10 million people die annually due to various diseases caused by the consumption of contaminated water [2]. Thus, exploitation of safe water sources to overcome the scarcity of water has been a global challenge for many countries like Algeria. These pollutants include organic and inorganic materials such as dyes, phenolic compounds, aromatic compounds and heavy metals [3]. Among these pollutants, industrial dyes are considered some of the most common and widespread contaminants due to their extensive use in various industrial sectors, including textile manufacturing, paper production, cosmetics, printing, food processing, and leather tanning [4]. Because of their high chemical stability, eliminating these dyes through conventional methods poses a major environmental challenge, necessitating the development of more efficient and environmentally friendly treatment technologies [5].

Several adsorbent materials have been used for pollutant removal from water, including graphene, zeolite, activated carbon, clay, cellulose, and chitosan. These materials are attracting increasing interest due to their effectiveness, availability, and biodegradability, making them among the most promising solutions in the field of water purification especially in light of the global trend toward adopting sustainable and environmentally friendly treatment technologies [6].

Research challenges have grown in the development of adsorbent materials that are biodegradable, low-cost, eco-friendly, and possess efficient adsorption properties. Among these materials, **chitosan (CTS)** has emerged as a leading candidate that has drawn significant attention from researchers not only due to its unique physical and chemical properties, but also for its wide-ranging applications in various fields [7].

Chitin and chitosan are commercially produced in countries like Japan, the U.S., India, Poland, Australia, and Norway, with smaller-scale production in Canada, Italy, Chile, and Brazil. Naturally abundant, chitin's global production is estimated at 10^1 to 10^{12} tons annually, making it a low-cost and widely available resource [8].

Chitosan is a cationic biopolymer derived from chitin and contains active functional groups such as amine ($-NH_2$) and hydroxyl (-OH), which serve as effective adsorption sites. These functional groups give chitosan a high capacity to adsorb

pollutants, especially anionic dyes. Numerous studies have demonstrated the high efficiency of chitosan in removing colored dyes, particularly when it is modified through physical or chemical methods [9].

According to data from the scientific search engine ***Science Direct***, there has been a significant increase in the number of scientific publications related to the use of **modified chitosan** for dye removal during the period from 2010 to 2025, with more than 30,000 articles and about 4,000 books on chitosan were published worldwide.

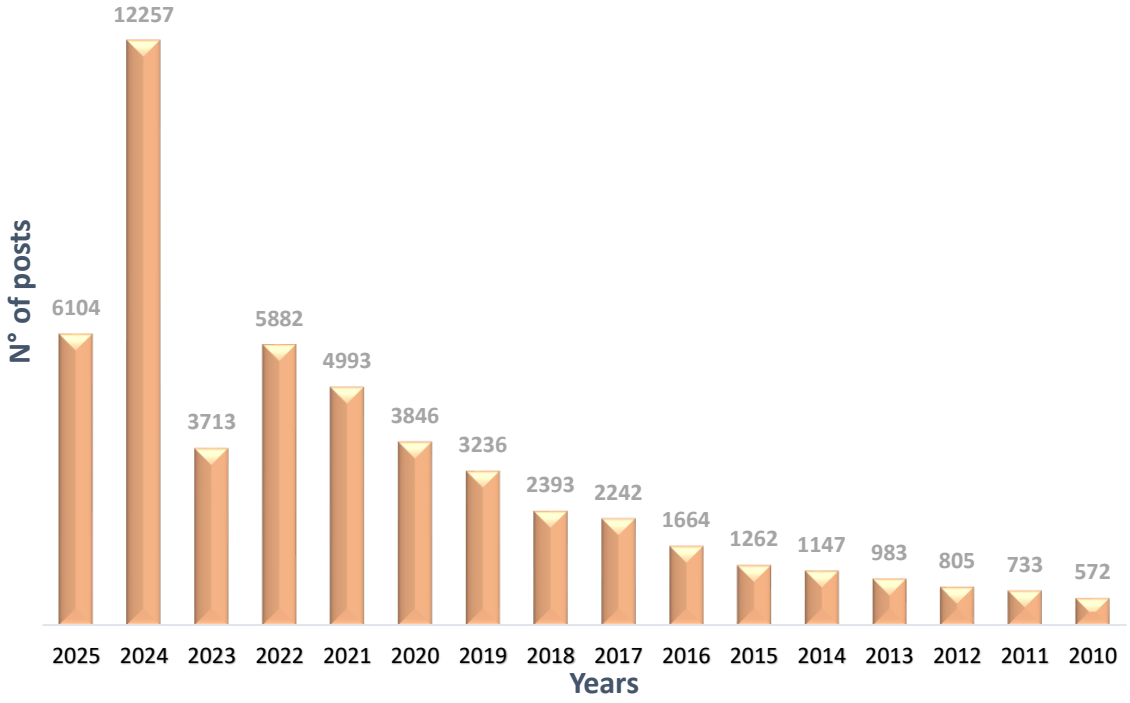

Figure I.1. The number of publications (2010-2025) on chitosan modifications for adsorption applications according to data taken from Web of Science and Scopus-indexed journals

Number of papers published in (Years, 2010-2025) focused on various chitosan materials, where the carbon materials are activated carbon (AC), Metal Oxide (MO), clay (CLY), Biochar (BC), and Carbon Nanotubes (CNTs) [10-12]. All data taken from Web of Science and Scopus-indexed journals.

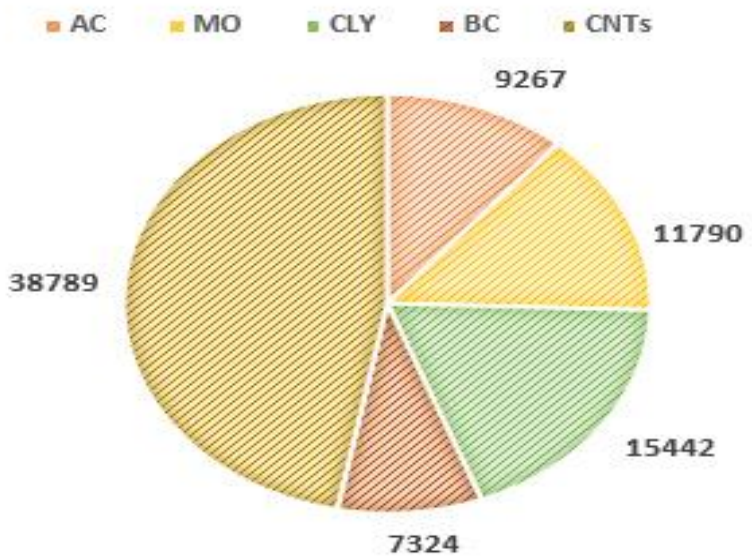

Figure I.2. Publication Trends of Chitosan-Based Materials with Carbon Composites (2010-2025): A Bibliometric Analysis of Web of Science and Scopus Data.

The main focus of this review will be on discussion 106 papers (Years, 2010–2025) from the Web of Science and Scopus-indexed journals, covering a total of 26 journals about the application of CTS and its derivatives to remove on cationic dyes and anionic dyes was discussed comprehensively, and factors affecting the adsorption performance of adsorbents, including adsorption isotherm model, adsorption kinetics process, etc. Based on the reviewed papers, it is clear, that while some challenges remain, chitosan-based materials are emerging as promising adsorbents **(See Table 01 in the appendices).**

I.2. Advances in chitosan-based dye adsorbents (2010-2025)

- A study conducted in **2010** aimed to develop an adsorbent material based on chitosan immobilized on glass plates **(CS/glass)**, as a preliminary step toward designing a bilayer system that synergistically combines photocatalysis and adsorption using titanium dioxide and chitosan for the removal of the **anionic** dye Reactive Red 4 **(RR4)** from aqueous solutions. The equilibrium adsorption data showed good agreement with both the **Langmuir and Freundlich** isotherm models, with a maximum adsorption capacity of **172.41 mg/g**. Kinetic analysis revealed that the adsorption process followed a pseudo-second-order **(PSO)** model, indicating that the rate-limiting step may be chemical adsorption. Thermodynamic analysis confirmed that the process is spontaneous and exothermic in nature [13].

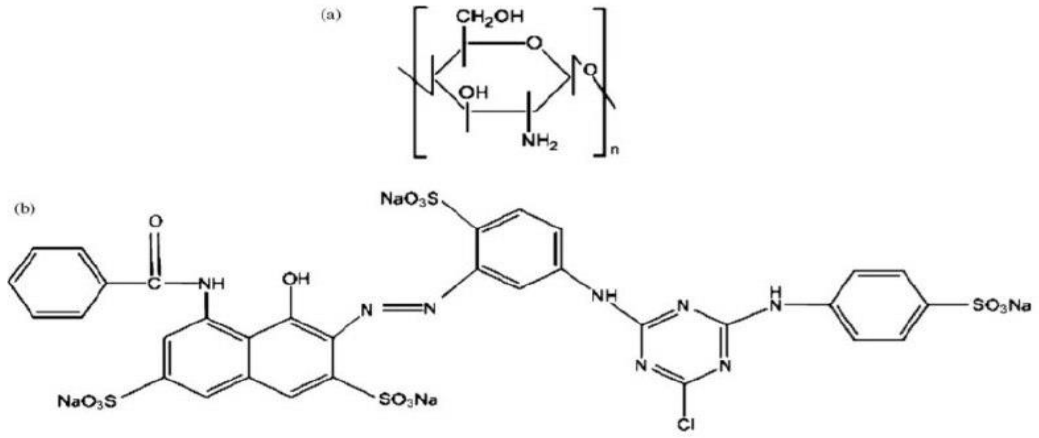

Figure I.3. The molecular structure of **(a)** chitosan, and **(b)** Reactive Red 4 (RR4)

- In **2011**, a study was conducted to evaluate the efficiency of chitosan modified with tetraethylenepentamine **(TEPA–CS)** for the removal of the **anionic** dye **Eosin Y** from aqueous solutions. The equilibrium results demonstrated a good fit with the **Langmuir** isotherm model, with a maximum adsorption capacity of **292.4 mg/g** at 298 K. Kinetic analysis showed that the adsorption followed a pseudo-second-order **(PSO)** model, indicating the possible involvement of chemical interactions in the adsorption mechanism. Thermodynamic analysis revealed negative values for both enthalpy and Gibbs free energy, confirming that the adsorption process is spontaneous and endothermic in nature [14].
- In **2012**, a study was conducted to develop a composite material consisting of hydroxyapatite and chitosan **(HAp-CS)** aimed at removing the **anionic** dye Congo Red **(CR)** from aqueous solutions. The findings indicated that the adsorption process followed a **pseudo-second-order** kinetic model and was spontaneous based on thermodynamic analysis. Moreover, the adsorption behavior was in good agreement with the **Langmuir** isotherm model. The composite containing 50 wt% chitosan demonstrated the highest adsorption capacity, reaching **769 mg/g** [15].
- With the aim of developing a new adsorbent for the removal of the **cationic** dye Methyl Blue **(MB)** from aqueous solutions, a study was conducted in **2013** to develop an adsorbent consisting of ethylenediamine tetraacetic anhydride (EDTA)-modified magnetic chitosan, referred to as **EMC**. The adsorption results showed good agreement with the **Sips** model, with a maximum adsorption capacity of **113.26 mg/g** under optimized conditions. The study also showed that

the adsorption behavior followed a **pseudo-second-order** model, suggesting the potential for chemical reactions in the adsorption mechanism. Reusability tests showed that the material maintained a significant portion of its efficiency after three consecutive adsorption-decomposition cycles, highlighting its potential for efficient reuse [16].

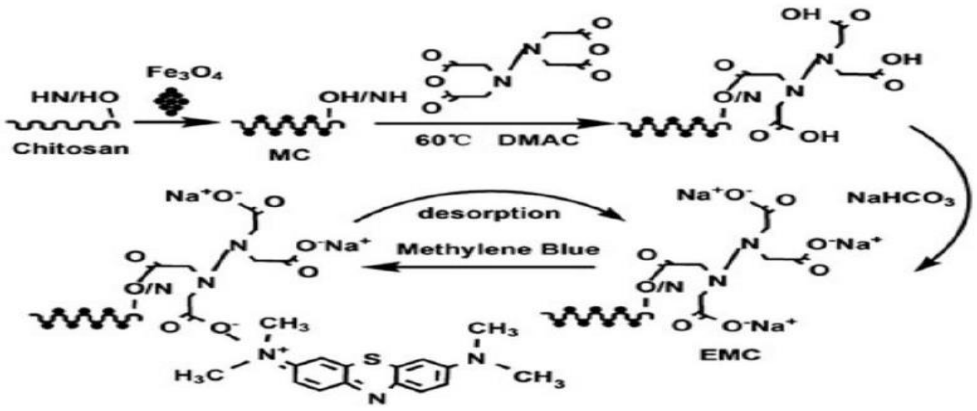

Figure I.4. Synthesis scheme of EMC and adsorption mechanism of MB on EMC.

- A study conducted in **2014** focused on the adsorption of the **anionic** dye **C.I. Reactive Blue 19** from aqueous solutions using grafted chitosan porous particles **CTS**. The equilibrium adsorption data were found to fit well with the **Langmuir** isotherm model, with a maximum dye uptake of **1498 mg/g**. Moreover, kinetic results indicated that the adsorption followed a **pseudo-second-order** model, suggesting that chemisorption is the dominant mechanism governing the process [17].

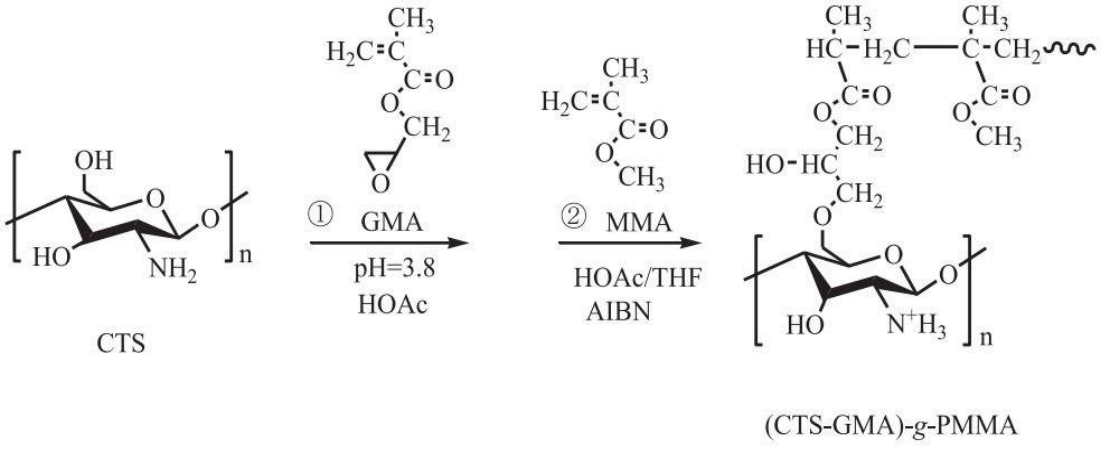

Figure I.5. The schematic route to modify CTS.

- In **2015**, a cross-linked chitosan/bentonite composite stabilized with zirconium(IV) was synthesized, referred to as **Zr-CCS/BT**. This composite was used to remove the **anionic** dye methyl orange **(MO)** from aqueous solutions. The adsorption heat data were accurately described using the **Langmuir** model, and the maximum adsorption capacity was **438.6 mg/g**. The kinetic data were accurately described using the **pseudo-second-order** model. The thermodynamic data demonstrated that the adsorption process of methyl orange is spontaneous and exothermic in nature [18].
- In **2016**, a research study was conducted aiming to prepare a cross-linked chitosan/bentonite composite surface-immobilized with zirconium (Zr(IV)) **(Zr-CCB)** for the adsorption of the **anionic** azo dye **Amido Black 10B** from aqueous solutions. The equilibrium adsorption data showed a good fit with the **Langmuir** isotherm model, with a maximum monolayer adsorption capacity of **418.4 mg/g**. Additionally, the study revealed that the adsorption behavior followed the **pseudo-second-order** kinetic model, indicating that the adsorption mechanism may be governed by chemical interactions [19].

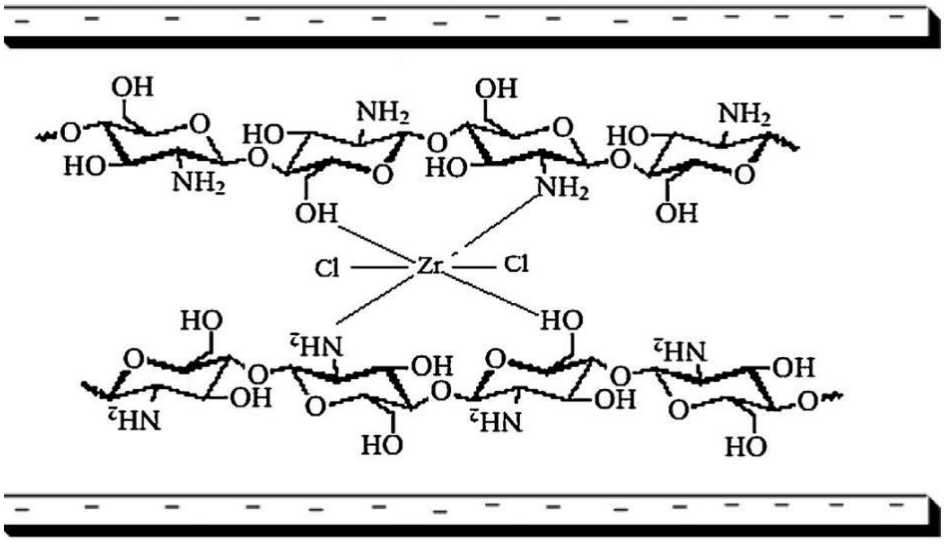

Figure I.6. Reaction mechanism between Zr(IV) and CCB.

- In **2017**, researchers conducted a study on the synthesis and characterization of a magnetic nanocomposite based on chitosan/silica/carbon nanotubes **(MNCSC)** and its application for the removal of the **anionic** dyes Direct Blue 71 **(DB71)** and Reactive Blue 19 **(RB19)** from aqueous solutions. The results showed a good fit with the **Langmuir** isotherm model, with maximum adsorption capacities of

61.35 mg/g for DB71 (R^2 = 0.996) and **97.08 mg/g** for RB19 (R^2 = 0.998). Additionally, the **pseudo-second-order** kinetic model was found to be the most appropriate to describe the adsorption behavior of the dyes [20].In this **2018** study, a **cross-linked poly(AA-co-VPA) hydrogel incorporating N-maleyl chitosan** was synthesized as an adsorbent for the removal of the **cationic** dyes crystal violet **(CV)** and methylene blue **(MB)** from aqueous solutions. The Redlich–Peterson isotherm model was found to best describe the adsorption behavior. Additionally, the results indicated that the pseudo-second-order kinetic model was the most suitable for fitting the experimental data. The maximum adsorption capacities for the removal of CV and MB from the solutions were **64.56 mg/g** and **66.89 mg/g**, respectively [21].

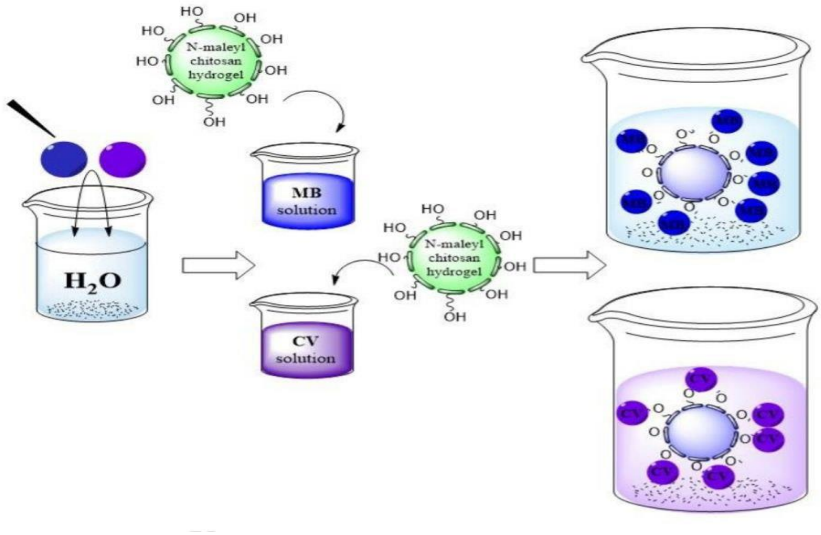

Figure I.7. The schematic cross-linked poly(AA-co-VPA) hydrogel incorporating N-maleyl chitosan.

- In a study published in **2019**, a hybrid nanocomposite of glyoxal cross-linked chitosan and titanium dioxide **(Chi-Gly/TNC)** was synthesized and applied for the removal of the **anionic** dyes Reactive Orange 16 **(RO16)** dye from aqueous solutions. The results showed that the highest removal efficiency reached 93.2% under optimal conditions: 50% TiO_2 loading, an adsorbent dose of 0.09 g/50 mL, solution pH around 4.0, and a temperature of 40°C. The kinetic data were consistent with the **pseudo-first-order** model, while the equilibrium data fit both **Langmuir and Freundlich** isotherm models, with a maximum adsorption capacity of **390.5 mg/g** [22].

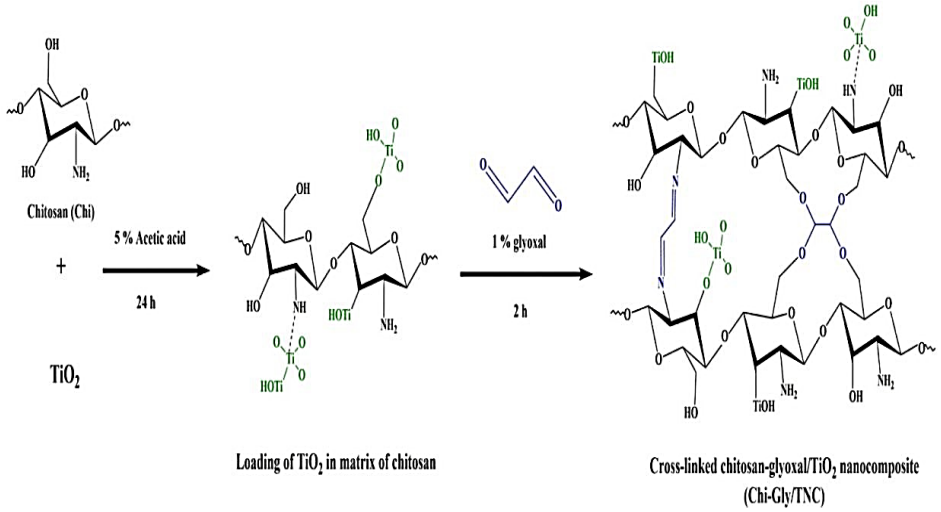

Figure I.8. Scheme of preparation cross linked chitosan-glyoxal/TiO2 nanocomposite

- In this **2020** study, a mesoporous chitosan–epichlorohydrin/activated charcoal composite **(CS-ECH/AC)** was synthesized by combining chitosan (CS) with activated charcoal (AC), followed by a crosslinking reaction using epichlorohydrin (ECH). The material was evaluated as an adsorbent for the removal of thionine **(TH)**, a model **cationic** dye, from aqueous solutions. The equilibrium data showed good agreement with the **Freundlich** isotherm model, with a maximum adsorption capacity of **60.9 mg/g** at 303 K. The kinetic data followed the **pseudo-second-order** model. Thermodynamic studies confirmed that the adsorption process was spontaneous and exothermic in nature[23] .

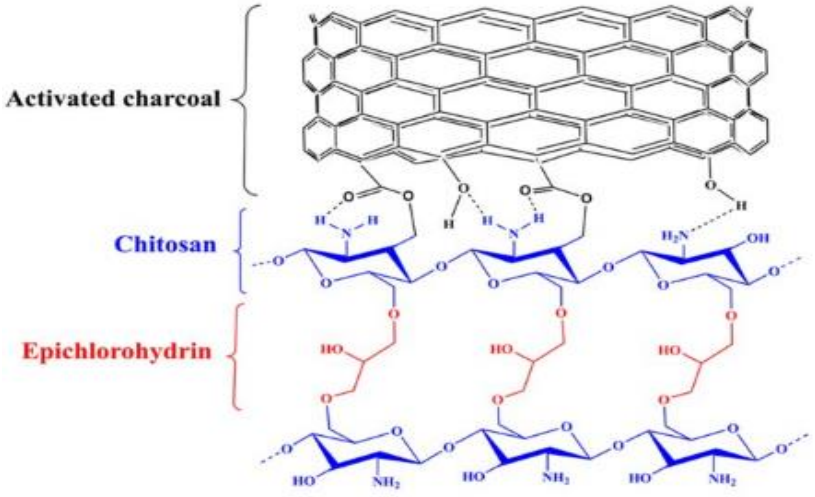

Figure I.9. The proposed molecular structure of CS-ECH/AC composite.

- In a study conducted in **2021**, a magnetic Schiff base composite of chitosan-glutaraldehyde/iron oxide **(CHT-GLA/ZnO/Fe_3O_4)** was developed by

incorporating zinc oxide (ZnO) nanoparticles into its structure to enhance its efficiency as an adsorbent for the removal of the **anionic** dye Remazol Brilliant Blue R **(RBBR)** from aqueous solutions. The kinetic data were found to follow the **pseudo-second-order** model, while the equilibrium data showed better fit with the **Freundlich and Temkin** isotherm models. The maximum adsorption capacity of the composite containing 25% ZnO (CHT-GLA/ZnO/Fe_3O_4-25) was approximately **176.6 mg/g** at a temperature of 60 °C [24].

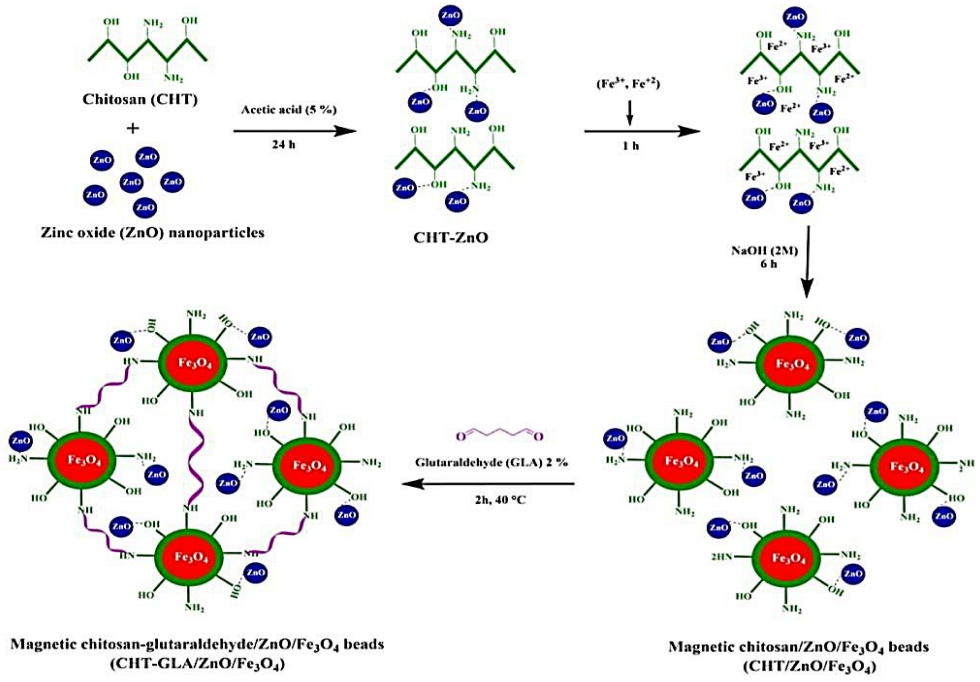

Figure I.10. Synthesis steps of CHT-GLA/ZnO/Fe_3O_4

- In a study conducted in **2022**, a novel nanocomposite biomaterial composed of cross-linked chitosan with magnesium oxide and iron oxide **(CTS-TPP/MgO/Fe_3O_4)** was synthesized and employed as an adsorbent for the removal of the anionic dye Reactive Blue 19 **(RB 19)** from aqueous solutions. The kinetic data were found to fit well with the **pseudo-second-order** model, while the equilibrium data followed the Freundlich isotherm model. The maximum adsorption capacity, as calculated from the Langmuir isotherm model, was **120.3 mg/g** [25].
- A study conducted in **2023** focused on the preparation of a biocomposite material made from chitosan/sepiolite clay/algae **(Chi/Sep/Alg)** for the adsorption and removal of **cationic** (malachite green, **MG**) and **anionic** (remazol brilliant blue R, **RBBR**) dyes from aqueous solutions. Kinetic and equilibrium results indicated

that the adsorption of both MG and RBBR dyes onto the Chi/Sep/Alg material followed the **pseudo-second-order** model and the **Freundlich** isotherm model, respectively. The maximum adsorption capacity of the Chi/Sep/Alg composite was **515.7 mg/g** for MG in a basic environment (pH 8) and **292.4 mg/g** for RBBR in an acidic environment (pH = 4) [26].

- This study from **2024** involved the development of a composite material made of chitosan-benzaldehyde/algae/coal fly ash **(CS-BD/Alg/FA)** as a promising adsorbent for the removal of the cationic dye, brilliant green **(BG)**. The kinetic and equilibrium data obtained under optimal conditions indicated that the adsorption of BG by CS-BD/Alg/FA followed the pseudo-second-order **(PSO)** model and **Langmuir** monolayer adsorption model, respectively. According to the thermodynamic parameters, it was determined that the adsorption process exhibited both spontaneous and exothermic nature. As a result, the maximum adsorption capacity (qmax) observed for CS-BD/Alg/FA towards BG was **239.3 mg/g** [27].

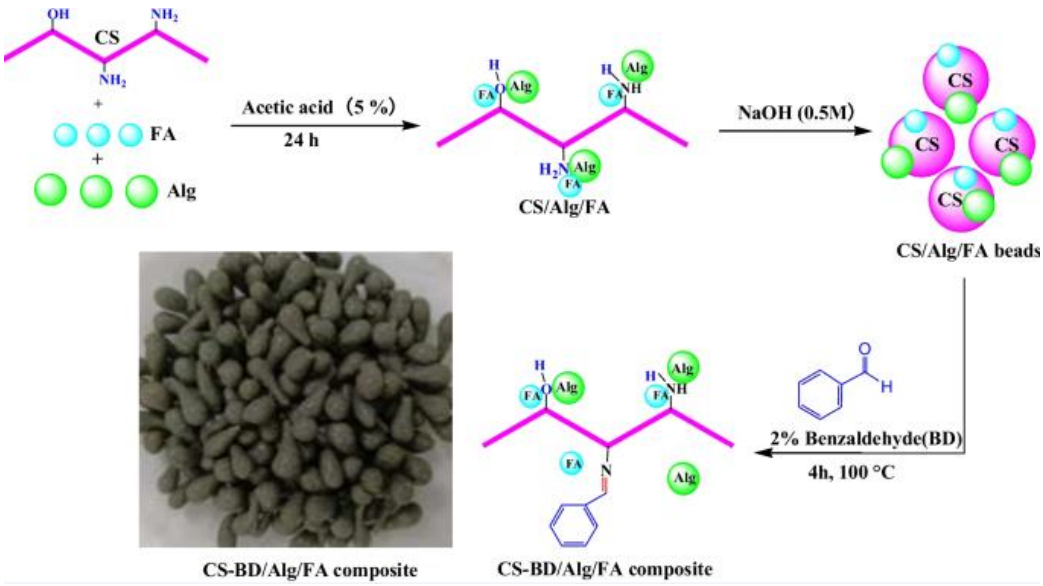

Figure I.11. Synthesis steps of CS-BD/Alg/FA Composite

- In **2025**, a chitosan-glutaraldehyde/algae **(CHS-GTD/AL)** composite was synthesized through a two-step process. First, the natural polymer chitosan (CHS) was functionalized with algae (AL). The adsorption behavior of the **cationic** dye methyl violet 2B **(MV 2B)** by CHS-GTD/AL was studied using the Box-Behnken design (BBD). The equilibrium adsorption data were well-described by the

Freundlich isotherm model. Kinetic studies revealed that the adsorption of MV 2B by CHS-GTD/AL followed a **pseudo-second-order** model. The adsorption capacity of CHS-GTD/AL towards MV 2B was determined to be **123.2 mg/g** [28].

References

[1] B. R. Scanlon, S. Fakhreddine, A. Rateb, I. de Graaf, J. Famiglietti, T. Gleeson, *et al.*, "Global water resources and the role of groundwater in a resilient water future," *Nature Reviews Earth & Environment,* vol. 4, pp. 87-101, 2023.

[2] N. J. Ashbolt, "Microbial contamination of drinking water and disease outcomes in developing regions," *Toxicology,* vol. 198, pp. 229-238, 2004.

[3] R. Mecheri, A. Zobeidi, S. Atia, S. Neghmouche Nacer, A. A. Salih, M. Benaissa, *et al.*, "Modeling and optimizing the crystal violet dye adsorption on kaolinite mixed with cellulose waste red bean peels: insights into the kinetic, isothermal, thermodynamic, and mechanistic study," *Materials,* vol. 16, p. 4082, 2023.

[4] S. Bahemmi, A. Zobeidi, S. Atia, S. Neghmouche Nacer, D. Ghernaout, and N. Elboughdiri, "Activating illite kaolinite clay with CTAB for adsorbing methylene blue: isotherms, kinetics, and thermodynamics studies," *Tuijin Jishu/Journal of Propulsion Technology,* vol. 44, p. 2023, 2023.

[5] N. Sjahro, R. Yunus, L. C. Abdullah, S. A. Rashid, A. J. Asis, and Z. Akhlisah, "Recent advances in the application of cellulose derivatives for removal of contaminants from aquatic environments," *Cellulose,* vol. 28, pp. 7521-7557, 2021.

[6] O. Akperov, E. Akperov, and F. Kamranzadeh, "Removal of Rhodamine 6G dye from water solution by alt-maleic anhydride-styrene-octene-1 terpolymer, cross-linked with triethanolamine," *New Materials, Compounds and Applications,* vol. 4, pp. 188-202, 2020.

[7] S. Islam, M. R. Bhuiyan, and M. Islam, "Chitin and chitosan: structure, properties and applications in biomedical engineering," *Journal of Polymers and the Environment,* vol. 25, pp. 854-866, 2017.

[8] B. T. Iber, N. A. Kasan, D. Torsabo, and J. W. Omuwa, "A review of various sources of chitin and chitosan in nature," *Journal of Renewable Materials,* vol. 10, p. 1097, 2022.

[9] A. Giannakas and M. Pissanou, "Chitosan/bentonite nanocomposites for wastewater treatment: a review," *SF J Nanochem Nanotechnol. 2018; 1 (1),* vol. 1010, 2018.

[10] G. Z. Kyzas and D. N. Bikiaris, "Recent modifications of chitosan for adsorption applications: a critical and systematic review," *Marine drugs,* vol. 13, pp. 312-337, 2015.

[11] D. Krajišnik, S. Uskoković-Marković, and A. Daković, "Chitosan–Clay Mineral Nanocomposites with Antibacterial Activity for Biomedical Application: Advantages and Future Perspectives," *International Journal of Molecular Sciences,* vol. 25, p. 10377, 2024.

[12] F. Tafraout and J. Isaad, "Recent research landscape on chitosan-mineral-based composites for wastewater treatment: a comprehensive bibliometric analysis (2014–2024)," *Environmental Science and Pollution Research*, pp. 1-23, 2025.

[13] M. Nawi, S. Sabar, A. Jawad, and W. W. Ngah, "Adsorption of Reactive Red 4 by immobilized chitosan on glass plates: towards the design of immobilized TiO2–chitosan synergistic photocatalyst-adsorption bilayer system," *Biochemical Engineering Journal*, vol. 49, pp. 317-325, 2010.

[14] X.-Y. Huang, X.-Y. Mao, H.-T. Bu, X.-Y. Yu, G.-B. Jiang, and M.-H. Zeng, "Chemical modification of chitosan by tetraethylenepentamine and adsorption study for anionic dye removal," *Carbohydrate Research*, vol. 346, pp. 1232-1240, 2011.

[15] H. Hou, R. Zhou, P. Wu, and L. Wu, "Removal of Congo red dye from aqueous solution with hydroxyapatite/chitosan composite," *Chemical engineering journal*, vol. 211, pp. 336-342, 2012.

[16] Y. Xia, X. Dai, S. Huang, X. Tian, H. Yang, Y. Li, *et al.*, "Fast and highly efficient removal of methylene blue by a novel EDTAD-modified magnetic chitosan material," *Desalination and Water Treatment*, vol. 51, pp. 7586-7595, 2013.

[17] X. Jiang, Y. Sun, L. Liu, S. Wang, and X. Tian, "Adsorption of CI Reactive Blue 19 from aqueous solutions by porous particles of the grafted chitosan," *Chemical Engineering Journal*, vol. 235, pp. 151-157, 2014.

[18] L. Zhang, P. Hu, J. Wang, Q. Liu, and R. Huang, "Adsorption of methyl orange (MO) by Zr (IV)-immobilized cross-linked chitosan/bentonite composite," *International journal of biological macromolecules*, vol. 81, pp. 818-827, 2015.

[19] L. Zhang, P. Hu, J. Wang, and R. Huang, "Adsorption of Amido Black 10B from aqueous solutions onto Zr (IV) surface-immobilized cross-linked chitosan/bentonite composite," *Applied Surface Science*, vol. 369, pp. 558-566, 2016.

[20] M. Abbasi, "Synthesis and characterization of magnetic nanocomposite of chitosan/SiO2/carbon nanotubes and its application for dyes removal," *Journal of Cleaner Production*, vol. 145, pp. 105-113, 2017.

[21] M. T. Nakhjiri, G. B. Marandi, and M. Kurdtabar, "Poly (AA-co-VPA) hydrogel cross-linked with N-maleyl chitosan as dye adsorbent: Isotherms, kinetics and thermodynamic investigation," *International Journal of Biological Macromolecules*, vol. 117, pp. 152-166, 2018.

[22] A. S. Abdulhameed, A.-T. Mohammad, and A. H. Jawad, "Modeling and mechanism of reactive orange 16 dye adsorption by chitosan-glyoxal/TiO2 nanocomposite: application of response surface methodology," *Desalination and Water Treatment*, vol. 164, pp. 346-360, 2019.

[23] A. H. Jawad, A. S. Abdulhameed, and M. S. Mastuli, "Mesoporous crosslinked chitosan-activated charcoal composite for the removal of thionine cationic dye: comprehensive adsorption and mechanism study," *Journal of Polymers and the Environment*, vol. 28, pp. 1095-1105, 2020.

[24] A. Reghioua, D. Barkat, A. H. Jawad, A. S. Abdulhameed, S. Rangabhashiyam, M. R. Khan, *et al.*, "Magnetic chitosan-glutaraldehyde/zinc oxide/Fe3O4 nanocomposite: optimization and adsorptive mechanism of remazol brilliant blue R dye removal," *Journal of Polymers and the Environment*, vol. 29, pp. 3932-3947, 2021.

[25] A. H. Jawad, U. K. Sahu, N. A. Jani, Z. A. ALOthman, and L. D. Wilson, "Magnetic crosslinked chitosan-tripolyphosphate/MgO/Fe3O4 nanocomposite for reactive blue 19 dye removal: Optimization using desirability function approach," *Surfaces and Interfaces*, vol. 28, p. 101698, 2022.

[26] Z. M. Zain, A. S. Abdulhameed, A. H. Jawad, Z. A. ALOthman, and Z. M. Yaseen, "A pH-sensitive surface of chitosan/sepiolite clay/algae biocomposite for the removal of malachite green and remazol brilliant blue R dyes: optimization and adsorption mechanism study," *Journal of Polymers and the Environment*, vol. 31, pp. 501-518, 2023.

[27] R. Wu, A. Suhaimi, A. H. Jawad, and Z. A. ALOthman, "Decoration of Chitosan-Benzaldehyde/Algae/Coal Fly Ash Adsorbent for Brilliant Green Dye Removal: Box–Benken Design Optimization and Mechanism Approach," *Journal of Inorganic and Organometallic Polymers and Materials*, vol. 34, pp. 5884-5900, 2024.

[28] H. M. Agha, A. S. Abdulhameed, A. H. Jawad, Z. A. ALOthman, L. D. Wilson, and S. Algburi, "Fabrication of glutaraldehyde crosslinked chitosan/algae biomaterial via hydrothermal process: Statistical optimization and adsorption mechanism for MV 2B dye removal," *Biomass Conversion and Biorefinery*, vol. 15, pp. 1105-1119, 2025.

Chapter II:

Bibliographic synthesis

PART I: Dyes

II.1. Dyes and Water Pollution

Dye is an organic compound that imparts colour to substances such as textile fibre, leather, hair, plastic materials or wax either is solution or dispersion [1].

Dyes have long been known to man and in the prehistoric times they were derived from natural plants, mainly for colouring fabric [2]. With the advent of the industrial revolution, industrial operations experienced a significant surge, resulting in a mismatch between the production of natural dyes and the growing industrial need. W. H. Perkin created aniline purple, the first artificially made dye, in 1856 [3]. Since then, there has been a substantial increase in the creation of synthetic colours. At present almost all the dyes are manufactured artificially even the natural dyes. The artificial dyes are thoughtfully delineated to have distinctive characteristics such as; ability to impart specific colour to the substance, resistance to fade when exposed to light, chemicals and washing [4], and resistance towards acids and bases. The groups that modify the ability of chromophores to absorb light are called **auxochromes** (NO_2, NO, N=N). The part of molecules which provides the colour by adsorbing wavelength is called **chromophores** (OH, NH2, NHR, NR_2, Cl and COOH) [5], as indicated in Table **II.1.**

Table II.1. Classification of Synthetic Dyes Based on Color Intensity [6]

Chromophore Groups (Color-Giving)	**Auxochrome Groups (Color Intensifiers)**
Azo (-N=N-)	Amine ($-NH_2$)
Nitro ($-NO_2$) or Nitroso (-NO, =N-OH)	Methyl Amine ($-NHCH_3$)
Carbonyl (=C=O)	Dimethyl Amine ($-N(CH_3)_2$)
Phenyl (-C=C-)	Hydroxyl (-OH)
Nitro ($-NO_2$, =NO-OH)	Alkoxyl (-OR)
Thioketone (>C=S)	Electron-Donating Groups

II.2. Classification of Dyes

There are two distinct ways to classify dyes: either by their chemical structure (chemical classes) or by their application method (classes ion charge). The reference work in terms of dyes and pigments is the colour index [7].

II.2.1. Classification Based on Ion Charge

Dyes can be classified based on their chemical structure, functional groups, or the ion charge they acquire upon dissolution in water. Since ion charge plays a significant

role in the adsorption process, dyes are categorized according to this criterion into **ionic dyes** and **non-ionic dyes**, as illustrated in Figure **II.1**[8, 9] **.**

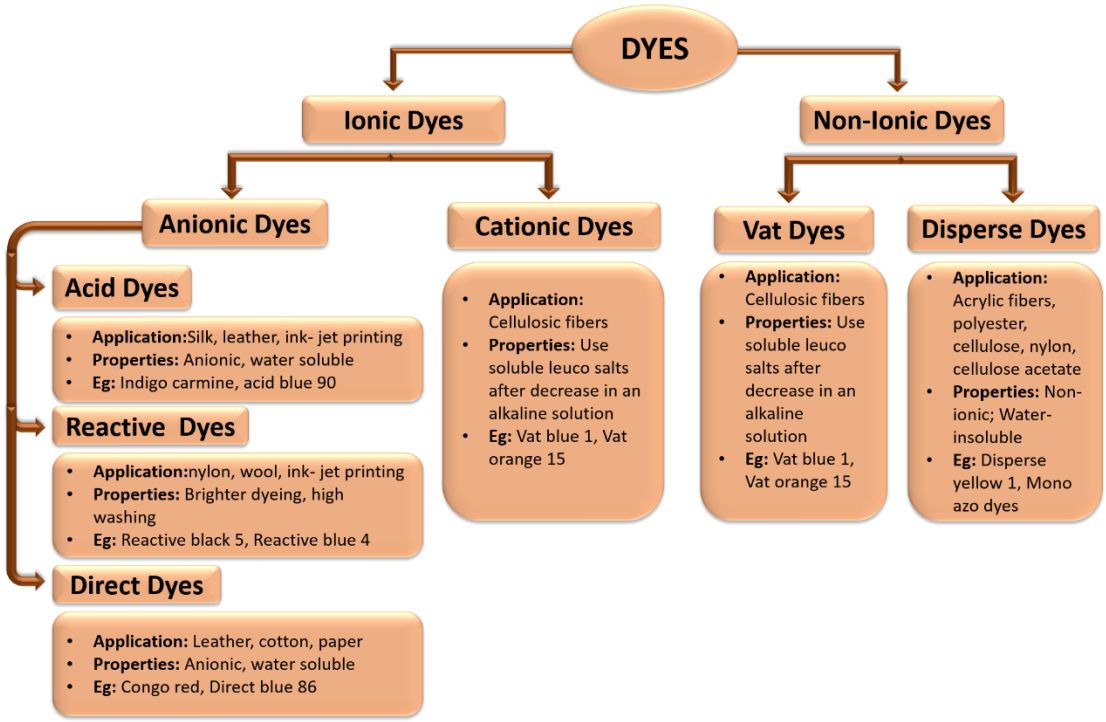

Figure II.1. Classification of dyes according to their ionic charge, application, and properties [10].

II.2.2. Chemical Classification

The categorization of dyes according to their chemical structure is determined by the characteristics of the chromophore group [11].

Table II.2. Classification of dyes based on chemical composition[4].

Classification	Definition	Basic Structure
Azo Dyes	Characterized by the presence of an azo (-N=N-) group that links two benzene nuclei. This category is currently the most widely applied, representing **60-70%** of the global production of coloring materials	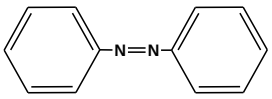
Anthraquinone Dyes	These are the second most important dyes after azo dyes. Their general structure is derived from anthracene, with the **chromophore being a quinone core**, which can be substituted with hydroxyl or amine groups.	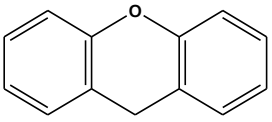
Xanthene Dyes	The main representative of this family is fluorescein. Although few xanthene dyes are used as colorants, they are employed in various applications, such as marking signals in maritime accidents and	

	tracking groundwater flow, wastewater streams, and other environmental studies.	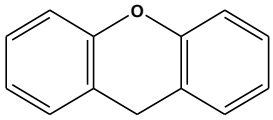
Nitro and Nitroso Dyes	These form a relatively small and older class of dyes that are still in use today due to their **very low cost** and **simple molecular structure**, which includes a **nitro (-NO_2) group at the ortho position** relative to an electron-donating group (such as hydroxyl or amine groups).	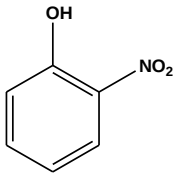
Phthalocyanine Dyes	These dyes have a **complex structure with a central metal atom** and are obtained through the reaction of **dicyanobenzene** in the presence of a **metal halide** (e.g., Cu, Ni, Co, Pt, etc.)	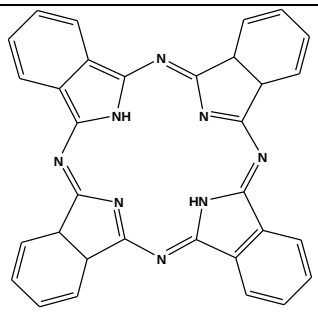
Triphenylmethane Dyes	This class consists of **hydrocarbons with three phenyl rings attached to a central carbon atom**. They represent **one of the oldest categories of synthetic dyes** and are used in **paper and textile industries**, as well as for dyeing **nylon, wool, silk, and cotton**. Additionally, they have applications in the **medical field**.	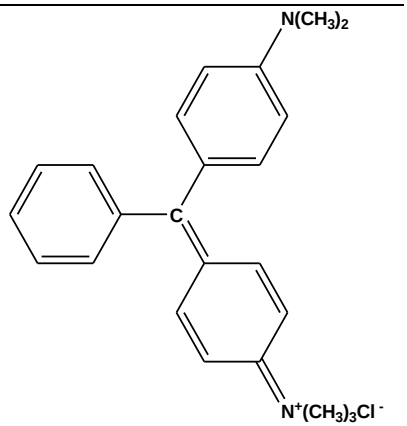
Indigoid Dyes	Derived from the **natural indigo color**, these dyes are widely used in **textiles, confectionery, pharmaceuticals, and medical diagnostics**	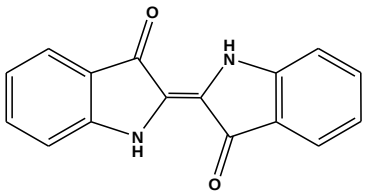

II.3. Uses of dyes

- Textile industry.
- Plastics and construction coatings industry.
- Food industry (food colorants).
- Cosmetics industry.
- Printing (ink and paper) [10].

II.4. Current Dye Removal Techniques

Various authors have reviewed and summarized dye removal methods in their publications [12-14]. In recent years, extensive research has been conducted to identify the most effective method for purifying dye-contaminated wastewater. Although a wide variety of approaches have been explored over the past three decades, only a few are currently employed by industries due to the limitations [12].

As it appears in the review articles referred to above, dye remediation strategies can be broadly classified into three categories: physical, chemical, and biological methods. Figure **II. 2** provides an overview of some commonly used techniques, along with their advantages and disadvantages [14]

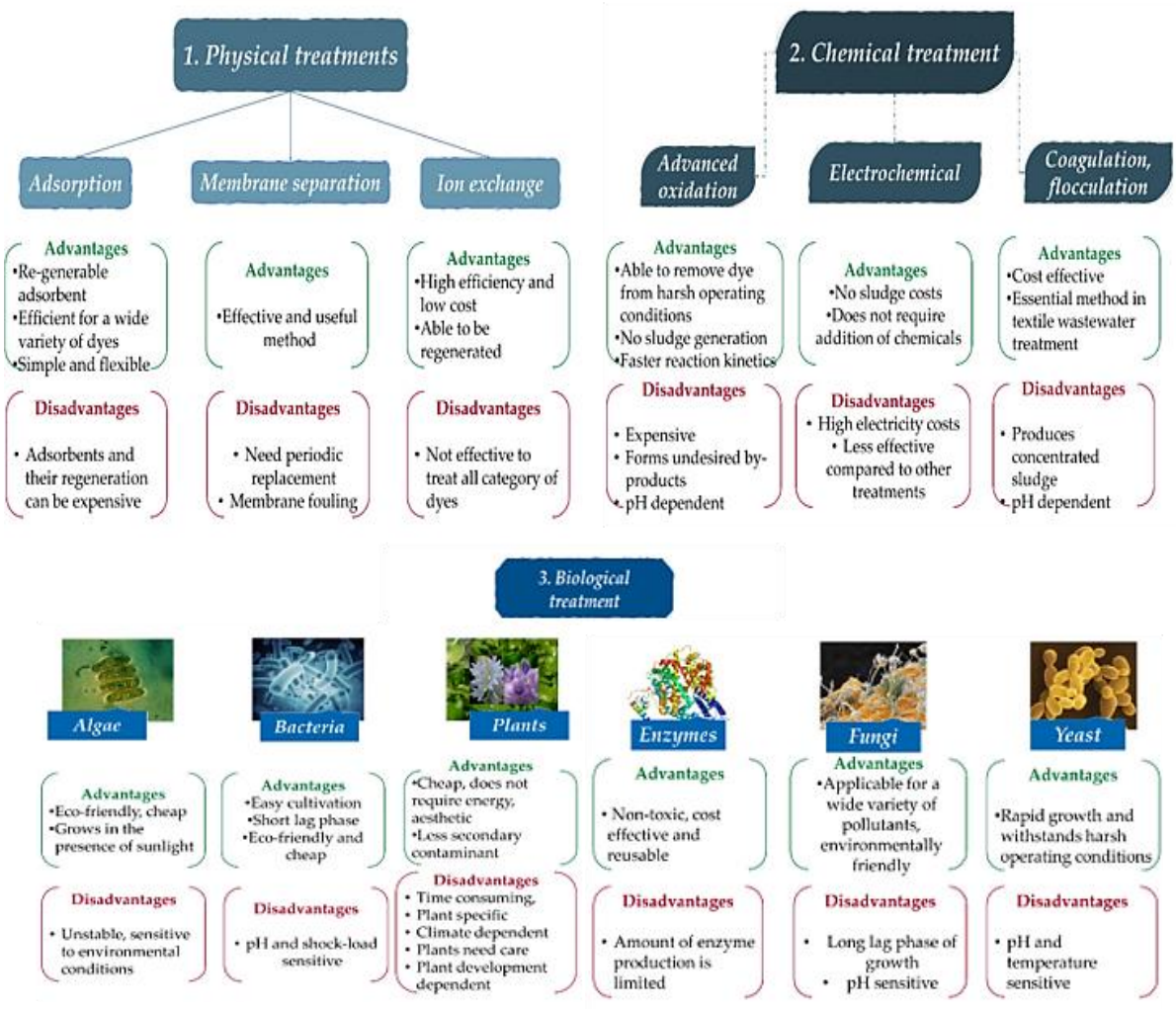

Figure II.2. Dye removal techniques (advantages/disadvantages) [14].

PART II: ADSORPTION

II.5. Introduction

First recorded in 1881, the term "adsorption" by Heinrich Kayser, a German scientist [15]. The adsorption phenomenon of attracting and retaining the molecules on the surface of a solid. The substance that adsorbs on the surface is called adsorbate, and the substance on which it adsorbs is called adsorbent [16]. Conversely, though, the adsorbed molecules' release is known as the process of desorption from the adsorbent's surface, and these contrasts with adsorption [13]. This procedure is shown in schematic form in Figure **II.3**.

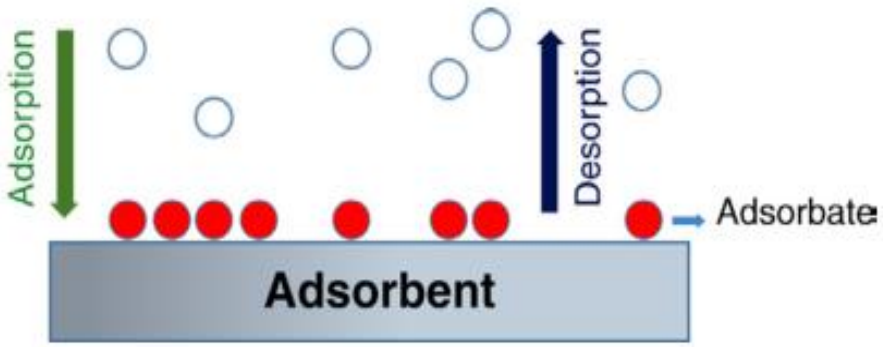

Figure II.3. Diagrammatic Illustration of Desorption and Adsorption Mechanisms [17].

II.6. Types of Adsorption

Adsorption of the molecules to the adsorbent surface can occur in two ways, which are “physical adsorption,” also called “physisorption,” and “chemical sorption,” also called “chemisorption”[17].

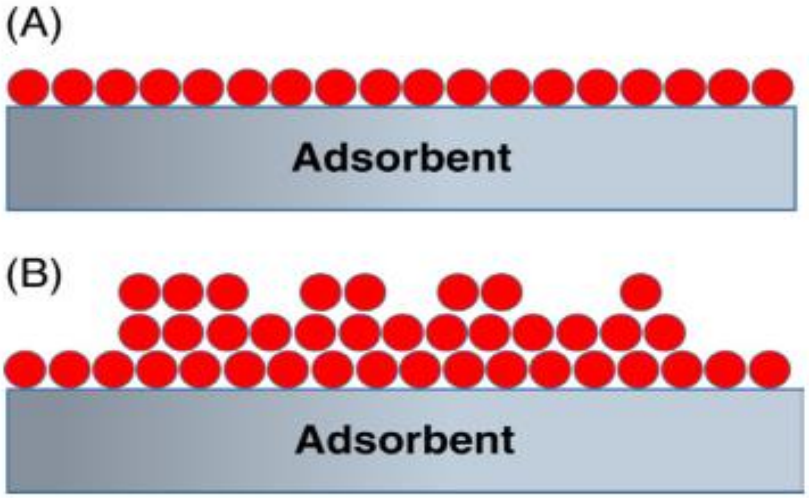

Figure II.4. (A) Monolayer and (B) multilayer adsorption [17].

The two types of adsorption can be distinguished using several criteria, as summarized in the following Table **II.3.**

Table II.3. Comparison between Physical Adsorption and Chemical Adsorption [18, 19]

Property	Physical Adsorption	Chemical Adsorption
Type of bonding	Physical forces (Van der Waals)	Chemical bonds
Operating temperature	Relatively low compared to the boiling point of the adsorbate	Very high compared to the boiling point of the adsorbate
Kinetics	Fast, independent of temperature	Very slow
Heat of adsorption	Less than 10 kcal/mol	Greater than 10 kcal/mol
Applied energy	Weak	Very high
Layer formation	Multilayer and monolayer formation	Monolayer formation only
Desorption	Easy	Difficult
Activation energy	No activation energy required	Requires activation energy
Pressure effect	Increases with pressure (directly proportional)	Not directly proportional; adsorbed amount may decrease with increasing pressure
Selectivity	Selective process	Non-selective process

II.7. Factors Affecting the Adsorption Phenomenon

The efficiency of liquid-phase adsorption, and therefore the optimal operation of the water treatment process, depends on several parameters. The sorption performance, as illustrated in Figure **II.5,** is influenced by physico-chemical factors such as the adsorbent/adsorptive interaction, the surface chemistry and pore structure of the adsorbent, particle size, nature of the adsorbent, presence of other ions in the aqueous solution, pH, temperature, pressure, and contact time. The properties of the adsorbate, its molecular weight, molecular structure, molecular size, and polarity should also be taken into account [20, 21].

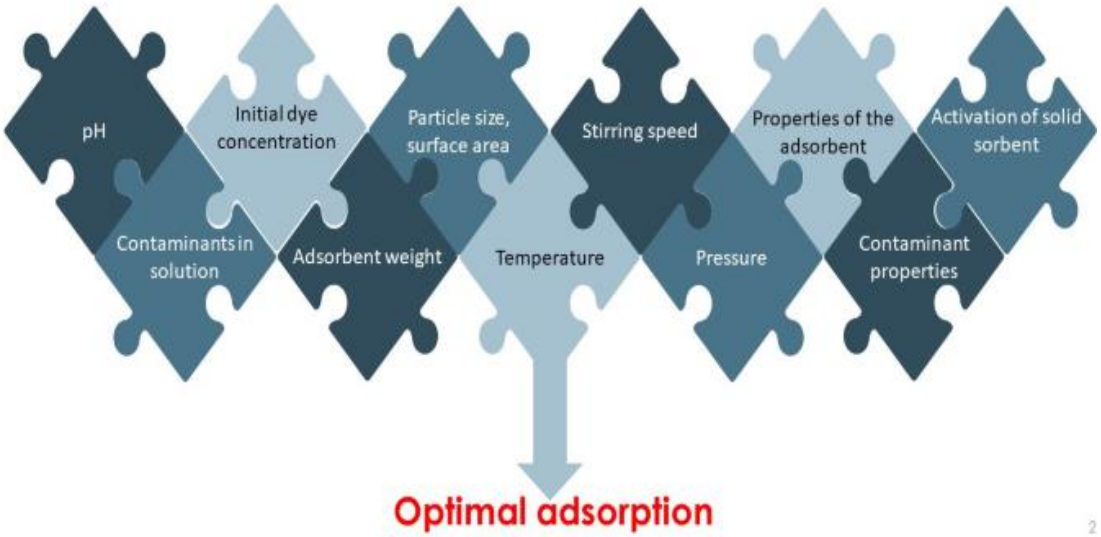

Figure II.5. Factors affecting adsorption process [22].

II.8. Equilibrium of adsorption

On solid adsorbents, liquid-phase adsorption takes place through equilibrium or dynamic processes. As was previously explained in brief, both batch and column methods can be used to carry out an adsorption procedure. The batch approach will be the main topic of this thesis [23]. In such water treatment systems, the efficiency of dye removal (E) and the maximum amount of dye bound in equilibrium q_e (mg/g) are directly related to the initial dye concentration [24]. Assuming that the ideal-dilute solution condition governs the adsorption process, q_e can be estimated using mass-balance considerations, the initial concentration of adsorbate C_0 (mg/L), equilibrium concentration of adsorbate C_e (mg/L), mass of the adsorbent W (g) and volume of solution V(L) according to Equation **(II.1)** [20]**.**

$$\mathbf{q_e = \frac{(C_0 - C_e)V}{W}} \qquad \textbf{(II.1)}$$

Within these kinds of systems for water purification, the dye's effectiveness adsorbed elimination, R (%) was established by employing Equation **(II.2)** [25]:

$$\mathbf{R(\%) = \frac{(C_0 - C_e)}{C_0} \times 100} \qquad \textbf{(II.2)}$$

II.9. Adsorption Models

II.9.1. Langmuir model

This model was proposed in 1918 based on the following assumptions:

- All active sites on the surface have identical energy.
- At low pressure, gases adsorbed onto a solid surface form a monolayer.
- The adsorbed molecules do not interact with one another.

- The adsorption process is reversible, meaning that an equilibrium exists between adsorption and desorption.
- The number of adsorption sites on the surface is limited.

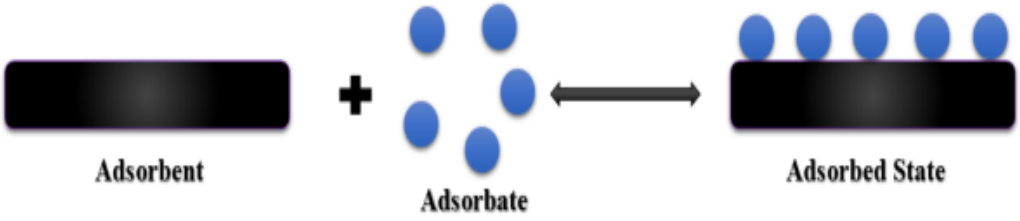

Figure II.6. Langmuir model of gas adsorption onto a solid adsorbent [17].

The Langmuir isotherm is expressed by the following equation [26]:

$$q_e = \frac{q_m k_L C_e}{1+k_L C_e} \qquad \textbf{(II.3)}$$

The model can also be expressed in its linear form by the following equation:

$$\frac{c_e}{q_e} = \frac{c_e}{q_{max}} + \frac{1}{q_{max \times K_L}}$$

In the equation above, q_{max} shows the maximum adsorption capacity (mg. g^{-1}) and K_L, represents the Langmuir constant (L. mg^{-1}).

The Langmuir constant K_L is given by the following equation:

$$K_L = \frac{q_m}{c_e(q_m - q_e)} \qquad \textbf{(II.4)}$$

This model is characterized by the equilibrium parameter R_L

$$R_L = \frac{1}{1+K_L . C_0} \qquad \textbf{(II.5)}$$

Where:

$R_L = R_0$: The adsorption is irreversible.

$0 < R_L < 1$: The adsorption process is favorable.

$R_L = 1$: The adsorption is linear.

$R_L > 1$: The adsorption process is unfavorable.

II.9.2. Freundlich model

In 1926, Freundlich developed an isotherm model that is considered one of the most accurate, having proven successful for gas adsorption, but primarily applied to adsorption from solutions. Freundlich observed that the adsorption mechanism is complex due to the heterogeneity of the surface, which results in a variation in the heat of adsorption. Because of the irregularities in the crystal structure of the adsorbent, not all adsorption sites can be considered energetically equivalent [27, 28] .

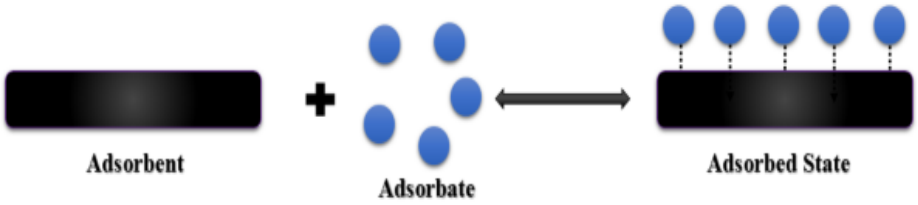

Figure II.7. The Sips and Freundlich isotherm model of gas, where surface heterogeneity is included [17].

The equation for this model is given as follows:

$$q_e = K_f \cdot c_e^{\frac{1}{n}} \qquad \textbf{(II.6)}$$

By taking the logarithm of both sides, the equation becomes:

$$ln\, q_e = ln\, K_f + \frac{1}{n}\, ln\, C_e \qquad \textbf{(II.7)}$$

Where; K_f, the Freundlich constant related to adsorption capacity (L/mg) and **n** is Adsorption intensity, generally ranging between 0 and 1.

The adsorption intensity can be interpreted based on the value of **n**:

- If **n<1**, the adsorption is considered chemical
- If **n>1**, the adsorption is considered physical

II.9.3. Temkin model

The Temkin isotherm is based on the assumption that the heat of adsorption decreases linearly with increasing surface coverage**.** The Temkin equation was originally developed to describe gas adsorption onto solid surfaces, but it has since been adapted to fit adsorption in the liquid phase as well [28]. The Temkin isotherm at equilibrium is expressed as follows:

$$q_e = \frac{R.T}{b} \ln(a\,.\,C_e) \qquad \textbf{(II.8)}$$

The Temkin model can also be represented by the linear equation[29]:

$$q_e = \frac{RT}{b} \ln k_T + \frac{RT}{b} \ln C_e \qquad \textbf{(II.9)}$$

Where, **T** is the temperature (K). **R** is the ideal gas constant (8.314 $J.mol^{-1}.K^{-1}$), **b**, represents the Temkin constant ($J.mol^{-1}$), which depends on the adsorption heat, and **a** is the equilibrium adsorption constant, which corresponds to the maximum adsorption energy ($L.mg^{-1}$).

II.10. Adsorption Kinetics

To determine the adsorption mechanism, investigating the kinetics is essential of thermodynamics and adsorption. The adsorption kinetics models of anionic dye onto various adsorbent substances, such as for this purpose, the pseudo first order was

employed, and pseudo second order models are commonly applied to the adsorption systems.

II.10.1. First-Order Pseudo-Kinetic (Lagergren Model)

The Lagergren kinetic model, also known as the pseudo-first-order (PFO), is used to describe the adsorption kinetics based on the hypothesis that the rate of change of the adsorbed amount is directly proportional to the difference between the amount of adsorption at equilibrium and the amount adsorbed at any given time[30].

This model is expressed by the following Lagergren equation:

$$\frac{dq_t}{dt} = K_1 (q_e - q_t) \qquad \textbf{(II.10)}$$

where, $\mathbf{q_e}$ (mg/g) and $\mathbf{q_t}$ (mg/g) are the uptake amounts of adsorbate at equilibrium, variable time (t) and $\mathbf{k_1}$ (min^{-1}) is the rate constant of the PFO kinetic equation

Integrating the previous equation gives the following form:

$$\ln(q_e - q_t) = \ln q_e - t\, K_1 \quad \textbf{(II.11)}$$

II.10.2. Second-Order Pseudo-Kinetic (Macka et Ho Model)

The pseudo-second-order (PSO) suggests that the adsorption process is not merely a weak physical interaction (such as van der Waals forces), but rather involves a chemical interaction between the adsorbed molecules and the surface of the adsorbent. This means there is a transfer of electrons or the formation of covalent or ionic bonds between the adsorbate (adsorbed molecules) and the adsorbent (material)[31].

$$\frac{dq_t}{dt} = K_2 (q_e - q_t)^2 \qquad \textbf{(II.12)}$$

And the integration of this equation gives

$$\frac{t}{q_t} = \frac{1}{K_2 q_e^{\,2}} + \frac{t}{q_e} \qquad \textbf{(II.13)}$$

Where, the parameter $\mathbf{k_2}$ is the adsorption rate constant (g/mg·min).

II.11. Thermodynamic Study

Thermodynamic studies are performed to investigate the temperature effect on the adsorption process. For this purpose, the following equations are used to calculate various thermodynamic parameters such as enthalpy change (ΔH°), Gibbs free energy change (ΔG°), and entropy change (ΔS°), which are the main characteristics of the adsorption process [32]. The nature of the adsorption process can be predicted by calculating these thermodynamic parameters [31].

These thermodynamic parameters highlight the influence of temperature on the adsorption process and can be determined using appropriate thermodynamic equations [33].

The Van't Hoff equation is expressed as:

$$\Delta G° = -RTLn\ K_d \qquad \textbf{(II.14)}$$

$$K_d = \frac{q_e}{C_e} \qquad \textbf{(II.15)}$$

$$\mathbf{LnK_d} = \frac{\mathbf{\Delta S°}}{\mathbf{R}} - \frac{\mathbf{\Delta H°}}{\mathbf{RT}} \qquad \textbf{(II.16)}$$

The ΔG° value indicates whether the adsorption process is spontaneous or not. If the ΔG° value is negative, the adsorption takes place spontaneously. On the other hand, ΔH° gives information about whether the adsorption process is endothermic or exothermic. The adsorption process is endothermic when exothermic (ΔH° < 0) or endothermic (ΔH° > 0) [34].

PART III: CHITOSAN

II.12. Introduction

Before delving into polymer chemistry, it is essential to look back at the historical milestones that have contributed to the development of this field. Since ancient times, humans have relied on natural polymers such as cellulose, starch, cotton, and natural rubber extracted from trees, as well as bioproteins like keratin, collagen, and others [35]. These materials are highly effective, biocompatible, and biodegradable [36]. Among these polymers, chitosan derived from chitin is considered one of the most widespread natural biopolymers on Earth. It is found in the exoskeletons of crustaceans, mollusk cartilage, insect shells, and the cell walls of microorganisms [37].

Chitosan is a promising material due to its exceptional physical properties, which include a unique molecular structure, biocompatibility, biodegradability, non-toxicity, and low cost. These diverse characteristics allow it to be used in a wide range of applications, including cosmetics, medical fields, membrane fabrication, and the food industry. Moreover, chitosan exhibits a high adsorption capacity, making it particularly valuable in water treatment and pollutant removal [38].

II.13. Historical Overview

Chitin was first discovered by the English scientist Hachett, who in 1797 reported on a substance resistant to chemical agents. However, due to the lack of follow-up on his findings, the discovery of chitin was later attributed to the French professor Henri Braconnot. In 1811, Braconnot managed to isolate a fibrous substance from a specific type of fungus. He observed that this material was insoluble in acidic aqueous solutions, which sparked interest among researchers.

In 1823, further studies revealed the presence of the same substance in certain insects. It was named *chitin*, a term derived from the Greek word *Kitos*, meaning "tunic" or "cover," in reference to its role in forming the exoskeletons of living organisms.

As for chitosan, it was first obtained from chitin by treating it with a strong alkaline solution, which resulted in a compound that is insoluble in organic acids [39]. Research and studies on chitosan continued, leading to the discovery of its unique properties and an expansion in its range of applications. A major breakthrough in the use of chitosan is credited to the Japanese professor Yoshio Ichimura in 1974. He developed an innovative preparation method that enabled the production of pure chitosan with specific and well-defined properties.

Since then, ongoing research and development efforts in this field have documented a wide range of physical and chemical properties of chitosan, as well as explored its diverse applications in medicine, industry, environmental science, and biotechnology [40].

II.14. Source and Production

Chitosan is extracted from chitin, which is typically obtained from natural sources such as shrimp, crab, and lobster shells, as well as fungi and green algae. This biopolymer can also be found in the exoskeletons of insects and fungal cell walls, as shown in Figure **II.8**, and Table **II.4.** [41] . Chitin content can vary with the proportion of minerals, proteins, and carotenoids, depending on the species, reproductive cycle phase, nutritional status, age, and also the peeling conditions during the processing [42].

Given the high economic value of these resources and based on scientific research findings, scientists and researchers have developed innovative techniques to convert this waste into valuable products across various fields. This not only promotes sustainability but also mitigates the negative environmental impact of such waste [43]

.

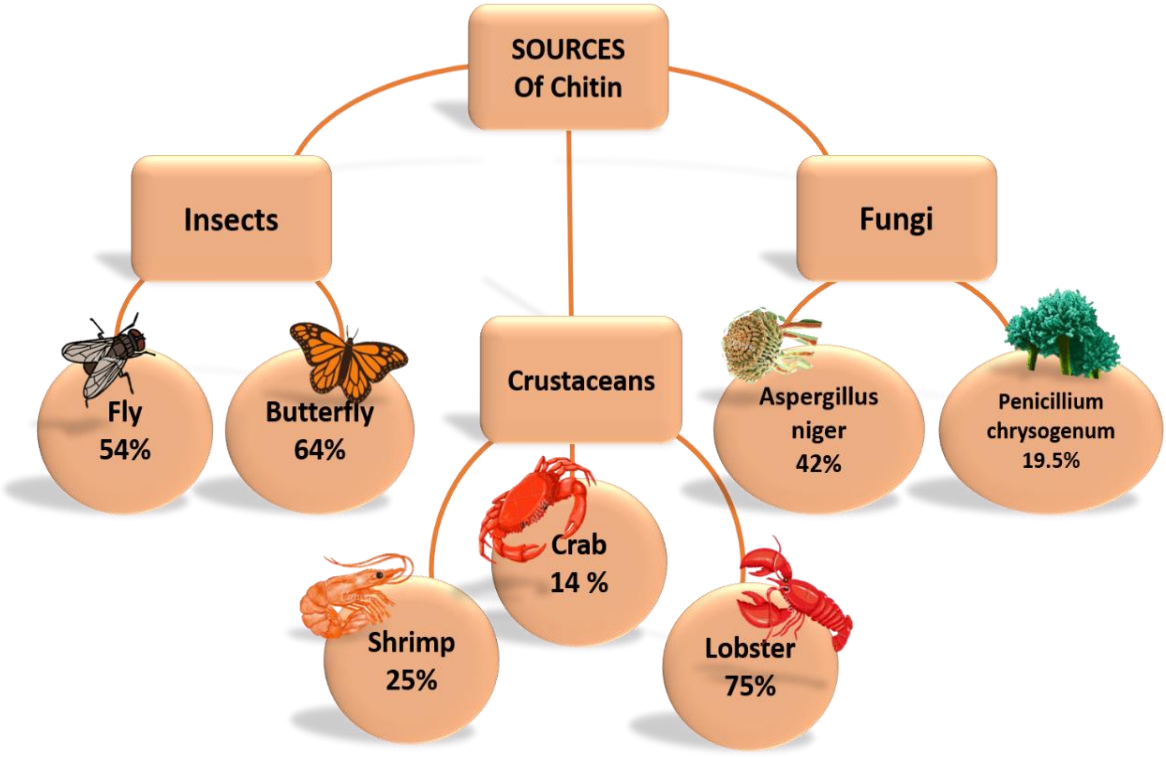

Figure II.8. Examples of chitin content from different sources [42]

Table II.4. Percentage of Chitin Found in Some of Its Main Sources [45 ,44]

Source	Chitin Content (%)
Crab	20 – 40
Lobster	20 – 40
Shrimp	20 – 40
Cockroaches	30 – 42
Flies	45
Algae	4.5
Yeasts	0.45
Filamentous Fungi	10 – 40
Squid	6 – 40
Octopus	6– 40

II.15. Methods for Extracting Chitin and Chitosan

Chitosan can be obtained by deacetylation of chitin through enzymatic or alkaline methods Figure **II.9**. However, the enzymatic method has been limited only to the laboratory scale, while the alkaline method has been more widely used on an industrial scale, due to its short processing time, simplicity, and low operational costs.

The chemical method is widely used in industry due to its simplicity and effectiveness in processing time. It involves several steps, beginning with demineralization of chitin using acids such as HCl or H_2SO_4 to remove calcium carbonate and calcium phosphate [46]. This is followed by deproteinization using alkaline solutions such as NaOH or KOH . Subsequently, organic pigments are removed using solvents like acetone or hydrogen peroxide (H_2O_2) [47]. In the final stage, deacetylation is carried out using concentrated alkaline solutions, typically NaOH, to convert chitin into chitosan, thereby enhancing its biodegradability [48].

On the other hand, the enzymatic method is considered more environmentally sustainable, as it relies on the use of microorganisms, such as bacteria, which secrete organic acids and proteolytic enzymes to remove both mineral and organic impurities from chitin. In this approach, lactic acid secreted by bacteria is used for the removal of minerals like calcium carbonate, while proteases break down proteins.

Additionally, the enzyme chitin deacetylase is employed to convert chitin into chitosan through deacetylation. Despite its environmental advantages, the enzymatic method remains limited in industrial applications due to challenges related to efficiency and cost [41, 49]

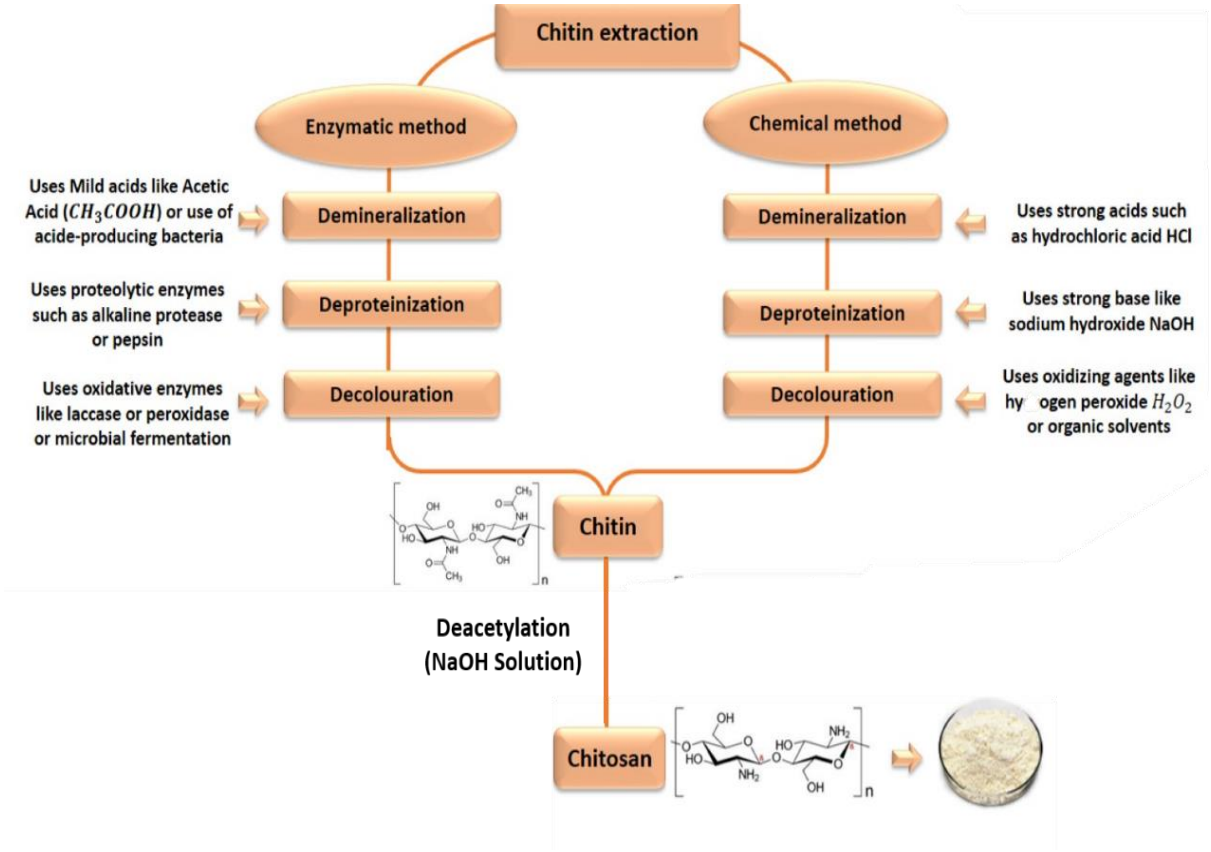

Figure II.9. Main Steps in the Extraction of Chitin and Chitosan

II.16. Physicochemical properties

The physicochemical properties of chitin and chitosan are depending by molecular chain orientation and packing. Their abundant hydroxyl and amino groups form hydrogen bonds, creating rigid crystalline structures [50].

In acidic conditions, chitosan's amino groups protonate, enhancing solubility and enabling electrostatic attraction of anionic compounds like dyes and halogens. The free -NH_2 and -OH groups also adsorb pollutants such as phenols, antibiotics, and pesticides. Adsorption capacity depends on crystallinity, water affinity, and deacetylation degree [51].

The main properties of chitosan are summarized in Table **II.5.** Include its polycationic nature, hydrogen bonding ability, and electrostatic interactions, making it an effective adsorbent. Factors like deacetylation degree (DD) [50], crystallinity [52], molecular weight (MW) [53], solubility [51], surface area[54], and particle size determine its adsorption potential. Optimizing these properties is crucial for developing efficient adsorbent materials.

Table II.5. Main chitosan properties, according to the information reported in [55].

Physicochemical properties	• Linear aminopolysaccharide with a high nitrogen content • Ionic conductive • Cationic biopolymer with high charge density • Flocculating agent • Complexing and chelating properties • Existence of reactive groups for chemical activation and cross-linking • Adsorption properties • pKa varies from 6.5 and 6.7 • Enable to form intermolecular hydrogen bonds
Biological properties	• Bioadhesivity • Non- toxic • Bioactivity • Adsorbable • Biodegradable • Antimicrobial activity • Blood anticoagulants • Antiacid, antiulcer and antitumoral • properties hypolipidermic activity

II.17. Advantages and Disadvantages of Chitosan

II.17.1. Advantages of Chitosan

- Insoluble in water, alkaline solutions, and organic solvents; biologically active and biocompatible [56].
- High adsorption capacity for reactive dyes and heavy metals [38].
- Biodegradable.
- High molecular weight.
- Non-homogeneous.
- Non-toxic.
- Cationic in nature.
- Linear polymer structure.

II.17.2. Disadvantages of Chitosan:

- Soluble in acidic solutions [56].
- Low thermal resistance.
- Low surface area.

- Low permeability and diffusivity.
- Low mechanical strength [57].

II.18. Chitosan Supports

Raw chitosan is generally unsuitable for use in many applications due to a set of limitations, such as poor mechanical properties, low stability in acidic media, limited solubility in acidic solutions, restricted porosity, low thermal resistance, and a small specific surface area [58]. To overcome these limitations, structural modification of chitosan is considered an effective approach to enhance its functional properties. Modified chitosan exhibits greater effectiveness compared to other polysaccharides, owing to the presence of reactive functional groups such as amino and hydroxyl groups, which allow for various modifications [59].

Among these, physical and chemical modifications are the most common and effective methods for improving chitosan's performance and adapting it to the requirements of various applications.

The physical modification approach involves direct incorporation of inorganic materials or nanoparticles, such as titanium dioxide (TiO_2) [60], zinc oxide (ZnO) nanoparticles [61], zeolites [62], and clay minerals [63].

On the other hand, chemical modification of chitosan involves forming chemical bonds with specific functional groups within the general structure of chitosan using organic cross-linking agents such as glyoxal, epichlorohydrin, tripolyphosphate, benzil, and polyaspartic acid sodium salt, via cross-linking reactions to form Schiff bases [64]. In this context, cross-linking reactions are considered among the most promising strategies for modifying chitosan, as they effectively enhance its properties by improving chemical stability in acidic environments, reducing its swelling and hydrophilicity in aqueous solutions, and increasing its mechanical resistance [65].

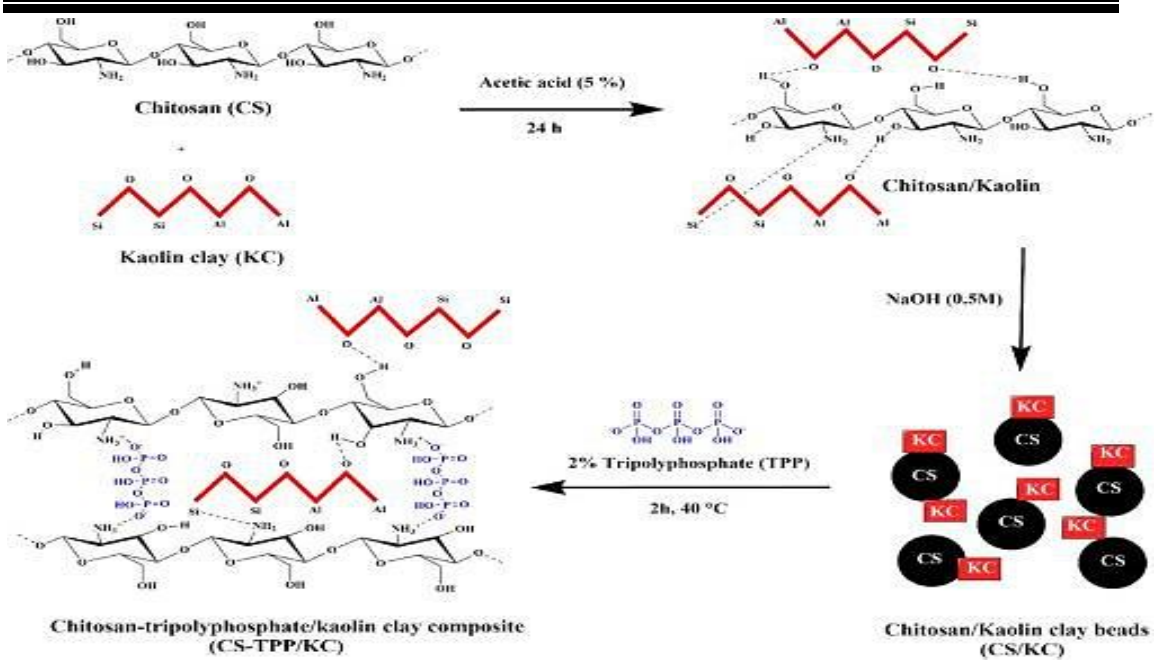

Figure II.10. Reaction Mechanism of Chitosan-Tripolyphosphate/Kaolin Clay Composite (CS-TPP/KC) [63].

II.19. Applications of Chitosan

In recent years, both chitin and chitosan have attracted considerable attention across a wide range of fields due to their excellent properties and biocompatibility. enabling broad applications in biomedicine [66], environmental remediation [67], food science [68], agriculture [69], and industry due to their biocompatibility [70], adsorption capacity[63], and functional adaptability, as summarized in Figure **II.11.**

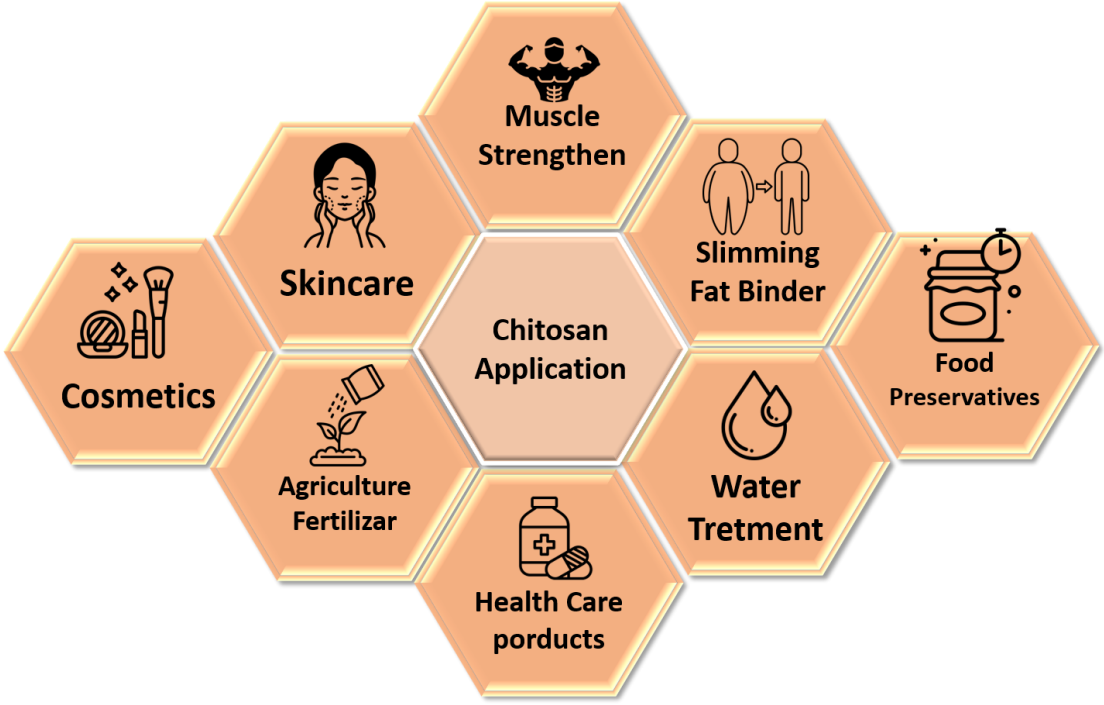

Figure II.11. Main Applications of Chitin and Chitosan [63].

PART IV: Optimization Methods

II.20. Introduction

Tools such as experimental design and optimization processes are used for the systematic investigation of potential problem areas. Therefore, it is evident that if experiments are conducted randomly, the results will also be random [71]. As a result, experiments must be organized to ensure the collection of valuable data [72].

In the following section, the methods of designing and optimizing experiments will be clarified to provide the researcher with the theoretical framework and practical tools suitable for the experimental work environment.

II.21. Experimental design

Experimental design is defined as a set of systematic steps for collecting and statistically analyzing data in order to reach generalizable conclusions. This methodology enables the optimal use of available resources to develop appropriate experimental designs based on accurate scientific principles, thus contributing to the reduction of experimental error.

The objective of modern experimental design lies in estimating and minimizing this error, in addition to performing the necessary tests and evaluations within the framework of scientific research. Given the novelty of this field and the presence of many unfamiliar terms, we have deemed it necessary to provide an explanation for them to maximize the benefit:

A. **Design:** The term "design" refers to the methodological framework or research plan that defines how a specific experiment will be conducted. This includes determining the objectives of the experiment, the experimental conditions, and the parameters to be controlled, with the aim of collecting analyzable data that can lead to scientifically meaningful conclusions.

B. **Unit of Sampling:** The unit of sampling is defined as the entity on which measurements are taken during the experiment. This unit may differ from the "experimental unit," which is the entity to which treatments are applied. Therefore, it is essential to distinguish between these two concepts during experimental planning.

C. **Analysis:** Analysis refers to the process of organizing, summarizing, and applying appropriate statistical tools to the data collected from the experiment in order to test hypotheses and draw conclusions that support the research objectives.

D. **Experiment:** An experiment is a structured scientific procedure used to test a specific hypothesis by examining the relationship between certain variables under controlled conditions. It serves as a fundamental tool for generating quantitative data from which reproducible scientific conclusions can be drawn.

E. **Treatments:** Treatments refer to the specific conditions or settings applied to the experimental units during the experiment. These treatments are designed to produce particular effects on the response variable and are usually applied in a randomized and controlled manner to ensure reliability.

F. **Factor or Variable Levels:** In the context of experimental design, factors or variables are expressed through levels that represent the range of their values. Typically, two main levels are defined, denoted as (-1) and (+1), to represent the lower and upper bounds, respectively. This helps in studying the impact of these factors on the response variable.

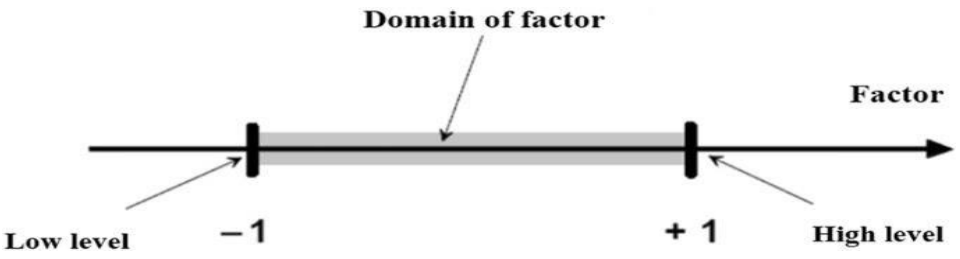

Figure II.12. Experimental Space [73]

II.22. Response Surface Methodology (RSM)

Response Surface Methodology (RSM) is a collection of statistical and mathematical techniques developed in the 1950s with the aim of determining optimal operating conditions in chemical industry applications [74]. It represents a specialized type of experimental design commonly used for modeling and optimizing complex systems, and it has broad applications in the design, development, and formulation of new products. This methodology is employed when the goal is to understand the relationship between several independent variables and a specific response variable (usually a quality or performance indicator) in a systematic and efficient way [75]. RSM seeks to analyze these relationships and identify the optimal values of the influential variables in order to improve the desired response.

II.22.1. Principle of RSM

RSM is based on designing a set of experiments in which the values of the variables are systematically and methodically varied, with the response measured in each experiment [76]. Once data are collected, they are analysed using a range of statistical methods, such as linear regression and stochastic regression. These analyses are used to estimate the relationship between the variables and the response, and to derive the optimal values that achieve the intended objective of the experiment [77].

II.22.2. Stages of Modelling Using the RSM

a. Experimental Planning for RSM

To ensure effective experimental planning, it is important to minimize the number of experiments as much as possible. This helps reduce computational processing requirements, as well as the time and costs associated with execution. Consequently, this leads to a reduction in the variance of the coefficients in the mathematical model used, thereby improving the accuracy of the resulting response surfaces. To achieve this, the optimal experimental design that meets the intended objectives must be selected. Among the quadratic designs commonly used in RSM studies are the *Central Composite Design (CCD)* and the *Box–Behnken Design (BBD)* [77].

b. RSM Modeling

When applying RSM, the goal is to establish a relationship between the continuous response to be optimized **(Y)** and a set of influencing factors **(K)**, using a linear regression model, which can be expressed as follows:

$$Y = f_B(X_1, X_2, \cdots X_K) \qquad \textbf{(II.17)}$$

Although the exact form of the response function is not known in advance, it can be effectively approximated using a polynomial model. In the case of two factors, for example, the linear regression model can be expressed as follows [78]:

$$\mathbf{Y = \sum_{i=1}^{k} \beta_i \chi_i + \sum_{i=1}^{k} \sum_{j=1}^{k} \beta_{ij} \chi_i \chi_j + \sum_{i=1}^{k} \beta_{ii} \chi_i^2 + \beta_0 + \varepsilon} \qquad \textbf{(II.18)}$$

Where:

The indices *i* and *j* are used to represent the number of variables.

$\boldsymbol{\beta_0}$: Constant coefficient.

$\boldsymbol{\beta_{ii}\beta_i}$: The linear and quadratic coefficients represent, respectively.

$\boldsymbol{\varepsilon}$:Random error.

$\boldsymbol{X_i X_j}$: The two values correspond to the response and the coded values of the independent factors (-1, 1, 0).

The quantity of testing was computed in the manner described below:

$$N = k + c_p + k^2 \quad \text{(II.19)}$$

In this case, c_p represents the central point's replicate number [79].

c. Analysis of Variance (ANOVA)

Analysis of Variance, abbreviated as ANOVA, is an important statistical tool often used in the context of regression analysis. It divides the total variance in the data into:

- A component due to the studied factors, which reflects the impact of the independent variables within the model,
- A residual component that represents the random variance or error.

These components are mathematically expressed using Mean Squares, which are calculated by dividing the sum of squares by their corresponding degrees of freedom.

The significance of ANOVA lies in its ability to conduct precise tests to determine whether the studied factors have a real effect on the response. Therefore, it is a critical tool for evaluating the suitability of the statistical model used [80].

The response surface is geometrically represented as follows:

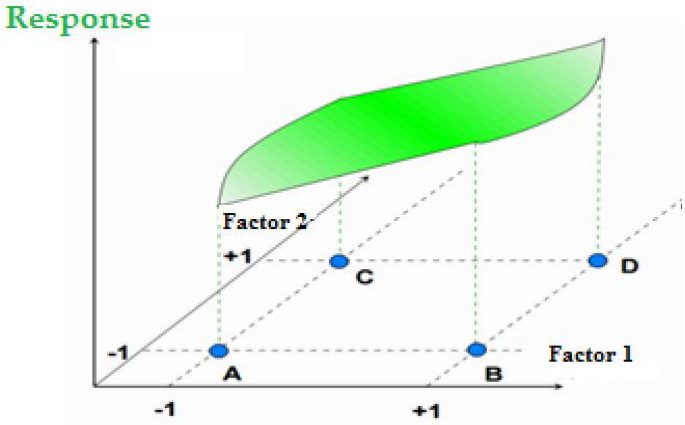

Figure II.13. Response Surface model plot [81]

II.22.3. Types of Designs

Response Surface Methodology (RSM) relies on a set of well-studied experimental designs to efficiently and effectively investigate the relationships between independent variables and the response variable. The appropriate type of experimental design is determined based on several factors, most notably the number of independent variables, the expected shape of the response surface, and the available research capabilities [82]. Each category of designs has specific characteristics, making it essential to choose the optimal design that aligns with the study objectives and the nature of the system under investigation to ensure the reliability and accuracy of the results [76]. Among the most commonly used designs in RSM studies are:

a. Central Composite Design (CCD)

The Central Composite Design (CCD) is one of the most prominent and widely used experimental designs within Response Surface Methodology (RSM). It is among the most common second-order designs for estimating quadratic response surfaces. First developed by Box and Wilson in 1951, it has since received considerable attention and study from many researchers due to its flexibility and effectiveness in constructing second-order response surface models [83].

This design combines factorial points, axial (or star) points, and center points to create a suitable layout for fitting second-order response surface models. It enables the estimation of both linear and quadratic effects of the variables, in addition to evaluating the curvature of the response surface [84].

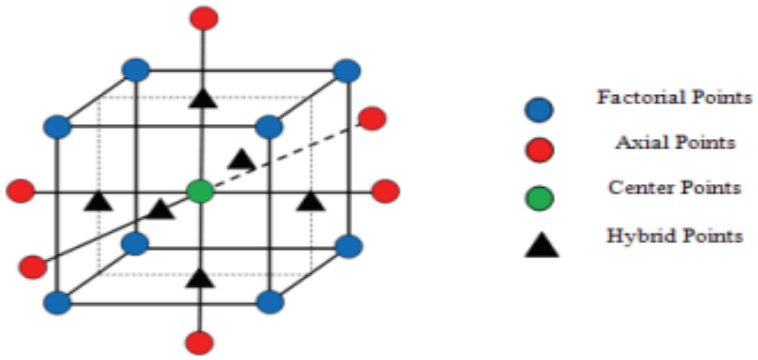

Figure II.14. CCD augmented with hybrid points [85].

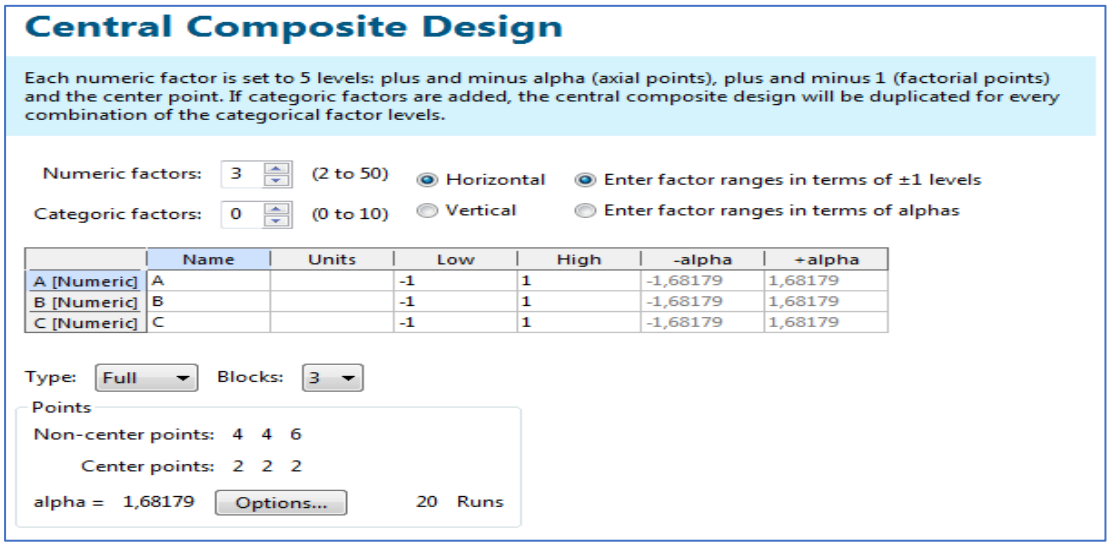

Figure II.15. CCD Design Generated by (Design-Expert 13)

b. Box-Behnken Design (BBD)

Box-Behnken Design (BBD) developed a standard model for handling multiple responses. This model provides each variable with three possible values (+1, 0, -1)

spaced at equal intervals. It aims to reduce the number of experiments while still allowing the approximation of linear and quadratic effects [86].

This model includes a set of points within a hypercube, excluding the center. As such, it is symmetrical and rotatable. Furthermore, it does not include any points at the cube's corners or at the upper and lower limits of each variable [79].

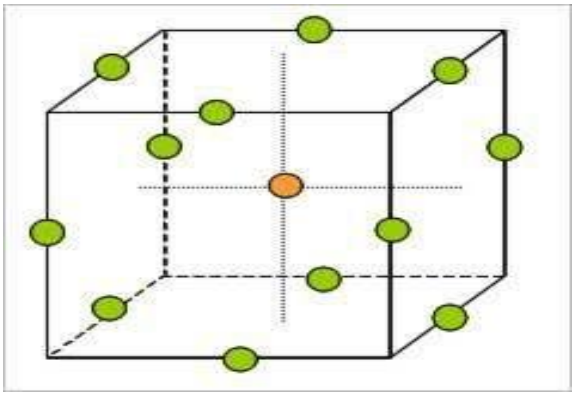

Figure II.16. Geometric Representation of the BBD

It is an alternative design used to optimize analytical methods and represents a common model for handling multiple responses using the desirability function (D), proposed by Dringroswick in 1980. This function, along with the response surface data, is used to determine the optimal conditions. From there, the exact values of each variable at optimal settings can be identified, as well as the maximum or minimum value of the response, depending on the desired outcome. Additionally, the design can be based on a mathematical model of the studied phenomenon.

This model is particularly valuable and practical, especially in general chemistry and in optimizing chromatographic separation conditions. One of the key advantages of this design is its ability to cover a large experimental space using a limited number of experimental points (fewer experiments) compared to the Full Factorial Design, which is due to its exclusion of corner and center points. While the outer faces of the cube resemble the structure of the CCD, it differs in other characteristics and does not include extended intersection points. For this reason, three levels per factor are used. This design provides researchers with a better understanding of the disturbances or effects, which contributes to constructing a more accurate model [74].

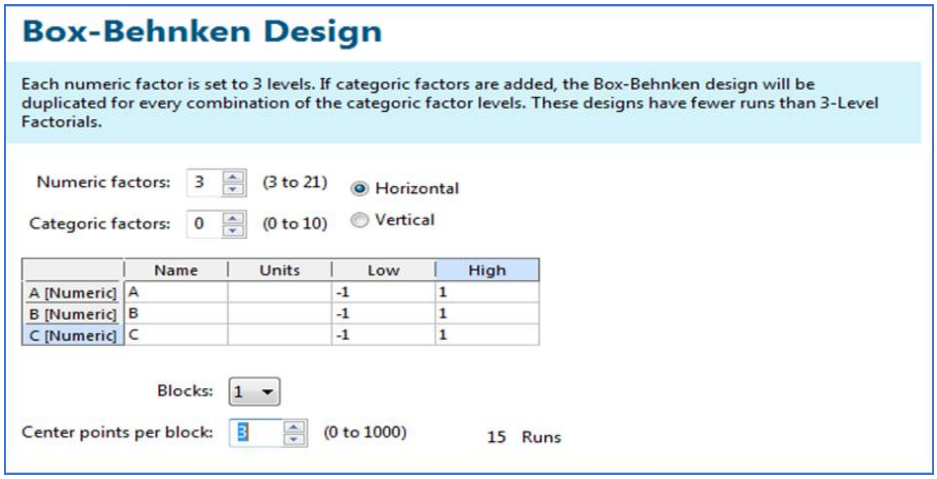

Figure II.17. BBD for Three Variables by (Design-Expert 13) [87]

c. BBD vs. CCD: A Comparison for Process Optimization

BBD and CCD respectively in RSM are employed to optimize processes also understand factor-response relationships. Here's a comparison [88, 89]:

- ***Number of Experimental Runs***: BBD needs fewer runs and is cost-effective with limited resources. CCD demands more runs, potentially resource-intensive.
- ***Design Space Coverage***: BBD efficiently explores but lacks the centre point. CCD assesses comprehensively, including centre and pivot points.
- ***Levels of Factors***: BBD uses three levels (±1, 0) for simpler models. CCD accommodates more levels, aiding detailed factor analysis.
- ***Point Arrangement***: BBD simplifies with a hypercube arrangement. CCD includes axial and centre points for interactions.
- ***Resource Efficiency***: BBD conserves resources, ideal for budget constraints. CCD is resource-intensive, offering in-depth understanding.
- **Model Complexity**: BBD suits simpler models (linear, quadratic). CCD handles complexity, capturing higher-order interactions.
- ***Application Areas***: BBD is common in chemistry, moderate factor studies. CCD spans various fields and diverse designs.

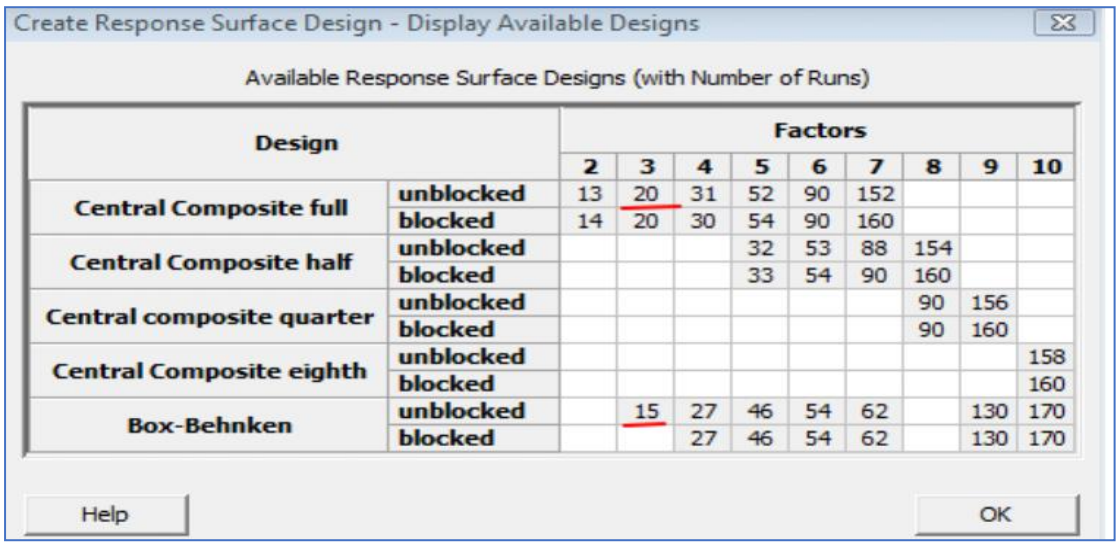

Design		Factors								
		2	3	4	5	6	7	8	9	10
Central Composite full	unblocked	13	20	31	52	90	152			
	blocked	14	20	30	54	90	160			
Central Composite half	unblocked				32	53	88	154		
	blocked				33	54	90	160		
Central composite quarter	unblocked							90	156	
	blocked							90	160	
Central Composite eighth	unblocked									158
	blocked									160
Box-Behnken	unblocked		15	27	46	54	62		130	170
	blocked			27	46	54	62		130	170

Figure II.18. BBD vs. CCD for three variables by (Design-Expert 13).

The BBD is a popular experimental design used in RSM for optimizing processes and studying the relationships between factors and responses. **This is the model adopted in this study.**

References

[1] H. Zollinger, "Some Thoughts on Innovative Impulses in Dyeing Research and Development," Textile Chemist & Colorist, vol. 23, 1991.

[2] A. Welham, "The theory of dyeing(and the secret of life)," Journal of the Society of Dyers and Colourists, vol. 116, pp. 140-3, 2000.

[3] V. K. Gupta, "Application of low-cost adsorbents for dye removal–a review," Journal of environmental management, vol. 90, pp. 2313-2342, 2009.

[4] A. T. Tasew, "Physicochemical characterization and activation of local bentonite to adsorb dye and chemical oxygen demand from the effluent of a textile factory," Addis Ababa Science and Technology University: Addis Ababa, Ethiopia, 2020.

[5] S. P. Gupta and M. S. J. Beg, "Structure and Properties of Dyes and Pigments," Dyes and Pigments: Novel Applications and Waste Treatment, p. 131, 2021.

[6] S. Attouti, "Activation de deux algues méditerranéennes par diverses méthodes pour l'élimination de colorants," Thèse doctorat université de Mostaganem, 2013.

[7] A. Gürses, M. Açıkyıldız, K. Güneş, M. S. Gürses, A. Gürses, M. Açıkyıldız, et al., "Classification of dye and pigments," Dyes and pigments, pp. 31-45, 2016.

[8] K. B. Tan, M. Vakili, B. A. Horri, P. E. Poh, A. Z. Abdullah, and B. Salamatinia, "Adsorption of dyes by nanomaterials: recent developments and adsorption mechanisms," Separation and purification technology, vol. 150, pp. 229-242, 2015.

[9] S. A. Dawood, "Development and characterization of biomass based novel adsorbent in the removal of Congo red dye by adsorption," Citeseer, 2013.

[10] M. Crepy, "Dermatoses professionnelles aux colorants," Documents pour le médecin du travail, pp. 565-576, 2004.

[11] J. A. Kiernan, "Classification and naming of dyes, stains and fluorochromes," Biotechnic & histochemistry, vol. 76, pp. 261-278, 2001.

[12] V. Katheresan, J. Kansedo, and S. Y. Lau, "Efficiency of various recent wastewater dye removal methods: A review," Journal of environmental chemical engineering, vol. 6, pp. 4676-4697, 2018.

[13] S. Madhav, A. Ahamad, P. Singh, and P. K. Mishra, "A review of textile industry: Wet processing, environmental impacts, and effluent treatment methods," Environmental Quality Management, vol. 27, pp. 31-41, 2018.

[14] S. Samsami, M. Mohamadizaniani, M.-H. Sarrafzadeh, E. R. Rene, and M. Firoozbahr, "Recent advances in the treatment of dye-containing wastewater from textile industries: Overview and perspectives," Process safety and environmental protection, vol. 143, pp. 138-163, 2020.

[15] G. Gaur and S. Sharma, "Study of Biosorbents for Removal of Dyes and Metals," Asian Journal of Chemistry, vol. 29, 2017.

[16] R. Treybal, "Drying," Mass Transfer Operations. 3rd ed. McGraw-Hill Book Co., Singapore, Singapore, pp. 655-716, 1981.

[17] R. Kecili and C. M. Hussain, "Mechanism of adsorption on nanomaterials," in Nanomaterials in chromatography, ed: Elsevier, 2018, pp. 89-115.

[18] N. Ouslimani née Terfaia, "Adsorption des colorants acides des effluents manufacturiers par des montmorillonites," Université de Boumerdès-M'hamed Bougara, 2012.

[19] T. Ryabukhova, A. Arzamastseva, N. Okisheva, and S. Konovalova, "Adsorption of alcohols from binary solutions on activated carbons," RUSSIAN JOURNAL OF PHYSICAL CHEMISTRY C/C OF ZHURNAL FIZICHESKOI KHIMII, vol. 74, pp. 281-283, 2000.

[20] M. T. Yagub, T. K. Sen, S. Afroze, and H. M. Ang, "Dye and its removal from aqueous solution by adsorption: a review," Advances in colloid and interface science, vol. 209, pp. 172-184, 2014.

[21] M. A. M. Razi, M. N. A. M. Hishammudin, and R. Hamdan, "Factor affecting textile dye removal using adsorbent from activated carbon: A review," in MATEC Web of Conferences, 2017, p. 06015.

[22] E. Rápó and S. Tonk, "Factors affecting synthetic dye adsorption; desorption studies: a review of results from the last five years (2017–2021)," Molecules, vol. 26, p. 5419, 2021.

[23] Y. Zhang, "Reduction of the water footprint in the textile dyeing process," Universitat Politècnica de Catalunya, 2022.

[24] P. Terangpi and S. Chakraborty, "Adsorption kinetics and equilibrium studies for removal of acid azo dyes by aniline formaldehyde condensate," Applied Water Science, vol. 7, pp. 3661-3671, 2017.

[25] R. D. Noble and P. A. Terry, Principles of chemical separations with environmental applications: Cambridge University Press, 2004.

[26] P. S. Ghosal and A. K. Gupta, "Determination of thermodynamic parameters from Langmuir isotherm constant-revisited," Journal of Molecular Liquids, vol. 225, pp. 137-146, 2017.

[27] G. D. Halsey, "The role of surface heterogeneity in adsorption," in Advances in catalysis. vol. 4, ed: Elsevier, 1952, pp. 259-269.

[28] A. Khoualdi and A. A. Medjani, "Adsorption du bleu de méthylène par le charbon actif et l'argile," 2016.

[29] I. D. Mall, V. C. Srivastava, N. K. Agarwal, and I. M. Mishra, "Removal of congo red from aqueous solution by bagasse fly ash and activated carbon: kinetic study and equilibrium isotherm analyses," Chemosphere, vol. 61, pp. 492-501, 2005.

[30] I. BELBACHIR, "Modification de la Bentonite de Maghnia et application dans l'adsorption de colorants textiles et de métaux lourds," Université de Tlemcen-Abou Bekr Belkaid, 2018.

[31] R. Chakraborty, A. Asthana, A. K. Singh, B. Jain, and A. B. H. Susan, "Adsorption of heavy metal ions by various low-cost adsorbents: a review,"

International Journal of Environmental Analytical Chemistry, vol. 102, pp. 342-379, 2022.

[32] N. Mohammadi, H. Khani, V. K. Gupta, E. Amereh, and S. Agarwal, "Adsorption process of methyl orange dye onto mesoporous carbon material–kinetic and thermodynamic studies," Journal of colloid and interface science, vol. 362, pp. 457-462, 2011.

[33] K. L. Kapoor, A textbook of physical chemistry vol. 3: Macmillan, 2001.

[34] R. Bushra, A. Ahmed, and M. Shahadat, "Mechanism of adsorption on nanomaterials," 2016.

[35] R. O. Ebewele, Polymer science and technology: CRC press, 2000.

[36] A. BOUCHETA, "Absorption de composés organiques par la houille et la bentonite," 2017.

[37] G. Crini, "Historical review on chitin and chitosan biopolymers," Environmental Chemistry Letters, vol. 17, pp. 1623-1643, 2019.

[38] G. Z. Kyzas and D. N. Bikiaris, "Recent modifications of chitosan for adsorption applications: a critical and systematic review," Marine drugs, vol. 13, pp. 312-337, 2015.

[39] N. Morin-Crini, E. Lichtfouse, G. Torri, and G. Crini, "Fundamentals and applications of chitosan," Sustainable agriculture reviews 35: chitin and chitosan: history, fundamentals and innovations, pp. 49-123, 2019.

[40] M. Berrada, Chitin and Chitosan: Physicochemical Properties and Industrial Applications: BoD–Books on Demand, 2021.

[41] D. C. da Silva Alves, B. Healy, L. A. d. A. Pinto, T. R. S. A. Cadaval Jr, and C. B. Breslin, "Recent developments in chitosan-based adsorbents for the removal of pollutants from aqueous environments," Molecules, vol. 26, p. 594, 2021.

[42] S. Subramanian, "International Journal of Biology and Nanobiomaterials."

[43] K. Divya and M. Jisha, "Chitosan nanoparticles preparation and applications," Environmental chemistry letters, vol. 16, pp. 101-112, 2018.

[44] S. M. Joseph, S. Krishnamoorthy, R. Paranthaman, J. Moses, and C. Anandharamakrishnan, "A review on source-specific chemistry, functionality, and applications of chitin and chitosan," Carbohydrate Polymer Technologies and Applications, vol. 2, p. 100036, 2021.

[45] B. T. Iber, N. A. Kasan, D. Torsabo, and J. W. Omuwa, "A review of various sources of chitin and chitosan in nature," Journal of Renewable Materials, vol. 10, p. 1097, 2022.

[46] M. Seenuvasan, G. Sarojini, and M. Dineshkumar, "Recovery of chitosan from natural biotic waste," in Current developments in biotechnology and bioengineering, ed: Elsevier, 2020, pp. 115-133.

[47] A. J. da Silva Lucas, E. Q. Oreste, H. L. G. Costa, H. M. López, C. D. M. Saad, and C. Prentice, "Extraction, physicochemical characterization, and morphological properties of chitin and chitosan from cuticles of edible insects," Food Chemistry, vol. 343, p. 128550, 2021.

[48] F. Nessa, S. M. Masum, M. Asaduzzaman, S. Roy, M. Hossain, and M. Jahan, "A process for the preparation of chitin and chitosan from prawn shell waste,"

Bangladesh Journal of Scientific and Industrial Research, vol. 45, pp. 323-330, 2010.

[49] S. G. Kou, L. M. Peters, and M. R. Mucalo, "Chitosan: A review of sources and preparation methods," International Journal of Biological Macromolecules, vol. 169, pp. 85-94, 2021.

[50] A. Ibram, A.-M. Ionescu, and E. Cadar, "Comparison of extraction methods of chitin and chitosan from different sources," European Journal of Natural Sciences and Medicine, vol. 2, pp. 23-36, 2019.

[51] C. Carrera, C. Bengoechea, F. Carrillo, and N. Calero, "Effect of deacetylation degree and molecular weight on surface properties of chitosan obtained from biowastes," Food Hydrocolloids, vol. 137, p. 108383, 2023.

[52] K. Kurita, "Chitin and chitosan: functional biopolymers from marine crustaceans," Marine biotechnology, vol. 8, pp. 203-226, 2006.

[53] A. Aljawish, "Fonctionnalisation enzymatique de chitosane par des composés phénoliques: évaluation des propriétés biologiques et physico-chimiques de ces nouveaux biopolymères," Thèse, Université De Lorraine, vol. 31, p. 35, 2013.

[54] M. Z. Elsabee, R. E. Morsi, and A. Al-Sabagh, "Surface active properties of chitosan and its derivatives," Colloids and Surfaces B: Biointerfaces, vol. 74, pp. 1-16, 2009.

[55] M. Rinaudo, "Chitin and chitosan: Properties and applications," Progress in polymer science, vol. 31, pp. 603-632, 2006.

[56] C. P. Jiménez-Gómez and J. A. Cecilia, "Chitosan: a natural biopolymer with a wide and varied range of applications," Molecules, vol. 25, p. 3981, 2020.

[57] C. K. Pillai, W. Paul, and C. P. Sharma, "Chitin and chitosan polymers: Chemistry, solubility and fiber formation," Progress in polymer science, vol. 34, pp. 641-678, 2009.

[58] M. Vakili, M. Rafatullah, B. Salamatinia, A. Z. Abdullah, M. H. Ibrahim, K. B. Tan, et al., "Application of chitosan and its derivatives as adsorbents for dye removal from water and wastewater: A review," Carbohydrate polymers, vol. 113, pp. 115-130, 2014.

[59] L. Xu, Y.-A. Huang, Q.-J. Zhu, and C. Ye, "Chitosan in molecularly-imprinted polymers: Current and future prospects," International Journal of Molecular Sciences, vol. 16, pp. 18328-18347, 2015.

[60] A. H. Jawad, N. S. A. Mubarak, and A. S. Abdulhameed, "Hybrid crosslinked chitosan-epichlorohydrin/TiO2 nanocomposite for reactive red 120 dye adsorption: kinetic, isotherm, thermodynamic, and mechanism study," Journal of Polymers and the Environment, vol. 28, pp. 624-637, 2020.

[61] S. Wang, Y. Lu, X.-k. Ouyang, X. X. Liang, D. Yu, L.-Y. Yang, et al., "Fabrication of chitosan-based MCS/ZnO@ Alg gel microspheres for efficient adsorption of As (V)," International journal of biological macromolecules, vol. 139, pp. 886-895, 2019.

[62] A. H. Jawad, A. S. Abdulhameed, A. Reghioua, and Z. M. Yaseen, "Zwitterion composite chitosan-epichlorohydrin/zeolite for adsorption of methylene blue

and reactive red 120 dyes," International Journal of Biological Macromolecules, vol. 163, pp. 756-765, 2020.

[63] A. H. Jawad and A. S. Abdulhameed, "Facile synthesis of crosslinked chitosan-tripolyphosphate/kaolin clay composite for decolourization and COD reduction of remazol brilliant blue R dye: optimization by using response surface methodology," Colloids and Surfaces A: Physicochemical and Engineering Aspects, vol. 605, p. 125329, 2020.

[64] Y. Zheng, W. Yang, C. Wang, J. Hu, S. Fu, L. Dong, et al., "Nanoparticles based on the complex of chitosan and polyaspartic acid sodium salt: preparation, characterization and the use for 5-fluorouracil delivery," European Journal of Pharmaceutics and Biopharmaceutics, vol. 67, pp. 621-631, 2007.

[65] A. H. Jawad, N. S. A. Mubarak, and A. S. Abdulhameed, "Tunable Schiff's base-cross-linked chitosan composite for the removal of reactive red 120 dye: adsorption and mechanism study," International journal of biological macromolecules, vol. 142, pp. 732-741, 2020.

[66] C. Choi, J.-P. Nam, and J.-W. Nah, "Application of chitosan and chitosan derivatives as biomaterials," Journal of Industrial and Engineering Chemistry, vol. 33, pp. 1-10, 2016.

[67] A. Anitha, S. Sowmya, P. S. Kumar, S. Deepthi, K. Chennazhi, H. Ehrlich, et al., "Chitin and chitosan in selected biomedical applications," Progress in polymer science, vol. 39, pp. 1644-1667, 2014.

[68] Y. Luo and Q. Wang, "Recent advances of chitosan and its derivatives for novel applications in food science," Journal of Food Processing & Beverages, vol. 1, pp. 1-13, 2013.

[69] Q. Li, E. Dunn, E. Grandmaison, and M. F. Goosen, "Applications and properties of chitosan," in Applications of Chitan and Chitosan, ed: CRC Press, 2020, pp. 3-29.

[70] A. l. Asdrubal, "Emulsions de Pickering à application dermo-cosmétique: Etude des interactions particules/ingrédients et projection sur leur impact environnemental," Normandie, 2023.

[71] D. C. Montgomery, Design and analysis of experiments: John wiley & sons, 2017.

[72] P. H. Mainardi and E. D. Bidoia, "Fundamental concepts and recent applications of factorial statistical designs," Brazilian Journal of Biometrics, vol. 40, 2022.

[73] L. C. Onyiah, Design and analysis of experiments: classical and regression approaches with SAS: CRC Press, 2008.

[74] M. A. Bezerra, R. E. Santelli, E. P. Oliveira, L. S. Villar, and L. A. Escaleira, "Response surface methodology (RSM) as a tool for optimization in analytical chemistry," Talanta, vol. 76, pp. 965-977, 2008.

[75] M. A. Bezerra, S. L. C. Ferreira, C. G. Novaes, A. M. P. Dos Santos, G. S. Valasques, U. M. F. da Mata Cerqueira, et al., "Simultaneous optimization of multiple responses and its application in Analytical Chemistry–A review," Talanta, vol. 194, pp. 941-959, 2019.

[76] A. I. Khuri and S. Mukhopadhyay, "Response surface methodology," Wiley interdisciplinary reviews: Computational statistics, vol. 2, pp. 128-149, 2010.

[77] A. M. Dean, M. Morris, J. Stufken, and D. Bingham, Handbook of design and analysis of experiments vol. 7: CRC Press Boca Raton, FL, USA:, 2015.

[78] K. A. M. Said and M. A. M. Amin, "Overview on the response surface methodology (RSM) in extraction processes," Journal of Applied Science & Process Engineering, vol. 2, 2015.

[79] M. Kousha, E. Daneshvar, H. Dopeikar, D. Taghavi, and A. Bhatnagar, "Box–Behnken design optimization of Acid Black 1 dye biosorption by different brown macroalgae," Chemical Engineering Journal, vol. 179, pp. 158-168, 2012.

[80] J. P. Kleijnen, "Response surface methodology," in Handbook of simulation optimization, ed: Springer, 2014, pp. 81-104.

[81] A. L. Muluken, "Multi-Objective Optimization of Tungsten Inert Gas Welding Process Parameters on 304L Stainless Steel Using Taguchi-Based Grey Relational Analysis," 2020.

[82] C. Manterola, M. Vial, V. Pineda, and A. Sanhueza, "Systematic Review of Literature with Different Types of Designs," International Journal of Morphology, vol. 27, 2009.

[83] B. Oyejola and J. Nwanya, "Selecting the right central composite design," Int. J. Stat. Appl, vol. 5, pp. 21-30, 2015.

[84] S. Somadasan, G. Subramaniyan, M. S. Athisayaraj, and S. K. Sukumaran, "Central composite design: an optimization tool for developing pharmaceutical formulations," Journal of Young Pharmacists, vol. 16, pp. 400-409, 2024.

[85] C. N. Njoku and S. K. Otisi, "Application of Central Composite Design with Design Expert v13 in Process Optimization," 2023.

[86] M. Manohar, J. Joseph, T. Selvaraj, and D. Sivakumar, "Application of Box Behnken design to optimize the parameters for turning Inconel 718 using coated carbide tools," International Journal of Scientific & Engineering Research, vol. 4, pp. 620-644, 2013.

[87] A. Aziz and S. Aziz, "Application of Box Behnken design to optimize the parameters for Kenaf-epoxy as noise absorber," in IOP conference series: materials science and engineering, 2018, p. 012001.

[88] M. Ozonoh, B. Oboirien, and M. Daramola, "Optimization of process variables during torrefaction of coal/biomass/waste tyre blends: Application of artificial neural network & response surface methodology," Biomass and Bioenergy, vol. 143, p. 105808, 2020.

[89] S. Beg, S. Swain, M. Rahman, M. S. Hasnain, and S. S. Imam, "Application of design of experiments (DoE) in pharmaceutical product and process optimization," in Pharmaceutical quality by design, ed: Elsevier, 2019, pp. 43-64.

Chapter III:

Materials and Methods

III.1. Introduction

The three laboratories where all of the experiments for this research project were carried out were the pedagogical laboratory in the Department of Chemistry, University of El-Oued; the Laboratory of Applied Chemistry and Environment, University of El-Oued; and the Physic-Chemical Analysis Scientific.

There are four main sections of this chapter that the following can be used to summarize. The initial step involves production of the biocomposite with commercial chitosan (CTS) 75% modified with Illite-kaolinite clay (IKaol) 25%. The adsorption properties were enhanced by chemically crosslinking the chitosan with epichlorohydrin (ECH) to improve its chemical stability and efficiency in pollutant removal, and we called it CTS-ECH/IKaol. In the second section, we used six different dyes anionic (Orange G, Orange II, Reactive Orange 16, Reactive Red 120) to select high-performance dyes to continue with for the rest of the study using CTS-ECH/IKaol. They are the two anionic dyes Orange G (OG) and Reactive Orange 16 (RO16). About the third section, it briefly explains the instruments: The techniques used in this work include pH_{pzc}, FTIR, XRD, and others. The fourth section provides an illustration of how to use the BBD by studying the effects of adsorbent dosage, solution pH, contact time, and temperature. Additionally, the adsorption results were analysed using various isotherm models, along with kinetic and thermodynamic models, to gain a deeper understanding of the adsorption mechanism to find the ideal adsorption operation parameters.

III.2. Chemical Solvents and Materials Used

In this study, CTS (deacetylation ≥75%, medium molecular weight) was obtained from Sigma-Aldrich, and illite-kaolinite clay, pretreated by another research team, was used. Glassware was initially soaked in dilute HNO_3 (10 % v/v) and washed with distilled water before use. The chemical reagents used included epichlorohydrin (98%), sodium hydroxide (NaOH), ethanol (EtOH), HCl (hydrochloric acid), sodium chloride (NaCl), and acetic acid (80%) of a high purity grade were bought from Merck, which was used without further purification. Similarly, Orange G, Orange II, Reactive Orange 16, Reactive Red 120. was purchased from Sigma-Aldrich. All of the chemicals and reagents utilized in the research were of analytical grade and didn't require any additional purification.

III.3. Preparation of Illite-Kaolinite Clay

The study employed illite-kaolinite clay (IKaol) that was collected from Djamaa in the south part of Algeria .and pretreated by other researchers. The clay was purified with the purpose of removing all crystalline phases and organic matter according to the method reported in the literature [1-3] as outlined in the accompanying Figure **III.1**.

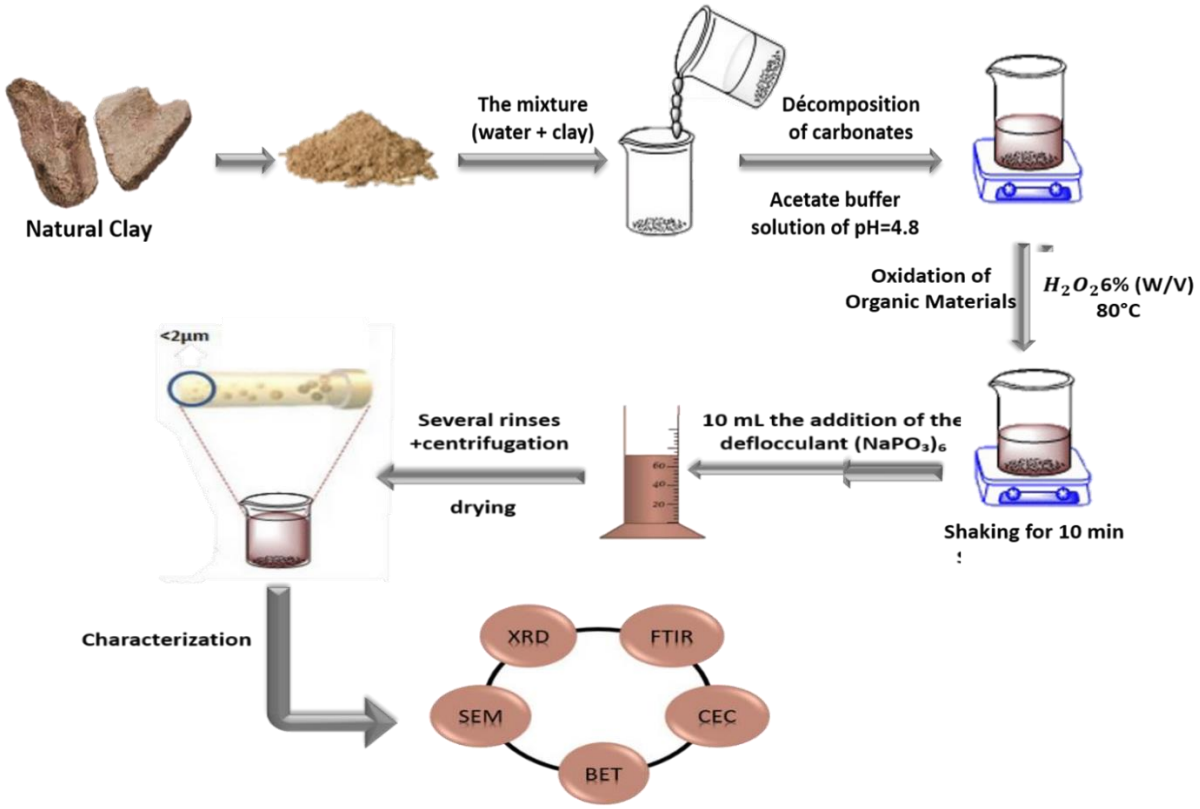

Figure III.1. Diagrammatic demonstration of preparation and analysis utilizing a clay sample [4].

III.4. Synthesis of CTS-ECH/IKaol biocomposite

The preparation of the adsorbent material (CTS-ECH/IKaol) was performed according to the procedure established in prior research, following the steps illustrated in the figure **III.2,3.**

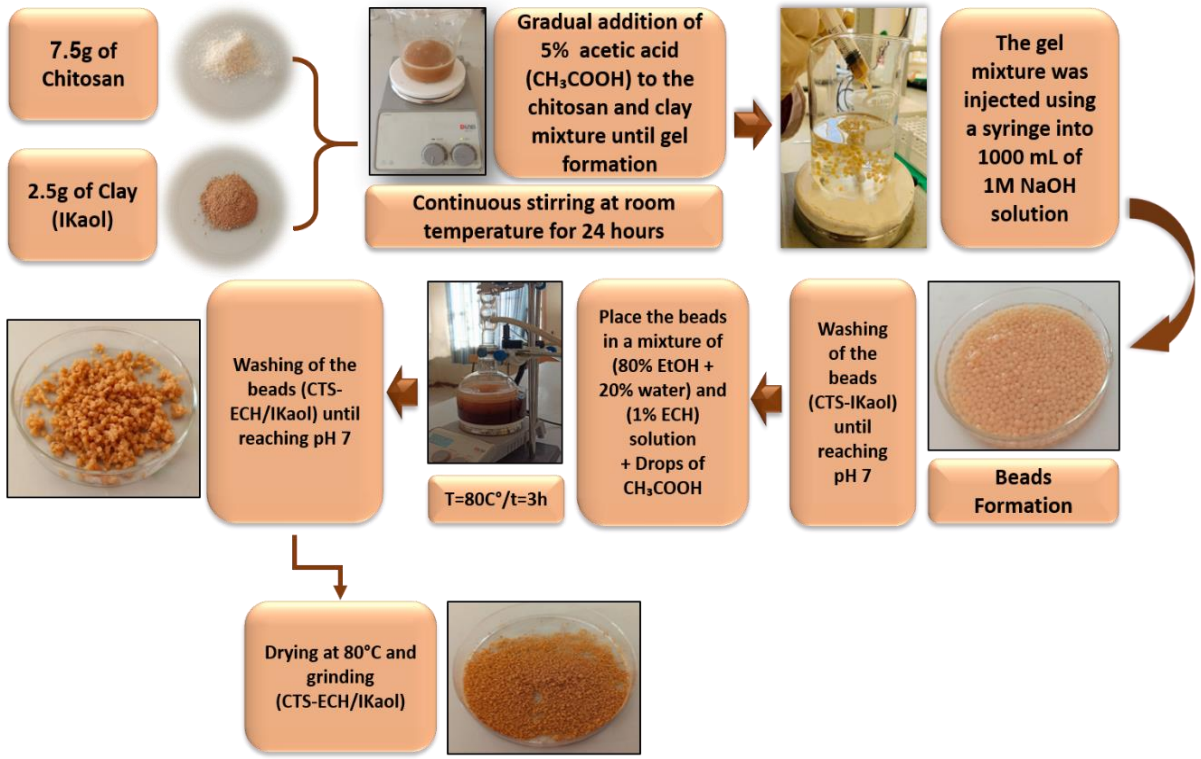

Figure III.2. The synthesis steps of CTS-ECH/IKaol biocomposite.

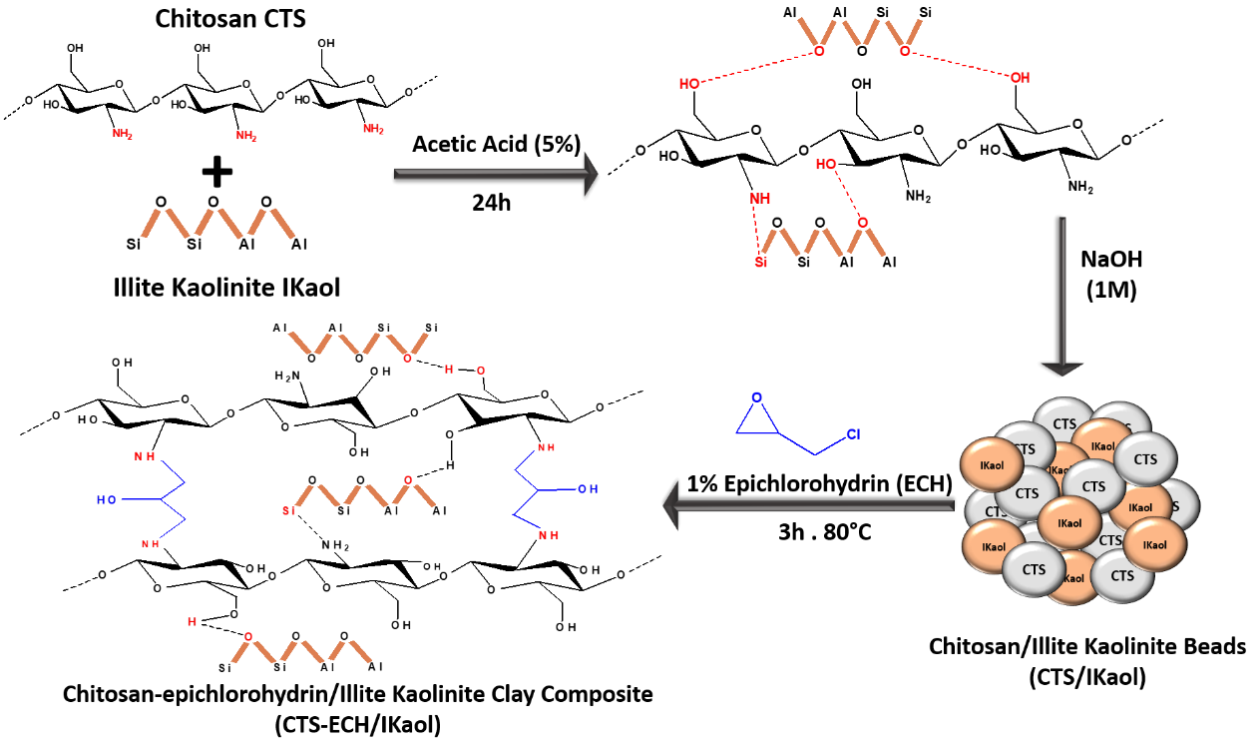

Figure III.3. Synthesis steps of CTS-ECH/IKaol

III.5. Characterization of samples

The effect of modification on the surface properties of clay was analysed using various characterization tools, including X-ray Diffraction Spectroscopy (XRD), Fourier transform infra-red spectroscopy (FTIR) and scanning electron microscopy (SEM). A brief description of these tools is discussed below.

III.5.1. Infrared (FTIR) spectra

The FT-IR is a widely used analytical technique for characterizing chemical materials. It aids in identifying the structures of simple molecules and detecting functional groups in organic compounds. It also provides important information regarding the nature of chemical bonds within a material [5]. In this study, infrared spectra were recorded using an FT-IR instrument (Agilent Technologies Cary 630 FTIR) to examine the samples before and after the adsorption process, aiming to identify chemical changes by detecting the present functional groups. The spectra were recorded in the range of 4000– 400cm^{-1}.

Figure III.4. A Photographic Image of the Fourier Transform Infrared (FT-IR) Spectroscopy Instrument

III.5.2. The XRD patterns

The XRD is an effective technique for the structural characterization of materials, particularly applied to crystalline media that exhibit a periodic and regular arrangement in their structure. The main objective of this technique is to determine the crystalline structure of sample powders and to study their compositional and structural properties with high precision [6]. For this purpose, the samples used in this study were examined using the (CTS-ECH/IKaol) device with (Miiflex600) radiation of a specific wavelength (Cu-Ka). The diffraction patterns were recorded at room temperature with

2θ varying between 10° to 80°. The scanning rate was (0.02°) per (S^{-1}). Subsequently, the crystallinity degree (Cr %) for each sample was calculated using the following equation:

$$\boldsymbol{Cr\%} = \frac{\boldsymbol{I_{200} - I_{am}}}{\boldsymbol{I_{200}}} \times \mathbf{100} \qquad \textbf{(III.1)}$$

$\boldsymbol{I_{200}}$ **:**The diffraction intensity at $(2\theta = 22 - 23)$

$\boldsymbol{I_{am}}$ **:** The diffraction intensity at $(2\theta = 16 - 20)$

Figure III.5. The BTX III Benchtop X-ray Diffraction Analyzer..

III.5.3. the point of zero charge (pH_{pzc})

The effect of pH was studied by measuring the point of zero charge (pH_{pzc}), which is the pH at which the net charge of the adsorbent material is zero. The method followed was based on the procedure described in reference [3, 7]. A quantity of 25 mg of the CTS-ECH/IKOL adsorbent material was added to each beaker containing 25 mL of NaCl solution with a concentration of 1 N.

The initial pH was adjusted within a range of 3 to 11 using NaOH (0.1 N) and HCl (0.1 N) solutions. The beakers were then placed on a magnetic stirrer and left overnight. The final pH of each sample was measured, and from this, the pH_{pzc} of the adsorbent material was determined.

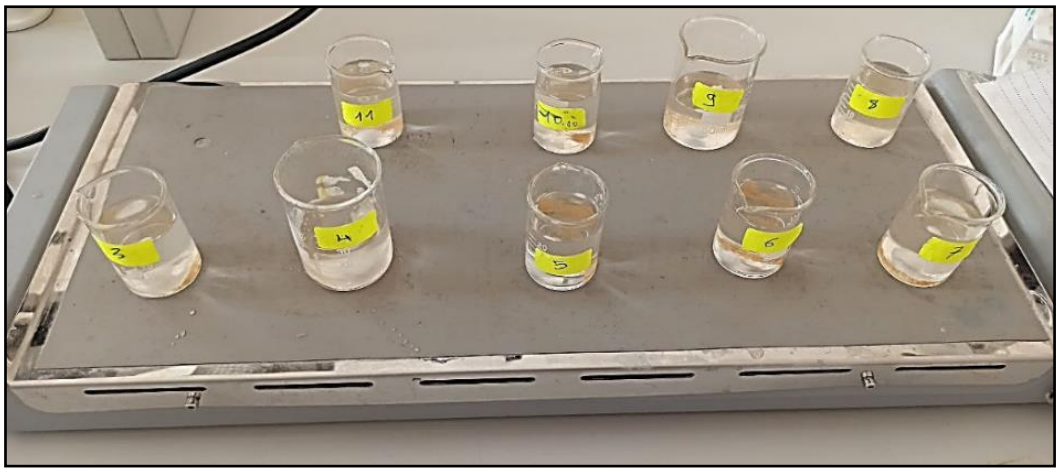

Figure III.6. Images of the point of zero charge (pH_{pzc}) of CTS-ECH/IKaol.

III.6. Preliminary study of anionic dyes adsorption using CTS-ECH/IKaol composite

A preliminary study was conducted to determine the effectiveness of CTS-ECH/IKaol in adsorbing different anionic dyes. Four dyes—Reactive Orange 16 (RO16), Reactive Red 120 (RR120), Orange II, and Orange G (OG)—were tested at 50 ppm to identify the most efficiently removed dyes for further investigation. Each dye solution (50 ppm) was treated with 0.1 g of CTS-ECH/IKaol. The mixtures were agitated on an orbital shaker at 250 rpm for varying contact times (5 to 120 min) at pH and temperature not controlled. After adsorption, the residual dye concentrations in the influent and effluent were measured using a spectrophotometer, and the removal efficiencies were calculated. The results showed that Orange G (OG) and Reactive Orange 16 (RO16) exhibited significantly higher adsorption efficiencies compared to the other optimization experiments to determine the best adsorption conditions.

Table III.1. Percentage of four anionic dyes removal by CTS-ECH/IKaol

Dye	Dye Removal (%)
Reactive Orange 16	**89.32**
Reactive Red 120	58.20
Orange G	**89.12**
Orange II	75.05

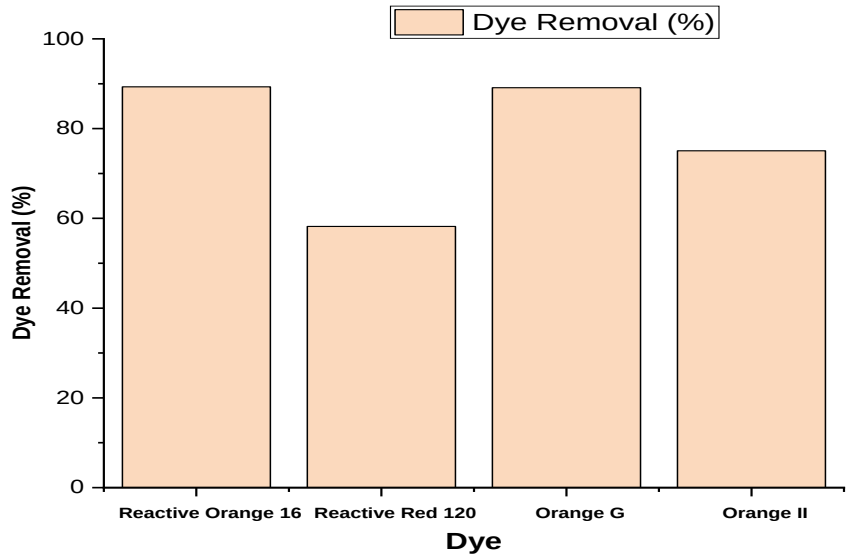

Figure III.7. Efficiency analysis of four anionic dyes removal by CTS-ECH/IKaol

III.7. Selection of the Dyes

A pretreatment study was carried out to determine which types of dyes the CTS-ECH/IKaol was effective on. Optimization studies were then carried out on the dye with the highest removal among five different anionic dyes under the same adsorption conditions. We used five different anionic dyes (Orange G, Orange II, Reactive Orange 16, Reactive Red 120) to select high-performance dyes to continue with for the rest of the study.

We conducted experiments on paint. Adsorption experiment sets were set up for each dye prepared at 50 ppm concentrations. In adsorption experiments, 0.1 g/L CTS-ECH/IKaol was added and mixed continuously on an orbital shaker at 250 rpm for 30 min contact time. Following the adsorption experiments, the influent and effluent concentrations of all after experiments were measured with a UV–vis spectrophotometer (SECOMAM PRIM), and the removal efficiencies were calculated. As a result of preliminary studies in adsorption experiments, higher removal efficiency was obtained for Orange G(OG) and Orange 16 (RO16) dyes compared to the other dyes used in our study. Therefore, these two dyes were chosen for optimization experiments of adsorption conditions.

Two anionic dyes, OG and RO16, were selected based on the following properties:

Table III.2. Physicochemical Properties of OG dye [8].

Name	Molecular formula	MW (g.mol^{-1})	Nature	λ_{max}(nm)
OG	$C_{16}H_{10}N_2Na_2O_7S_2$	452.4	Anionic	478

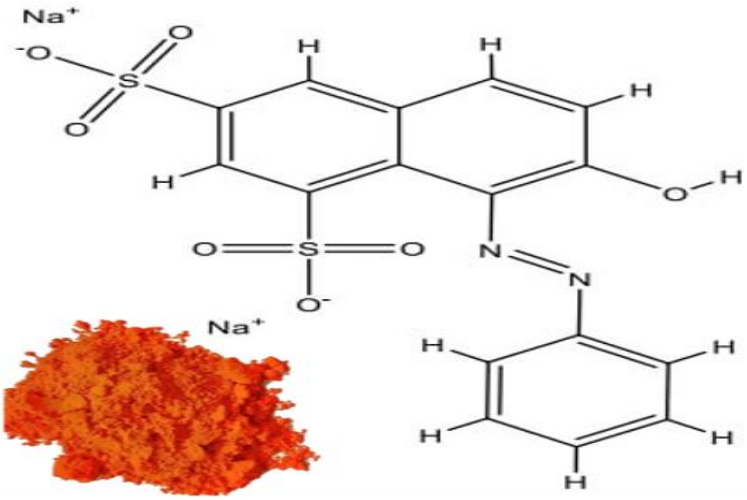

Figure III.8. Structure molecular formula of O G dye

Table III.3. Physicochemical Properties of RO16 dye [9]

Name	Molecular formula	MW (g.mol^{-1})	Nature	λ_{max}(nm)
RO16	$C_{20}H_{17}N_3Na_2O_{11}S_3$	617.54	Anionic	496

Figure III.9. Structure molecular formula of Reactive Orange 16 Dye

III.8. Design of experiment

The RSM Design-Expert is a specific functionality present in the Design-Expert program developed by Stat-Ease. It emphasizes RSM for process optimization. It facilitates investigators in designing experiments, fitting response surface models, and effectively analyzing data. In this work, the Design Expert 13.0 software was used as a statistical tool for designing the experiments and performing statistical analysis. RSM-BBD was applied for optimizing and studying the impact of four adsorption key factors,

such as CTS-ECH/IKaol dosage, solution pH, contact time, and temperature, on the OG and RO16 dyes. Table **III.4** presents the levels of independent adsorption key factors applied in BBD model. A quadratic equation was adopted to predict the OG and RO16 dyes' removal.

besides experimental data analysis as Equation (II.18) mentioned in the chapter (II).

$$Y = \beta_0 + \sum_{i=1}^{k} \beta_i X_i + \sum_{i=1}^{k} \beta_i X^2{}_i + \sum_{i=1}^{k} \sum_{j=1}^{k} \beta_{ij} X_i X_j + \varepsilon \qquad \textbf{(III.2)}$$

Where, ϒ is the predicted response (OG and RO16 dyes decolourization), k is the number of variables, *i* and j are the variable indices, β_0 is the constant coefficient, β_i and β_{ii} are linear and quadratic coefficients, β_{ij} is the interaction coefficient, and ε is a random error. X_i and X_j are the response and coded values for independent factors (-1, 0, and +1), respectively. Positive coefficients show synergy, while negative ones indicate antagonism between variables.

Table III.4. BBD codes for independent factor experimental levels for OG and RO16 dyes removal.

Factor	Level		
	Low	**Medium**	**High**
Adsorbent dose(g)	0.02	0.04	0.06
Contact time(min)	5	25	45
Temperature(C°)	30	45	60
Ph	4	7	10

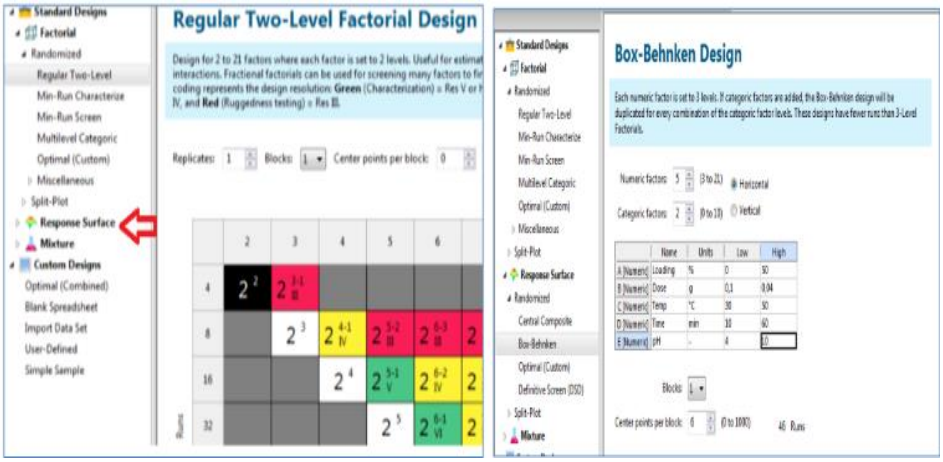

Figure III.10. The Response Surface Methodology (RSM) software

Using analysis of variance (ANOVA), researchers evaluated the accuracy of the model by calculating the coefficients, which included p-value, F-value, determination coefficient (R2), predicted determination coefficient (R2 pred), adjusted determination coefficient (R2 adj), acceptable precision, degree of freedom (DF), and standard deviation [10]. These factors were essential in assessing the precision of both empirical data and the theoretical framework. The researchers utilized a dependable second-order quadratic model equation to forecast optimal values and investigate the interrelationships among the components. The optimal factor values were achieved by utilizing the regression equation, counter-response surface map, and imposing restrictions on the levels of variables. An initial set of tests was performed to detect extreme values of variables.

III.9. Adsorption Studies in Batch

Adsorption studies of OG and RO16 dye pollutants on CTS-ECH/IKaol were carried out under the same working conditions. According to BBD, a total of 29 experimental (runs) were conducted to optimize and analyze the effects of four key variables—A: CTS-ECH/IKaol dosage (0.02 to 0.06 g) were employed to eliminate OG and RO16 in dye concentrations (25 to 250 mg/L), B: contact time (5 to 60 min, C: temperatures ranging (30 to 60 °C), and D: pH levels ranging (4 to 10) which were adjusted by HCl and NaOH (0.1 M). The outcomes of these 29 runs for both OG and RO16 dye removal are detailed in Table **III.5.**

A specified quantity of adsorbent was taken in a set of Erlenmeyer flasks (250 mL) containing 100 mL of dye solution before being placed in an isothermal water bath shaker (Waterbath WNB 29, Memmert, Germany) and set with 110 rpm, the mixture was separated using a centrifuge (SCILOGEX SCI412) at 4500 rpm for 2 minutes. Finally, the concentrations of OG and RO16 dyes were calculated by UV- Vis spectroscopy (SECOMAM PRIM) at λ_{max} = 478 nm and λ_{max} = 496 nm, respectively. The OG and RO16 dye removal percentage (R%), and the adsorption capacity (q_e, mg/g) of both dyes at various time intervals are calculated by Eqs. (3) and (4), respectively.

$$\boldsymbol{R}(\%) = \frac{\boldsymbol{C_0 - C_e}}{\boldsymbol{C_0}} \times \mathbf{100} \qquad \textbf{(III.3)}$$

$$\boldsymbol{q_e} = \frac{\boldsymbol{V}}{\boldsymbol{W}} (\boldsymbol{C_0 - C_e}) \qquad \textbf{(III.4)}$$

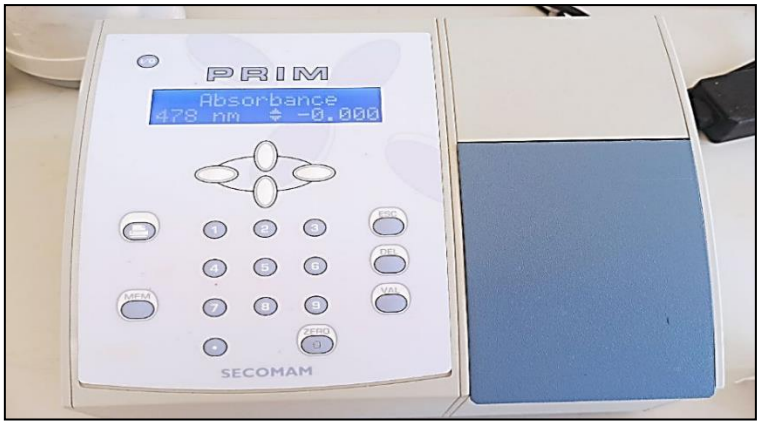

Figure III.11. Image of the UV–Visible (UV-Vis) spectrophotometer

Figure III.12. Image of rotary shaker used for dye adsorption experiments

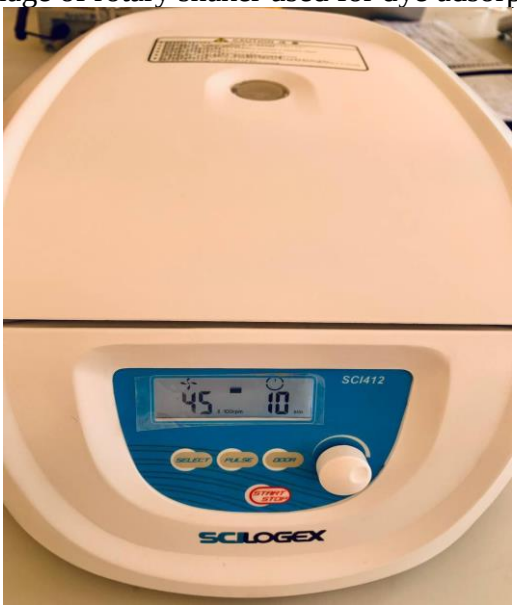

Figure III.13. Eppendorf Centrifuge SCILOGEX SCI412

Table III.5. The 4-varibles BBD matrix and experimental data for OG and RO16 dyes removal

Run	A: Dose (g)	B: Time (min)	C: Temp (°C)	D: pH	OG removal (%)	RO16 removal (%)
1	0.04	5	45	10	36.97	36.49
2	0.02	25	60	7	26.21	46.63
3	0.04	5	45	4	61.19	57.98
4	0.06	45	45	7	89.93	91.72
5	0.04	5	60	7	28.2	59.95
6	0.06	25	45	10	63.88	46.18
7	0.02	45	45	7	43.75	49.96
8	0.06	5	45	7	70.79	60.63
9	0.02	25	45	10	22.43	6.96
10	0.04	25	45	7	72.82	76.23
11	0.02	25	30	7	44.07	36.93
12	0.02	25	45	4	60.94	65.93
13	0.04	45	45	10	32.5	41.55
14	0.04	25	45	7	73.19	75.24
15	0.04	25	45	7	79.27	75.85
16	0.04	25	30	10	20.12	34.34
17	0.04	45	60	7	81.64	88.72
18	0.04	45	45	4	91.71	95.83
19	0.04	25	30	4	64.47	71.2
20	0.04	45	30	7	32.29	69.45
21	0.04	25	60	4	**92.14**	90.53
22	0.04	25	45	7	79.25	75.92
23	0.06	25	45	4	88.1	**96.52**
24	0.06	25	30	7	44.45	86.85
25	0.02	5	45	7	30.82	30.81
26	0.04	25	45	7	74.12	75.17
27	0.06	25	60	7	87.83	92.83
28	0.04	5	30	7	19.1	36.39
29	0.04	25	60	10	25.88	37.54

III.10. Adsorption kinetics

The adsorption kinetics can be tested by two common types of models: the pseudo first order (PFO), pseudo-second-order (PSO)

III.10.1. Pseudo-first order model

The linear equation **(III.5)**, PFO kinetic models are defined by the following equations:

$$\ln(q_e - q_t) = \ln q_e - K_1 t \qquad \textbf{(III.5)}$$

The PFO kinetic model for adsorption is expressed as plots of ln (q_e- q_t) vs t for linear PFO models. The values of K_1 (min^{-1}) the rate constant of adsorption according PSO can be obtained from the slope and q_e (cal) (mg/g) from the intercept.

III.10.2. Pseudo-second order model

The linear equation **(III.6)**, PSO kinetic models are defined by the following equations:

$$\frac{t}{q_t} = \frac{1}{K_2 q_e^2} + \frac{t}{q_e} \qquad \textbf{(III.6)}$$

The PSO kinetic model for adsorption is expressed as a plot of $\frac{t}{q_t}$ vs t. The q_e (cal) (mg/g) parameter can be obtained from the intercept, and The k_2 ($g \cdot mol^{-1} \cdot min^{-1}$) the rate constant of adsorption according PSO from slope.

III.11. Adsorption isotherms

Adsorption isotherms explain the interaction between adsorbate with adsorbent, where it describes the interaction on how the dye molecules distribute between the bulk dye solution and the solid adsorbent once the system attended equilibrium state. The linear Freundlich isotherm, Langmuir and Temkin can be obtained from the equilibrium data. [11].

The Freundlich model is an empirical model that accounts for the heterogeneity of adsorption energies on the surface of the adsorbent. Its linear form is given by the following equation [12]:

$$\ln q_e = \ln K_f + \frac{1}{n} \ln C_e \qquad \textbf{(III.7)}$$

When plot of ln q_e versus ln C_e , a straight line is obtained, and its slope is a measure of the adsorption intensity (n), while the intercept of K_f represents the adsorption capacity.

The Langmuir model is the most commonly used equation, and the linearized form is written as follows [13]:

$$\frac{C_e}{q_e} = \frac{1}{q_{max} \times K_L} + \frac{C_e}{q_{max}} \qquad \textbf{(III.8)}$$

Hence, a straight line with a slope $\left(\frac{1}{q_{max}}\right)$ and an intercept as $\frac{1}{K_L \times q_{max}}$ can be obtained by plotting $\frac{C_e}{q_e}$ versus $\mathbf{C_e}$

The Temkin model assumes that the adsorption energy of all molecules decreases linearly with increasing surface coverage. The Temkin model can be described by the following linear equation [14]:

$$q_e = \frac{RT}{b} \ln K_T + \frac{RT}{b} \ln C_e \qquad \textbf{(III.9)}$$

The equilibrium binding constant (K_T) can be obtained by plotting (q_e) versus ($\ln C_e$), which yields a linear relationship. The slope of the resulting straight line corresponds to ($\frac{RT}{b}$), while the intercept is ($\frac{RT}{b} \ln K_T$). From these values, the Temkin parameters—the heat-related constant (b) and the equilibrium binding constant (K_T) can be calculated.

III.12. Adsorption thermodynamics

The adsorption behavior of OG and RO16 dyes onto the CTS–ECH/IKaol composite was evaluated through thermodynamic analysis. Key parameters—including the standard Gibbs free energy change (ΔG°), standard enthalpy change (ΔH°), and standard entropy change (ΔS°) were determined to elucidate the nature of the adsorption process. Adsorption experiments were conducted at temperatures ranging from 30°C to 60°C using a shaking water bath.

$$\ln K_d = \frac{\Delta S}{R} - \frac{\Delta H}{RT} \qquad \textbf{(III.10)}$$

$$K_d = \frac{(C_i - C_t)}{C_t} \times \frac{V}{m} \left[\frac{l}{g}\right]$$

$$\Delta G° = \Delta H° - T\Delta S°$$

The thermodynamic parameters ΔH° (enthalpy change) and ΔS° (entropy change) were determined from the linear van't Hoff plot of ln K_d versus $\left(\frac{1}{T}\right)$, where the slope corresponds to $\left(\frac{-\Delta H^\circ}{R}\right)$ and the intercept equals $\left(\frac{\Delta S^\circ}{R}\right)$

III.13. Regeneration Study

To enhance cost-effectiveness, the regeneration and reuse of the adsorbent are essential. The CTS-ECH/IKaol composite was saturated with OG or RO 16 dyes at a concentration of 50 mg/L under optimized conditions: an adsorbent dose of 0.04 g for OG and 0.06 g for RO 16, temperatures of 60°C (OG) and 45°C (RO 16), a constant pH of 4, and a contact time of 25 minutes for both dyes. After adsorption, the dye-laden composite was rinsed to remove residual dye and dried. Desorption was performed using 0.1 M NaOH, the solution was aerated for 5 h at room temperature, after which the material was thoroughly washed, dried [15, 16], and the level of OG and RO16 dyes desorbed (R, %) was estimated using Eq. (III.11):

$$\boldsymbol{R}(\%) = \frac{\boldsymbol{C_0 - C_e}}{\boldsymbol{C_0}} \times \mathbf{100} \qquad \textbf{(III.11)}$$

After each cycle of adsorption–desorption, the spent adsorbent was washed with distilled water and reused in a follow-up cycle, ensuring efficient adsorbent recovery and process sustainability.

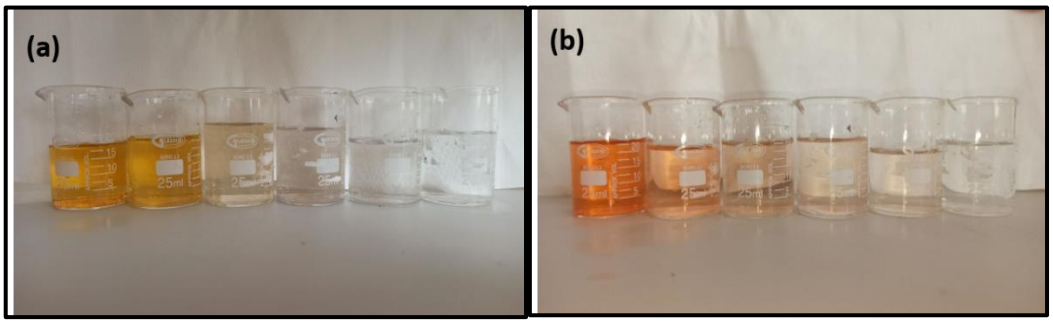

Figure III.14. Study of the Desorption Process of Dye-Saturated Adsorbent for the Removal of Residual Dye in the Cases of (a) Orange G and (b) RO16

References

[1] D. Atia and A. Zobeidi, "An investigation into the mineralogical and physicochemical characterization of El-Oued (Algeria) clay," *Neuroquantology*, vol. 20, pp. 1048-1058, 2022.

[2] A. Hamidi, D. Atia, A. Rebiai, A. Reghioua, A. Zobeidi, M. Messaoudi, *et al.*, "Investigation of adsorption kinetics and isothermal thermodynamics for optimizing methylene blue adsorption onto a modified clay with cellulose using the response surface approach," *Biomass Conversion and Biorefinery*, pp. 1-15, 2023.

[3] R. Mecheri, A. Zobeidi, S. Atia, S. Neghmouche Nacer, A. A. Salih, M. Benaissa, *et al.*, "Modeling and optimizing the crystal violet dye adsorption on kaolinite mixed with cellulose waste red bean peels: insights into the kinetic, isothermal, thermodynamic, and mechanistic study," *Materials*, vol. 16, p. 4082, 2023.

[4] S. Aghris, F. Laghrib, Y. Koumya, S. El Kasmi, M. Azaitraoui, A. Farahi, *et al.*, "Exploration of a new source of sustainable aluminosilicate clay minerals from morocco: mineralogical and physico-chemical characterizations for clear upcoming applications," *Journal of Inorganic and Organometallic Polymers and Materials*, vol. 31, pp. 2925-2938, 2021.

[5] A. H. Jawad, S. Rangabhashiyam, A. S. Abdulhameed, S. S. A. Syed-Hassan, Z. A. ALOthman, and L. D. Wilson, "Process optimization and adsorptive mechanism for reactive blue 19 dye by magnetic crosslinked chitosan/MgO/Fe3O4 biocomposite," *Journal of Polymers and the Environment*, vol. 30, pp. 2759-2773, 2022.

[6] F. J. Muhana, B. I. El-Eswed, and F. I. Khalili, "Synthesis of immobilized chitosan/humic acid coupling product for removal of Pb (II), Cd (II) and Cr2O72–from aqueous solutions," *Desalination and Water Treatment*, vol. 87, pp. 292-305, 2017.

[7] B. M. Babić, S. K. Milonjić, M. J. Polovina, and B. Kaludierović, "Point of zero charge and intrinsic equilibrium constants of activated carbon cloth," *Carbon*, vol. 37, pp. 477-481, 1999.

[8] Z. Taibi, K. Bentaleb, Z. Bouberka, C. Pierlot, M. Vandewalle, C. Volkringer, *et al.*, "Adsorption of orange G dye on hydrophobic activated bentonite from aqueous solution," *Crystals*, vol. 13, p. 211, 2023.

[9] J. Y. Tong, "Batch study and experimental design for the removal of reactive orange 16 from aqueous solution using chitosan beads," UTAR, 2024.

[10] S. Zhu, R. Shi, J. Wang, J.-F. Wang, and X.-M. Li, "Unpredictable chronic mild stress not chronic restraint stress induces depressive behaviours in mice," *Neuroreport*, vol. 25, pp. 1151-1155, 2014.

[11] N. Ayawei, A. N. Ebelegi, and D. Wankasi, "Modelling and interpretation of adsorption isotherms," *Journal of chemistry*, vol. 2017, p. 3039817, 2017.

[12] Y. A. E. H. Ali, L. Hejji, N. B. Seddik, A. Azzouz, L. Pérez-Villarejo, M. Stitou, *et al.*, "Remediation of malachite-green dye from textile wastewater using biosorbent almond shell-based cellulose," *Journal of Molecular Liquids*, vol. 399, p. 124435, 2024.

[13] S. Banerjee, G. C. Sharma, R. K. Gautam, M. Chattopadhyaya, S. N. Upadhyay, and Y. C. Sharma, "Removal of Malachite Green, a hazardous dye from aqueous solutions using Avena sativa (oat) hull as a potential adsorbent," *Journal of Molecular Liquids*, vol. 213, pp. 162-172, 2016.

[14] E. Dundar, "Modélisation par la théorie du potentiel des processus d'adsorption dans les matériaux microporeux," Université du Québec à Trois-Rivières, 2014.

[15] N. S. Abdul Mubarak, T. Chuan, H. Khor, A. H. Jawad, L. Wilson, and S. Sabar, "Immobilized Fe-loaded chitosan film for methyl orange dye removal: competitive ions, reusability, and mechanism," *Journal of Polymers and the Environment*, vol. 29, pp. 1050-1062, 2021.

[16] S. Elhady, M. Bassyouni, M. Elshikhiby, M. Y. Saleh, and M. H. Elzahar, "Optimization of anionic dye removal using cross-linked chitosan composite as eco-friendly bio-adsorbent," *Applied Water Science*, vol. 14, p. 159, 2024.

Chapter IV:

Results and Discussion

IV.1. Introduction

In this chapter, the physicochemical properties of the (CTS-ECH/IKaol) composite were investigated with the aim of evaluating its efficiency in removing the dyes Orange G (OG) and Reactive Orange 16 (RO16) from aqueous solutions. This study is part of the ongoing search for effective and environmentally friendly adsorbent materials for the treatment of dye-contaminated wastewater. The factors influencing the adsorption process were analyzed using the Box–Behnken design within the framework of Response Surface Methodology (RSM), in order to determine the optimal operating conditions for achieving maximum adsorption efficiency. Furthermore, the study addressed the thermodynamic and kinetic aspects of the adsorption process, as well as the evaluation of adsorption isotherm models.

IV.2. Characterization of CTS-ECH/IKaol composite

IV.2.1. Fourier Transform Infrared Spectroscopy (FT-IR):

The FT-IR absorption spectrum provides information about the type and quantity of chemical bonds within the material. By identifying the constituent chemical elements, it is possible to infer the molecular structure of the compound. Moreover, the infrared spectrum enables the identification of the main functional groups present in the studied sample and offers insights into the functional groups before and after the adsorption process, based on the specific wavenumber range characteristic of each functional group [1].

The FTIR spectra of the adsorbent CTS-ECH/IKaol before adsorption and after the adsorption of Orange G (OG) and Reactive Orange 16 (RO16) dyes are presented in Figure **IV.1 (a, b and c)** respectively.

The FTIR spectrum of CTS-ECH/IKaol Figure **IV.1.a** displays distinguished peaks at 3500 cm^{-1}, 1645 cm^{-1}, and 1340 cm^{-1}, corresponding to the stretching vibrations of O–H, N–H, and C–N groups, respectively [2]. Additionally, peaks appeared at 1150 cm^{-1} and 1040 cm^{-1}, attributed to the stretching vibrations of C–O–C and C–O bonds. These peaks indicate the reaction of epoxy groups (ECH) with the carbon atoms of hydroxyl groups in CTS, forming covalent bonds that lead to epoxide ring opening and the release of a chlorine atom [3]. Moreover, a peak at 1049 cm^{-1} was observed, corresponding to the stretching vibration of the Si–O–Si bond. Other peaks appeared at 940 cm^{-1} and within the range of 500–795 cm^{-1}, which are attributed to the bending vibrations of OH groups in Al–OH and to the vibrations of Si–O–Al bonds, respectively [4].

After the adsorption of OG dye Figure **IV.1.c**, the FTIR spectrum exhibited a new peak around 1040 cm^{-1}, which can be attributed to the adsorption of the S=O stretching vibration of the sulfonic group (SO^{-}), indicating the interaction of the dye with active sites on the adsorbent surface. Additionally, a change in both intensity and bandwidth was observed at 1645 cm^{-1}, a region typically associated with C=C or C=O vibrations in the dye structure, suggesting partial interactions between the aromatic ring in OG and the polymeric matrix [5].

Following the adsorption of RO16 dye Figure **IV.1.b**, a distinct new peak appeared at 1032 cm^{-1}, also corresponding to the S=O group, but with higher intensity, reflecting a stronger interaction between the SO_3^- group of RO16 and the positively charged sites of chitosan. Moreover, a peak at approximately 1618 cm^{-1} was recorded, attributed to N=N stretching vibrations, indicating the immobilization of the azo group (–N=N–) of the dye onto the adsorbent surface. A slight shift was also observed in the vibration band associated with OH/NH groups around 3300–3400 cm^{-1}, suggesting the occurrence of hydrogen bonding interactions between the dye and the adsorbent [6, 7].

These spectral changes confirm that both OG and RO16 dyes were effectively anchored onto the surface of the adsorbent through specific functional interactions involving the S=O, N=N, and C=C groups, thereby validating the successful adsorption process and the efficacy of the composite in dye removal.

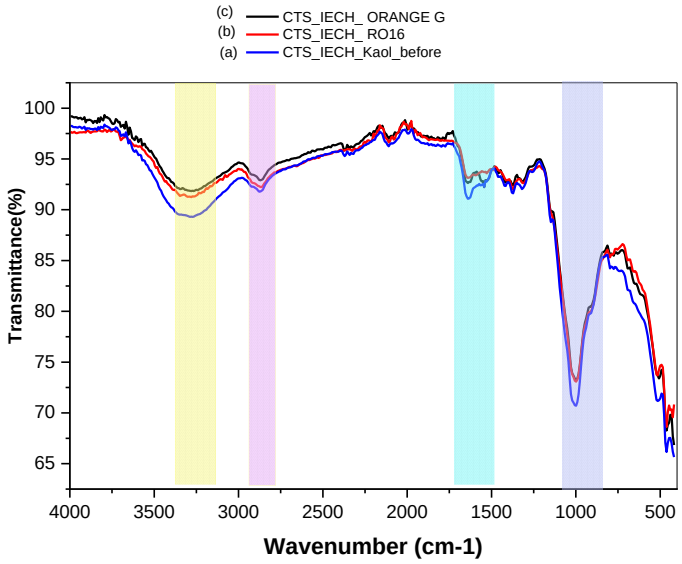

Figure IV.1. FT-IR spectra of **(a)** CTS–ECH/IKaol, **(b)** CTS–ECH/IKaol- RO16 **(c)** CTS–ECH/IKaol-OG.

IV.2.2. X-ray Diffraction (XRD) Analysis:

Figure **IV.2** displays the X-ray diffraction (XRD) patterns of the CTS–ECH/IKaol composite. In the XRD pattern of the raw composite, a sharp characteristic diffraction peaks corresponding to the IKaol as follows:2θ = 19.8°, 29.5°, 38.5°, and 77.5°, which correspond to the crystallographic planes (110), (220), (311), and (440), respectively. A similar observation was reported by Ali H. Jawad et al. [8] for the synthesis of Chitosan-Epichlorohydrin/TiO2 nanocomposite , and for the CS-TPP/KC composite [2]. These distinct peaks confirm the crystalline structure of CTS–ECH/IKaol, which reflects the crystalline nature of IKaol and indicates the presence of intramolecular hydrogen bonding between CTS and IKaol. Furthermore, these results reaffirm the successful incorporation of IKaol particles into the CTS–ECH/IKaol composite [8].

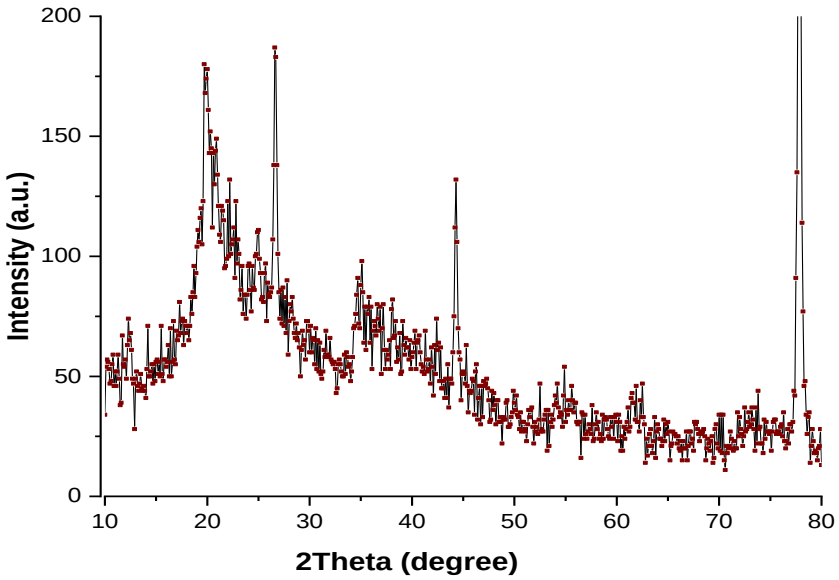

Figure IV.2. XRD patterns of CTS–ECH/IKaol composite

IV.3. Optimization with BBD- RSM

Table **III.5** show that the Box–Behnken Design (BBD) included 29 experimental runs. This design was adopted to investigate the individual and interactive effects of various factors on the removal efficiency of OG and RO16 dyes, considered as response variables. The independent factors taken into account were: adsorbent dosage (A), contact time (B), temperature (C), and solution pH (D). The results indicated that the highest removal efficiencies for OG and RO16 were **92.14%** and **96.52%**, respectively, achieved in runs number **21** and **23** (Table **III.5**).

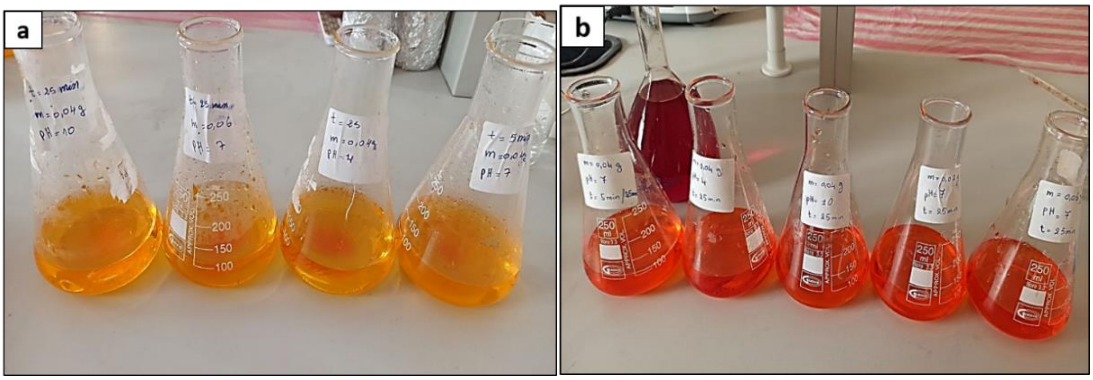

Figure IV.3. Deposition of natural dyes following adsorption onto the CTS-ECH/IKaol composite (a – OG; b – RO16)

IV.4. Model fitting and statistical analysis

The independent and interactive impact of the adsorption key factors, such as adsorbent dosage (A), contact time (B), temperature (C), and pH (D), on the OG and RO16 dye removal was evaluated by BBD-RSM. To test the significance of binary combination and the adequacy of the model, the analysis of variance (ANOVA) was used. The outcomes of the ANOVA statistics for OG and RO16 dye, as shown in Table **IV.1-2**. The model is deemed to have statistical significance, and the factor effects deemed real when the F- value is greater than unity and the p- value is< 0.05 [9].

Moreover, the coefficient of determination (R^2) values for OG and RO16 dye are 0.948 and 0.971, respectively, which specified that the regressions model is statistically significant. From statistical perspective, the codes of the BBD model are statistically significant when the p- value is< 0.05. Therefore, the following codes in BBD: A, B, C, D, AC, BC, BD, B^2, C^2, and D^2, for OG dye are significant; A, B, C, D, and BD are considered statistically significant for RO16 dye. The other model terms with p- value> 0.05 were ignored in model equation to achieve the best- fit results. The empirical model equation in terms of coded parameters for responses OG and RO16 dye removal are expressed by Eqs. (IV.1) and (IV.2), respectively:

$$\textbf{OG removal}\ (\%) = +75.73 + 18.0633A + 10.3958B + 9.78333C - 21.3975D + 15.31AC + 10.0625BC - 8.7475BD - 6.19042\,A2 - 12.9792B^2 - 19.5404C^2 - 7.79917D^2 \quad \textbf{(IV.1)}$$

$$\textbf{RO\_16 removal}\ (\%) = +75.682 + 19.915A + 12.915B + 6.75333C - 22.9108D - 8.1975BD - 8.51058A^2 - 7.56933B^2 - 12.3731D^2 \quad (\textbf{IV.2})$$

Table IV.1. Analysis of variance (ANOVA) for OG dye removal (%)

Source	Sum of Squares	df	Mean Square	F-value	p-value
Model	16791.43	14	1199.39	18.50	< 0.0001
A-Dose	3915.41	1	3915.41	60.38	< 0.0001
B-Time	1296.88	1	1296.88	20.00	0.0005
C-Temp	1148.56	1	1148.56	17.71	0.0009
D-pH	5494.24	1	5494.24	84.73	< 0.0001
AB	9.64	1	9.64	0.1487	0.7056
AC	937.58	1	937.58	14.46	0.0019
AD	51.05	1	51.05	0.7873	0.3899
BC	405.02	1	405.02	6.25	0.0255
BD	306.08	1	306.08	4.72	0.0475
CD	120.01	1	120.01	1.85	0.1952
A^2	248.57	1	248.57	3.83	0.0705
B^2	1092.71	1	1092.71	16.85	0.0011
C^2	2476.72	1	2476.72	38.20	< 0.0001
D^2	394.55	1	394.55	6.08	0.0272
Residual	907.79	14	64.84		
Lack of Fit	865.36	10	86.54	8.16	0.0289
Pure Error	42.43	4	10.61		
Cor Total	17699.22	28			

Table IV.2. Analysis of variance (ANOVA) for RO16 dye removal (%)

Source	Sum of Squares	Df	Mean Square	F-value	p-value
Model	15319,14	14	1094,22	33,60	< 0.0001
A-Dose	4700,92	1	4700,92	144,33	< 0.0001
B-Time	2001,57	1	2001,57	61,45	< 0.0001
C-Temp	547,29	1	547,29	16,80	0,0011
D-pH	6298,88	1	6298,88	193,39	< 0.0001
AB	35,64	1	35,64	1,09	0,3133
AC	3,46	1	3,46	0,1062	0,7493
AD	18,62	1	18,62	0,5717	0,4621
BC	4,60	1	4,60	0,1413	0,7127
BD	268,80	1	268,80	8,25	0,0123
CD	65,04	1	65,04	2,00	0,1795

A^2	469,82	1	469,82	14,42	0,0020
B^2	371,64	1	371,64	11,41	0,0045
C^2	83,33	1	83,33	2,56	0,1320
D^2	993,04	1	993,04	30,49	< 0.0001
Residual	455,98	14	32,57		
Lack of Fit	455,14	10	45,51	216,04	< 0.0001
Pure Error	0,8427	4	0,2107		
Cor Total	15775,12	28			

BBD graphical ways can be utilized to analyze the residual distribution and the relations between real and theoretical values for the OG removal (%) and RO16 removal (%), thus giving an indication of the strength of the developed models. The normal probability of the residuals in the BBD model for both responses is illustrated in Figure **IV.4 a** and **b**, respectively. The points in both figures exhibit a close alignment with a straight line, indicating an ideal normal distribution and independent residuals. Furthermore, Figure **IV.4 c** and **d** display the relationship between the actual and expected values for the outcomes (OG removal (%) and RO16 removal). The statistical validation of the BBD model is supported by the proximity of the actual and expected values in Figure **IV.5 c** and **d**, which indicates the actual and expected values are close to each other [10].

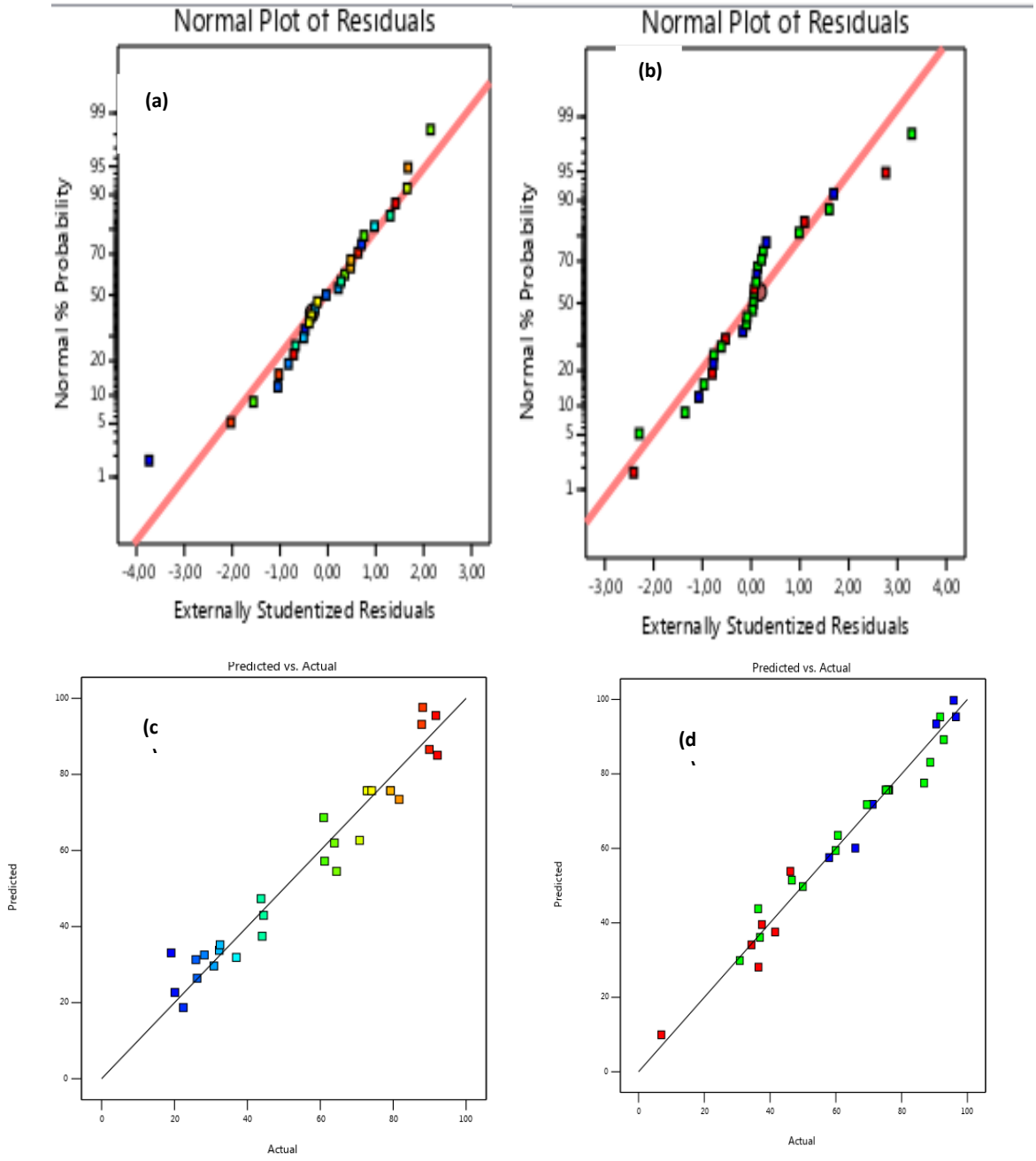

Figure IV.4. Normal probability plots of residuals for **(a)** OG dye removal and **(b)** RO16 dye removal; plots of the relationship between the estimated and real values of **(c)** OG dye removal and **(d)** RO16 dye removal.

Plotting the response surface graphs for OG and RO16 dye removal allowed us to demonstrate how the individual parameters affected the response (Figure **IV.5.**). The study reveals that the variables CTS-ECH/IKaol dose (A), contact time (B), temperature (C) and pH (D), directly affect the removal rate of OG and RO16 dye. An increase in all the previous variables leads to an improvement in the removal rate. The direct

proportionality of the studied variables to the removal rate is interpreted as follows: Increasing the adsorbent dose, contact time, and temperature enhances dye removal by providing more active sites, allowing longer interactions, and improving molecular kinetics, whereas higher pH decreases removal efficiency by reducing electrostatic attraction. These results align with the Equation (**IV.1** and **IV.2**) for removing OG and RO16 dye (%), as the coefficients of factors CTS-ECH/IKaol dose (A), contact time (B), temperature (C) are positive. In contrast, the coefficient of factor and pH (D) is negative.

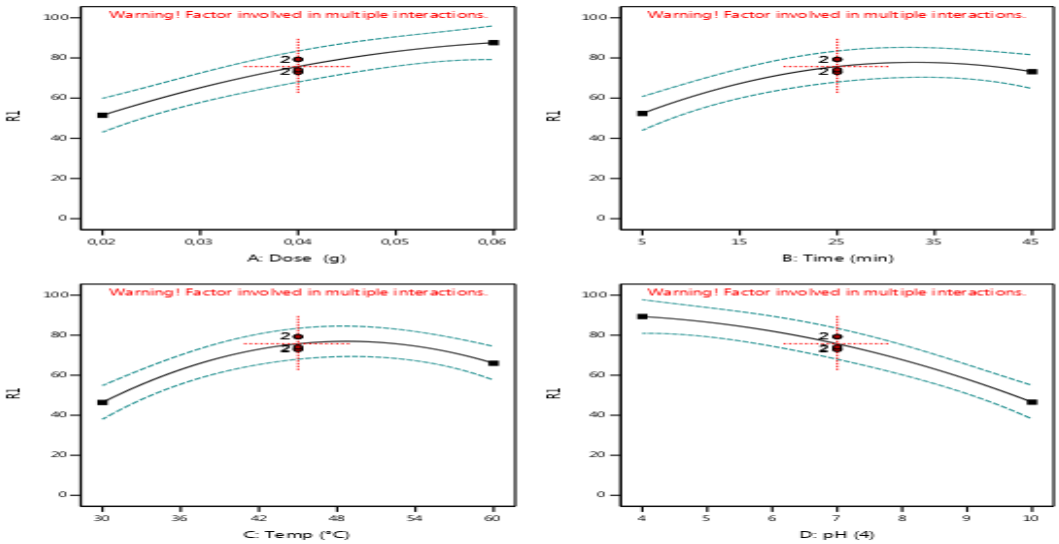

Figure IV.5. Influence of the main working parameters on OG dye adsorption process.

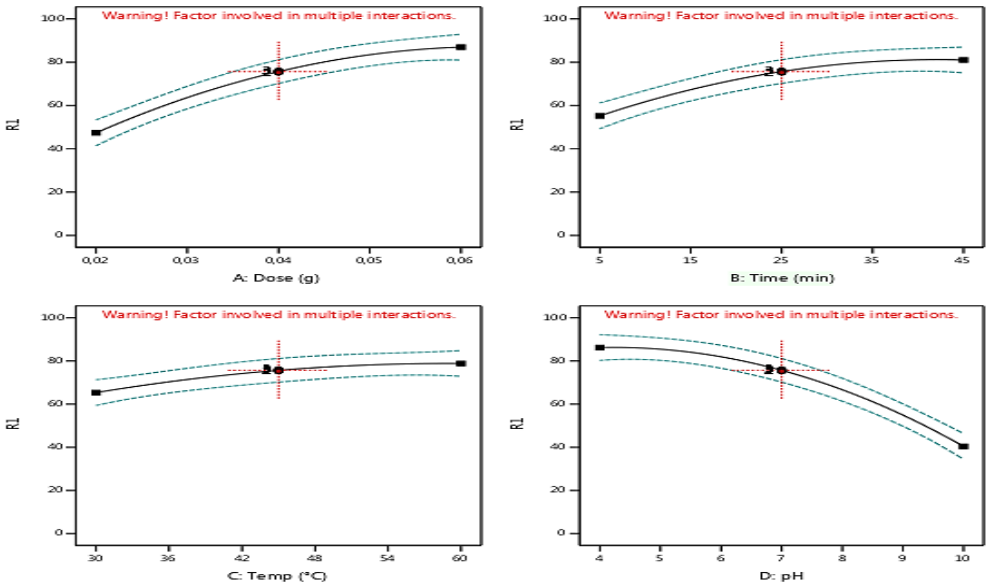

Figure IV.6. Influence of the main working parameters on RO16 dye adsorption process.

IV.5. Interactions Significant for OG and RO16 dye removal

The interaction effect between the CTS-ECH/IKaol dosage (A) and temperature (C) is statistically significant on the OG dye removal (p-value = 0.0019). Meanwhile, another key parameter (time (B) = 25 min and pH (D) = 4) was held constant. The plots of three- dimensional (3D) response surfaces were used to further analyze the relationship between the temperature and the adsorbent dose, as shown in Figures **IV.7**, respectively, clearly illustrates that increasing the temperature from 30 °C to 60 ° C led to a higher percentage of OG removal (as indicated in Table **IV.1**). These results will be covered in more detail in our discussion of adsorption thermodynamics in Section (**IV.9)**. It is worth noting that similar findings regarding the uptake of RO16 dye by chitosan-glyoxal/fly ash/Fe_3O_4 biocomposite were previously reported by Twinkle et al.[11].

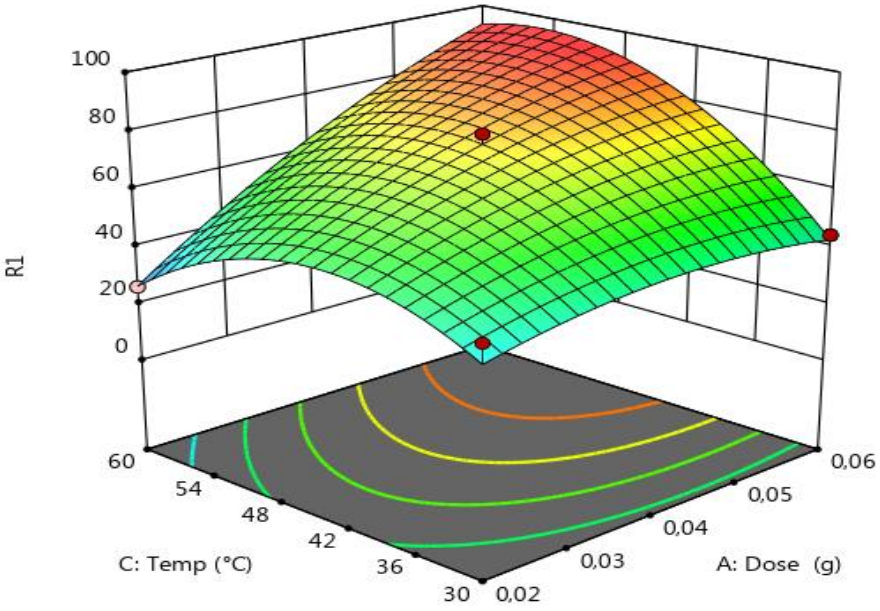

Figures. IV.7. 3D response surfaces of the AC interaction (A: adsorbent dose, and C: temperature) interaction for OG dye removal.

Another significant interaction (p-value = 0.0255) on the OG dye removal (%) was between contact time (B) and temperature (C), while the other parameters (adsorbent dose (A) 0.04 g and solution pH (D) 4) remained constant. The 3D response surface plots for the impacts and interaction of time (B) and temperature (C) on OG dye removal (%) are shown in Figure **IV.8**. From Figure **IV.8** provides further clarification, showing that the removal of OG was enhanced by increasing the time from 5 to 25 min,

In fact, longer contact time will offer longer exposure time of OG dye molecules to functional groups available on the surface of CTS-ECH/IKaol composite, and will also provide sufficient time for OG dye molecules to penetrate deeper toward inner adsorption active sites on the surface of CTS-ECH/IKaol composite, which is consistent with the findings of the kinetics study discussed in Section (**IV.7**)

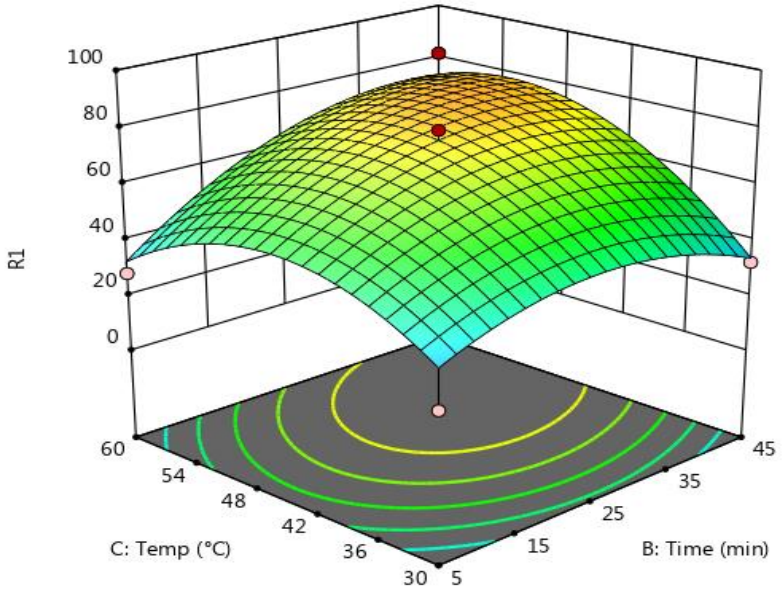

Figures IV.8. 3D response surfaces of the BC interaction (B: contact time, and C: temperature) interaction for OG dye removal.

Finally, the interaction between contact time (B) and solution pH (D) significantly influenced the removal of GO and RO16 dyes, with p-values of 0.0475 and 0.0123, respectively, while the other factors adsorbent dose (0.04 g) and temperature (60°C) for OG dye removal, and adsorbent dose (0.06 g) and temperature (45°C) for RO16 dye removal were kept constant. The plots of three- dimensional (3D) response surfaces for the impacts and interaction of time (B) and pH (D) on OG and Ro16 dye removal (%) are shown in Figure **IV.9 a** and **b**. From Figure **IV.9 a** and **b** it can be noticed that the lowering in solution pH from 10 to 4 was responsible for increasing the OG and RO16 dye removal (%) from 19.1% to 92.14% and 6,96% to 96,52%, respectively. The pH_{pzc} value of CTS-ECH/IKaol composite was 6.90 as depicted in Figure **IV.9.c**. This result elucidates that the CTS-ECH/IKaol composite has a cationic character and reconfirms the availability of the amino ($-NH_3$) cationic group on the CTS-ECH/IKaol composite surface, which is in line with the result obtained from the potentiometric titrations test. The surface of CTS-ECH/IKaol composite can be converted into a positive charge at

solution pH with a value below the pH_{pzc}, thus promoting the adsorption of anions species like OG or RO16 dye molecules. As a result, a strong electrostatic interaction can be created between the protonated amino ($-NH_3$) functional group of the CTS-ECH/IKaol composite and sulfonate ($-SO_3$) group of the OG or RO16 dye. This mechanism aligns with findings by Anaya-Esparza et al. (2020), who reported similar behavior in dye adsorption using titanium dioxide-impregnated chitosan beads[12]. Consequently, pH 4.0 was selected as the optimal condition for further experiments. The enhanced adsorption at lower pH can be attributed to the protonation of amino groups, as described in Eq. (IV.3 and IV.4).

$$\mathbf{IKaol\text{-}R\text{-}NH_3^+ + OG\text{-}SO_3^- \leftrightharpoons IKaol\text{-}R\text{-}NH_3^+\text{----}O_3S\text{-}OG} \quad \mathbf{(IV.3)}$$

$$\mathbf{IKaol\text{-}R\text{-}NH_3^+ + RO16\text{-}SO_3^- \leftrightharpoons IKaol\text{-}R\text{-}NH_3^+\text{---}\ O_3S\text{--}RO16} \quad \mathbf{(IV.4)}$$

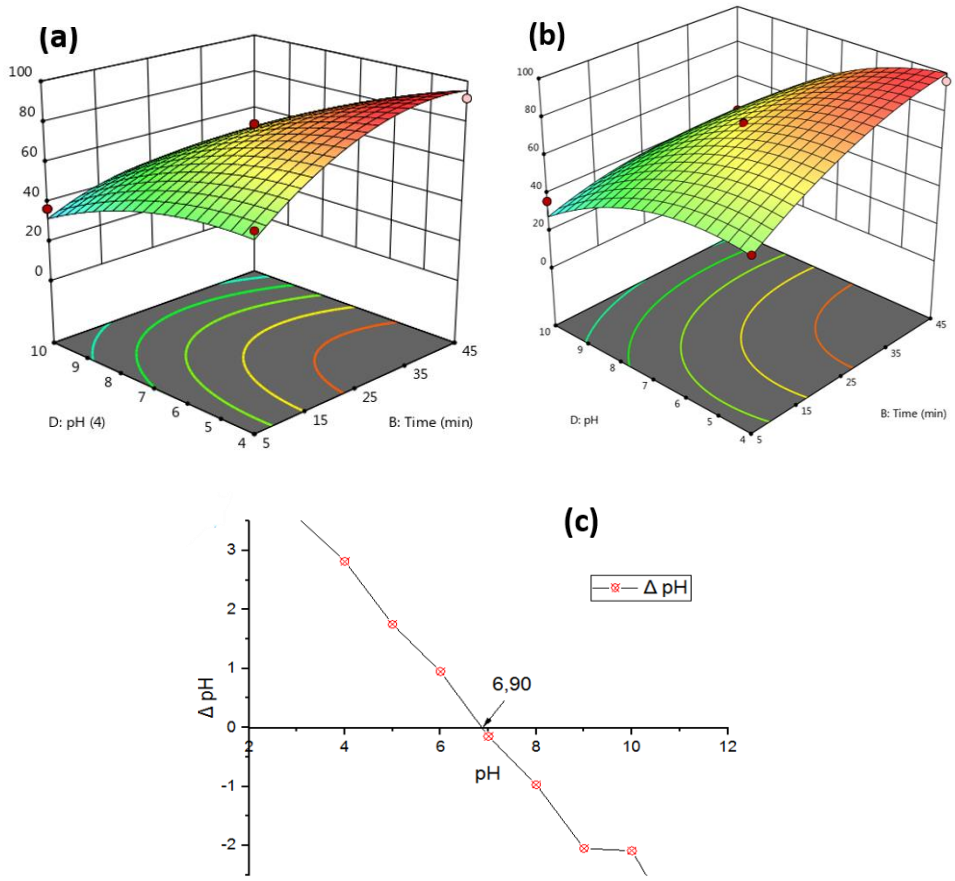

Figures IV.9. 3D response surfaces plots of **(a)** the BD interaction for OG dye removal, **(b)** the BD interaction for RO16 dye removal (B: contact time, and D:pH) and **(c)** pH_{pzc} of CTS-ECH/IKaol

IV.6. Impact of initial OG and RO16 dye concentration vs contact time

The concentration test is often adopted to further evaluate the effectiveness of an adsorbent and its impact on the dye molecules. Figure **IV.10.a,b** illustrates the relationship between the adsorption performance of CTS-ECH/IKaol and the initial concentration of OG and RO16 solutions. For this test, the dose of CTS-ECH/IKaol was 0.04 g for OG, and 0.06 g for RO16, the solution pH was set to 4 for OG and RO16 dyes. While varying the initial adsorbate concentrations from 25 to 250 mg/ L, the adsorption efficiency of CTS-ECH/IKaol improved from 39.21 to 192.05 mg/ g for OG dye and from 34.52 to 276.66 mg/ g for RO16 dye. The gradual increase in the adsorption rate is plausibly attributed to the presence of an attractive force that expedites mass transfer. This force likely facilitates the movement of dye molecules [13].

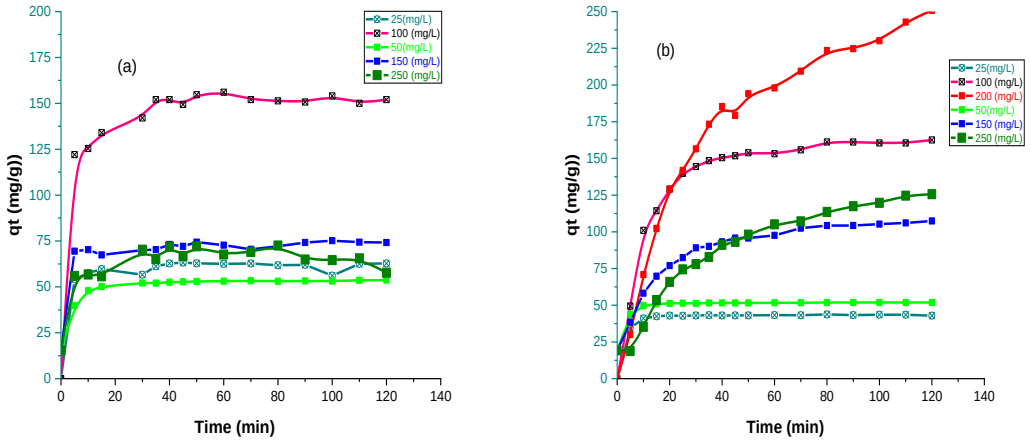

Figure IV. 10. Effect of the contact time on OG dye **(a)** and RO16 dye **(b)** adsorption at different initial concentrations by CTS-ECH/IKaol composite

IV.7. Adsorption kinetics

Another test to assess the efficiency of CTS-ECH/IKaol composite versus time is the kinetic study, which offers extra information on the adsorption rate, the equilibrium time as well as determine the best kinetic model . In this respect, two types of kinetic models were applied to analyze the experimental results, namely The pseudo- first-order (PFO) [14], and pseudo- second- order (PSO) [15]. The obtained kinetics parameters are summarized in Table **IV.3**. The highest determined coefficient (R^2) and the accuracy of theoretical values were considered in choosing the best kinetic models.

According to experimental data presented in Table **IV.3**, it can be concluded that the adsorption of OG and RO16 dye molecules by the CTS-ECH/IKaol composite followed PSO model due to the higher correlation coefficient (R^2) values. Additionally,

compared to the q_e values computed using the PFO model, the qe (i.e., q_e, cal) values estimated using the PSO model are closer to the experimental qe (i.e., q_e, exp) values. These findings and FT-IR analyses indicate that the adsorption process depends critically on the chemical interaction between the OG or RO16 dye and the active functional groups on the CTS-ECH/IKaol surface. This result indicates that the adsorption of OG and RO16 dye by CTS-ECH/IKaol composite was governed by chemisorption process and can involve the electrostatic interaction force between the positively charged functional groups available on the surface of CTS-ECH/IKaol composite and the OG and RO16 dye anions [16]

Table IV.3. PFO and PSO kinetic parameters for OG and RO16 adsorption on CTS-ECH/IKaol composite

OG Concentration (mg/L)	$q_{e\ exp}$ (mg/g)	Pseudo-first-order			Pseudo-second-order		
		$q_{e\ cal}$ (mg/g)	K_1 (1/min)	R^2	$q_{e\ cal}$ (mg/g)	K_2*10^{-2} (g/mg. min)	R^2
25	62.55	62.18	0.403	0.999	62.50	0.952	0.996
50	124.58	119,33	0.207	0.997	125.00	0.610	0.999
100	153.38	143,21	0.031	0.973	153.85	0.454	0.999
150	178.38	177,68	0.027	0.999	178.57	2.509	0.998
250	185.71	183.09	0.245	0.999	185.19	0.164	0.991

RO16 Concentration (mg/L)	$q_{e\ exp}$ (mg/g)	Pseudo-first-order			Pseudo-second-order		
		$q_{e\ cal}$ (mg/g)	K_1 (1/min)	R^2	$q_{e\ cal}$ (mg/g)	K_2*10^{-2} (g/mg. min)	R^2
25	43.76	36.14	0.403	0.999	43.67	0.0419	0.999
50	84.89	82.27	0.269	0.997	84.75	0.0140	0.999
100	161.20	139.73	0.031	0.973	161.2	0.065	0.999
150	199.02	204.38	0.073	0.994	200.00	0.027	0.973
200	250.89	248.29	0.037	0.990	250.00	0.011	0.982
250	276.66	292.95	0.293	0.972	277.78	0.08	0.983

IV.8. Adsorption isotherm

Different isotherm models were used to verify the adsorbate deposition onto the adsorbent's surface and to estimate the maximum adsorption capacity of CTS-ECH/IKaol to ward OG and RO16 dyes at constant temperature. They included Langmuir [17], Freundlich [18], Temkin [19]. The non- linear curves of the equilibrium models are shown in Table **IV.4** and Figure **IV.11**.

The parameters of equilibrium models are recorded in Table **IV.4**. According to the R^2 values (Table **IV.4**) obtained from the isotherm models, it was observed that the Freundlich isotherm has the highest R^2 values compared to other R^2 values obtained from Langmuir and Temkin isotherms. This indicates that the RO16 dye adsorption occurred on a heterogeneous surface and multi-layered adsorption [20].Furthermore, the adsorption intensity factor (n) is used to assess the potency of adsorption or surface roughness [21]The values of (1/n) in the Freundlich isotherm were estimated to be 0.46 and 0.11 for OG and RO16 dyes, respectively, which is favorable because it is less than 1, biosorption suggests a strong connection between OG and RO16 dyes and CTS-ECH/IKaol [22, 23].

The maximal adsorption capacities (q_{max}) for a monolayer were calculated and compared with other adsorbents for OG and RO16 adsorption, as summarized in Table **IV.4**. The composite material CTS-ECH/IKaol exhibited a maximum adsorption capacity (q_{max}) of 416.67 mg/g for OG dye at 60°C and 357.14 mg/g for RO16 dye at 45°C.

Table IV.4. Langmuir, Freundlich, and Temkin constants for the adsorption of OG dye onto the CTS-ECH/IKaol composite.

Adsorption isotherm	Parameter	Value OG	Value RO16
Langmuir	q_{max} **(mg/g)**	416,67	357,14
	K_L **(L/mg)**	0,026	0,0447
	R^2	0,984	0,984
Freandlich	K_f **(mg/g) (L/mg)$^{1/n}$**	32,97	172,71
	N	2,16	8,63
	R^2	**0,999**	**0,996**
Temkin	K_T **(L/mg)**	0,465	114,23
	b_T **(JHZ[J/mol)**	34,68	12,21
	R^2	0,946	0,947

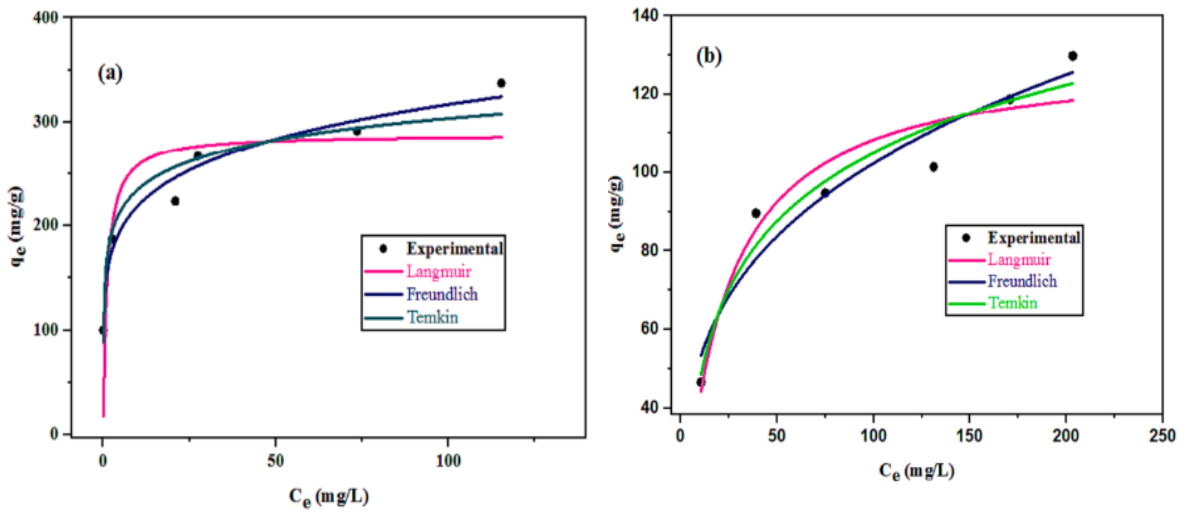

Figure IV. 11. Isotherm Model Fitting for (a) OG and (b) RO16 dye Adsorption Experimental Data.

The adsorption capacity of RO16 dye by the CTS-ECH/IKaol composite was compared with various other chitosan composite materials as given in Table **IV.5**. From Table **IV.5**, it is evident that the CTS-ECH/IKaol composite is a highly effective bio adsorbent for removing OG and RO16 dyes from aqueous solutions, respectively. The findings of this study underscore the significance of reassessing plentiful natural waste and extracting valuable compounds, such as chitosan, to maintain the environment and attain economic advantages. The development of an effective adsorbent from CTS-ECH/IKaol composite represents an environmentally friendly alternative adsorbent for the treatment of water pollution.

Table IV.5. Comparison of the adsorption capacity of OG and RO16 dyes by various chitosan composites.

Adsorbents	**Dye**	**q_{max} (mg/g)**	**Ref**
octadecylamine nanoclay ODA	OG	39.4	[24]
Bacillus subtilis bacteria @ chitosan biopolymer CHS@BCLS	RO16	120	[25]
Biochar	OG	38.2	[26]
chitosan-genipin/SiO2 composite CHI-GNP/SiO2	RO16	57.1	[27]
crosslinked chitosan-glutaraldehyde matrix (QS@Ch-Glu)	OG	206.65	[28]
Chitosan and watermelon seed shell CS/WSS	RO16	158.6	[29]
polyaniline-modified almond (PANI@ WS)	OG	17.65	[30]
cross-linked chitosan-epichlorohydrin/nanosilica (CS-EPH/NSi)	RO16	110.2	[31]
arginine-doped polyaniline/silicon dioxide (Arg-PANI@SiO2)	OG	387.16	[32]
chitosan/nano SiO2 (CTS/NS)	RO16	97.8	[33]

Activated carbon (MTLAC)	OG	318.5	[34]
Activated Carbon	RO16	112.27	[35]
tetrafluoroterephthalonitrile crosslinked quercetin/chitosan (T-QT/CS)	OG	349.9	[36]
humin immobilized on silica	RO16	19.45	[37]
Aminated covalent organic polymer (ACOP)	OG	227.9	[38]
polysulfone-immobilized esterified Corynebacterium glutamicum (PIEC)	RO16	248.1	[39]
polystyrene modified-chitin	OG	17.86	[40]
activated carbon	RO16	13.32	[41]
hydrophobic activated bentonite clay	OG	102.8	[42]
biochar derived from coconut shell	RO16	46.63	[43]
CTS-ECH/IKaol	OG	**416.67**	**This study**
	RO16	**357.14**	**This study**

IV.9. Adsorption thermodynamics

Various thermodynamic parameters were determined to evaluate the feasibility and spontaneity of the adsorption process of OG and RO16 dyes onto the CTS-ECH/IKaol composite, as well as to assess the degree of randomness at the dye/sorbent interface. These parameters include the change in entropy (ΔS°) in kJ/mol·K, the change in enthalpy (ΔH°) in kJ/mol, and the change in Gibbs free energy (ΔG°) in kJ/mol.

The plots of lnKd versus 1/T are presented in **Figure IV. 12.a, b.** From these plots, the thermodynamic parameters ΔH° and ΔS° were derived. The intercept of the linear plot corresponds to ΔS°, while the slope represents ΔH°.

The results presented in Table **VI.6** for the OG dye indicate that with increasing temperature, the values of K_d also increase, leading to an increase in adsorption capacity. This suggests that the adsorption process is endothermic, which is further confirmed by the positive value of ΔH°.

Additionally, the positive ΔS° values suggest that the adsorption of OG onto CTS-ECH/IKaol results in an increased randomness during adsorption studies at the solid/liquid solution interface [44].The adsorption of OG dye onto CTS-ECH/IKaol also yielded negative values of ΔG°, indicating that the process is spontaneous. These negative ΔG° values reflect a high adsorption affinity of the material [45].

Furthermore, the internal structure of the CTS-ECH/IKaol may be influenced by the increasing in temperature, leading to facilitate the OG and RO16 dye molecules distribution in the CTS-ECH/IKaol 's interspaces structure. Besides, the protonation process of amino (-NH_2) and hydroxyl (-OH) groups promotes at high temperature,

which leads more cationic sites available on the CTS-ECH/IKaol surface for adsorption of anionic species of dye [2].

Table IV.6. Thermodynamic parameters for OG dye adsorption onto CTS-ECH/IKaol.

T(k)	Ln K_d	ΔG° (kJ/mol)	ΔH° (kJ/mol)	ΔS° (kJ/mol K)
303,15	-0.14	-7.20	**44.31**	**0.168**
313.15	0.806	-8.50		
318.15	1.752	-10.61		
333.15	2.699	-10.93		
		-9.31		

The results presented in Table **VI.7** for RO16 dye show that the change in Gibbs free energy (ΔG°) is negative, indicating that the studied adsorption process is spontaneous and physical in nature. Moreover, the process is exothermic, as evidenced by the negative enthalpy value (ΔH°), which also explains the observed decrease in RO16 adsorption capacity with increasing temperature. The negative ΔS° value suggests that the dye ions become more ordered at the interface between the liquid phase and the adsorbent due to binding interactions, leading to a decrease in system randomness [46, 47].

Table IV.7. Thermodynamic parameters for RO16 dye adsorption onto CTS-ECH/IKaol.

T(k)	Ln K_d	ΔG° (kJ/mol)	ΔH° (kJ/mol)	ΔS°(kJ/mol K)
303,15	-0.14	0.35	**-78.65**	**-0.238**
313.15	0.806	-2.10		
318.15	1.752	-4.63		
333.15	2.699	-7.47		
		-3.46		

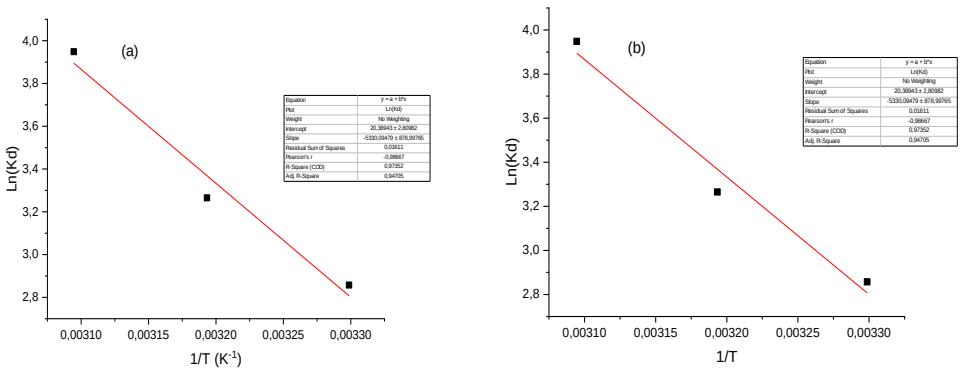

Figure IV.12. Van'tHoff plot for OG dye (a) and RO16 dye (b) adsorption onto CTS-ECH/IKaol.

IV.10. Mechanisms of adsorption

The surface properties of the adsorbent material—particularly the active functional groups and the surface charge variation with pH—are key factors governing the adsorption mechanism. The point of zero charge (pH_{pzc}) of the CTS-ECH/IKaol composite is approximately 6.90, indicating that the material's surface is positively charged at pH values below 6.90 and negatively charged at higher pH values.

Since both OG and RO16 are anionic dyes, adsorption is more effective in acidic media, where the material's surface exhibits a positive charge, thereby enhancing electrostatic interactions with the negatively charged dye molecules, as illustrated in Figure **IV.13**.

In addition to electrostatic interactions, n–π interactions between the lone pair electrons on oxygen atoms in the adsorbent and the aromatic rings in the dye molecules may also contribute to enhanced adsorption. Furthermore, dipole–dipole hydrogen bonding may occur between OH or NH_2 groups on the surface and O or N atoms within the dye structures. Additionally, Yoshida-type hydrogen bonds can form between –OH groups on the CTS-ECH/IKaol surface and the aromatic rings of the dyes. Collectively, these interactions enhance the adsorption efficiency of OG and RO16 dyes onto the CTS-ECH/IKaol surface, making it an effective material for the removal of anionic dyes from aqueous solutions [48].

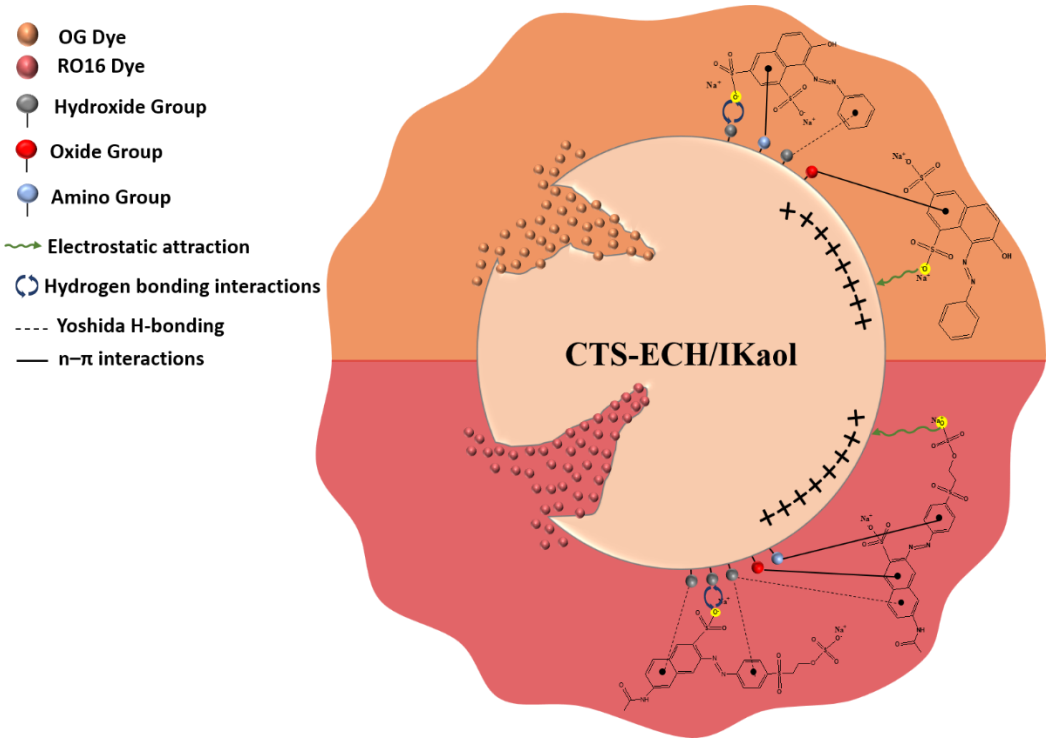

Figure IV.13. Possible mechanism between the CTS-ECH/IKaol surface and the dyes (Orange G and Reactive Orange 16)

IV.11. Regeneration Studies

The ability to recycle biosorbents is crucial for enhancing the cost- effectiveness, affordability, and eco- friendliness of the adsorption process, particularly when considering their potential utility on a pilot scale [49]. The reusability of the CTS-ECH/IKaol composite was evaluated by conducting several biosorption cycles with the OG and RO16 dye. Figure **IV.14** shows the adsorption-desorption results of OG and RO16 dye for two cycles. The adsorption was slightly reduced by 32% and 21% for OG and RO16 dye, respectively, after the second cycle and remained constant until the second cycle, with an average OG or RO16 dye adsorption near 31%. The results show that MO dye could be effectively desorbed from the adsorbent using 0.1 M NaOH solution. During the desorption process, the adsorbed anionic OG or RO16 dye onto the CTS-ECH/IKaol composite would be replaced with OH- ions [50]. The decline in dye removal efficacy may be ascribed to the saturation of the CTS-ECH/IKaol surface with dye molecules, resulting from the equilibrium state between OG or RO16 dye, and the accessible functional groups on the biocomposite surface. This refers to a change in the biocomposite morphology due to a reduction in its surface area and pore volume [51]. This observation highlights a potential limitation of the CTS-ECH/IKaol adsorption properties in the case of multiple adsorption-desorption cycles [52]. Hence, the synthesized CTS-ECH/IKaol has significant potential for wastewater treatment due to its environmentally friendly and cost-effectiveness, together with its impressive adsorption capacity and its moderate reusability over multiple cycles.

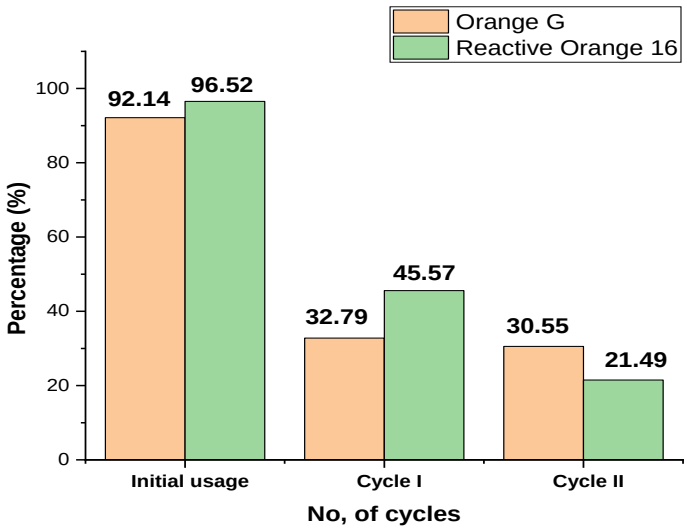

Figure IV.14. Effect of reusability for the adsorption of OG and RO16 dye on CTS-ECH/IKaol composite

References

[1] P. Djomgoue and D. Njopwouo, "FT-IR spectroscopy applied for surface clays characterization," *Journal of Surface Engineered Materials and Advanced Technology*, vol. 3, pp. 275-282, 2013.

[2] A. H. Jawad and A. S. Abdulhameed, "Facile synthesis of crosslinked chitosan-tripolyphosphate/kaolin clay composite for decolourization and COD reduction of remazol brilliant blue R dye: optimization by using response surface methodology," *Colloids and Surfaces A: Physicochemical and Engineering Aspects*, vol. 605, p. 125329, 2020.

[3] M. Monier and D. Abdel-Latif, "Fabrication of Au (III) ion-imprinted polymer based on thiol-modified chitosan," *International journal of biological macromolecules*, vol. 105, pp. 777-787, 2017.

[4] M. Auta and B. Hameed, "Chitosan–clay composite as highly effective and low-cost adsorbent for batch and fixed-bed adsorption of methylene blue," *Chemical Engineering Journal*, vol. 237, pp. 352-361, 2014.

[5] X. Sun, Z. Tang, M. Pan, Z. Wang, H. Yang, and H. Liu, "Chitosan/kaolin composite porous microspheres with high hemostatic efficacy," *Carbohydrate Polymers*, vol. 177, pp. 135-143, 2017.

[6] H. Vardikar, B. Bhanvase, A. Rathod, and S. Sonawane, "Sonochemical synthesis, characterization and sorption study of Kaolin-Chitosan-TiO2 ternary nanocomposite: advantage over conventional method," *Materials Chemistry and Physics*, vol. 217, pp. 457-467, 2018.

[7] P. S. Palanivel Sathishkumar, M. A. Mani Arulkumar, and T. P. Thayumanavan Palvannan, "Utilization of agro-industrial waste Jatropha curcas pods as an activated carbon for the adsorption of reactive dye Remazol Brilliant Blue R (RBBR)," 2011.

[8] A. H. Jawad, N. S. A. Mubarak, and A. S. Abdulhameed, "Hybrid crosslinked chitosan-epichlorohydrin/TiO2 nanocomposite for reactive red 120 dye adsorption: kinetic, isotherm, thermodynamic, and mechanism study," *Journal of Polymers and the Environment*, vol. 28, pp. 624-637, 2020.

[9] A. Ritter and R. Muñoz-Carpena, "Performance evaluation of hydrological models: Statistical significance for reducing subjectivity in goodness-of-fit assessments," *Journal of Hydrology*, vol. 480, pp. 33-45, 2013.

[10] S. Pandey and S. Tiwari, "Facile approach to synthesize chitosan based composite—characterization and cadmium (II) ion adsorption studies," *Carbohydrate Polymers*, vol. 134, pp. 646-656, 2015.

[11] Twinkle, H. Tewatia, J. Kaushik, A. Sahu, S. K. Chaudhary, and S. K. Sonkar, "Waste iron dust derived iron oxide nanoparticles for efficient adsorption of multiple azo dyes," *ACS Sustainable Resource Management*, vol. 1, pp. 278-288, 2024.

[12] L. M. Anaya-Esparza, J. M. Ruvalcaba-Gómez, C. I. Maytorena-Verdugo, N. González-Silva, R. Romero-Toledo, S. Aguilera-Aguirre, *et al.*, "Chitosan-TiO2: A versatile hybrid composite," *Materials*, vol. 13, p. 811, 2020.

[13] A. Reghioua, D. Atia, A. Hamidi, A. H. Jawad, A. S. Abdulhameed, and H. M. Mbuvi, "Production of eco-friendly adsorbent of kaolin clay and cellulose extracted from peanut shells for removal of methylene blue and congo red

removal dyes," *International journal of biological macromolecules,* vol. 263, p. 130304, 2024.

[14] I. BELBACHIR, "Modification de la Bentonite de Maghnia et application dans l'adsorption de colorants textiles et de métaux lourds," Université de Tlemcen-Abou Bekr Belkaid, 2018.

[15] R. Chakraborty, A. Asthana, A. K. Singh, B. Jain, and A. B. H. Susan, "Adsorption of heavy metal ions by various low-cost adsorbents: a review," *International Journal of Environmental Analytical Chemistry,* vol. 102, pp. 342-379, 2022.

[16] A. Hamidi, D. Atia, A. Rebiai, A. Reghioua, A. Zobeidi, M. Messaoudi, *et al.*, "Investigation of adsorption kinetics and isothermal thermodynamics for optimizing methylene blue adsorption onto a modified clay with cellulose using the response surface approach," *Biomass Conversion and Biorefinery,* vol. 14, pp. 22573-22587, 2024.

[17] A. P. Rovai, J. D. Baker, and M. K. Ponton, *Social science research design and statistics: A practitioner's guide to research methods and IBM SPSS*: Watertree Press LLC, 2013.

[18] S. A. Siddiqui, O. Zannou, I. Karim, Kasmiati, N. M. Awad, J. Gołaszewski, *et al.*, "Avoiding food neophobia and increasing consumer acceptance of new food trends—A decade of research," *Sustainability*, vol. 14, p. 10391, 2022.

[19] R. H. Myers, A. I. Khuri, and W. H. Carter, "Response surface methodology: 1966–l988," *Technometrics,* vol. 31, pp. 137-157, 1989.

[20] E. Mosaffa, R. I. Patel, A. Banerjee, B. B. Basak, and M. Oroujzadeh, "Comprehensive analysis of cationic dye removal from synthetic and industrial wastewater using a semi-natural curcumin grafted biochar/poly acrylic acid composite hydrogel," *RSC advances*, vol. 14, pp. 7745-7762, 2024.

[21] K. Rechendorff, M. B. Hovgaard, M. Foss, V. Zhdanov, and F. Besenbacher, "Enhancement of protein adsorption induced by surface roughness," *Langmuir*, vol. 22, pp. 10885-10888, 2006.

[22] H. Bensalah, S. A. Younssi, M. Ouammou, A. Gurlo, and M. F. Bekheet, "Azo dye adsorption on an industrial waste-transformed hydroxyapatite adsorbent: Kinetics, isotherms, mechanism and regeneration studies," *Journal of Environmental Chemical Engineering*, vol. 8, p. 103807, 2020.

[23] P. Zhang, Y. Li, Y. Cao, and L. Han, "Characteristics of tetracycline adsorption by cow manure biochar prepared at different pyrolysis temperatures," *Bioresource Technology,* vol. 285, p. 121348, 2019.

[24] M. A. Salam, S. A. Kosa, and A. A. Al-Beladi, "Application of nanoclay for the adsorptive removal of Orange G dye from aqueous solution," *Journal of molecular liquids*, vol. 241, pp. 469-477, 2017.

[25] H. M. Agha, R. Wu, A. H. Jawad, and Z. A. ALOthman, "Bacillus subtilis bacteria@ chitosan biopolymer for Reactive Orange 16 dye removal: multivariable optimization and desirability functions by response surface methodology," *Biomass Conversion and Biorefinery*, pp. 1-17, 2025.

[26] J.-H. Park, J. J. Wang, Y. Meng, Z. Wei, R. D. DeLaune, and D.-C. Seo, "Adsorption/desorption behavior of cationic and anionic dyes by biochars prepared at normal and high pyrolysis temperatures," *Colloids and Surfaces A: Physicochemical and Engineering Aspects,* vol. 572, pp. 274-282, 2019.

[27] R. Wu, A. S. Abdulhameed, A. H. Jawad, S. A. Musa, Y. De Luna, Z. A. ALOthman, *et al.*, "An eco-friendly chitosan-genipin/SiO2 composite for reactive orange 16 dye removal: Insights into adsorption statistical modeling

and mechanism," *International Journal of Biological Macromolecules,* vol. 270, p. 132329, 2024.

[28] A. Amjlef, S. Farsad, A. Chaoui, A. B. Hamou, M. Ezzahery, S. Et-Taleb, *et al.*, "Effective adsorption of Orange G dye using chitosan cross-linked by glutaraldehyde and reinforced with quartz sand," *International Journal of Biological Macromolecules,* vol. 239, p. 124373, 2023.

[29] H. M. Agha, A. H. Jawad, Z. A. ALOthman, and L. D. Wilson, "Design of chitosan and watermelon (Citrullus lanatus) seed shell composite adsorbent for reactive orange 16 dye removal: multivariable optimization and dye adsorption mechanism study," *Biomass Conversion and Biorefinery,* pp. 1-16, 2024.

[30] A. Imgharn, A. Hsini, Y. Naciri, M. Laabd, H. Kabli, M. Elamine, *et al.*, "Synthesis and characterization of polyaniline-based biocomposites and their application for effective removal of Orange G dye using adsorption in dynamic regime," *Chemical Physics Letters,* vol. 778, p. 138811, 2021.

[31] R. Wu, A. S. Abdulhameed, R. Selvasembian, E. Yousif, Z. A. ALOthman, and A. H. Jawad, "Optimized hydrothermal synthesis of chitosan-epichlorohydrin/nanosilica for efficient reactive dye removal: mechanistic insights," *Water, Air, & Soil Pollution,* vol. 235, p. 128, 2024.

[32] Z. Ennajih, T. Bouzid, O. Doughmi, R. El-bardai, I. Daou, I. El Mrabet, *et al.*, "Innovative arginine-polyaniline@ SiO2 for Orange G removal: adsorption experiments and DFT insights," *Separation and Purification Technology,* p. 133008, 2025.

[33] A. S. Abdulhameed, R. Wu, S. A. Musa, H. M. Agha, Z. A. ALOthman, A. H. Jawad, *et al.*, "Bisphenol-A-diglycidyl ether modified chitosan/nano-SiO2 via hydrothermal process: A statistical modeling and adsorption mechanism for reactive orange 16 dye removal," *International Journal of Biological Macromolecules,* vol. 256, p. 128267, 2024.

[34] M. Goswami and P. Phukan, "Enhanced adsorption of cationic dyes using sulfonic acid modified activated carbon," *Journal of Environmental Chemical Engineering,* vol. 5, pp. 3508-3517, 2017.

[35] J. J. Lee, "Study on of Process Parameters for Adsorption of Reactive Orange 16 Dye by Activated Carbon," *Journal of the Korea Academia-Industrial cooperation Society,* vol. 21, pp. 667-674, 2020.

[36] Z.-R. Zhong, H.-L. Jiang, N. Shi, H.-W. Lv, Z.-J. Liu, and F.-A. He, "A novel tetrafluoroterephthalonitrile-crosslinked quercetin/chitosan adsorbent and its adsorption properties for dyes," *Journal of Molecular Structure,* vol. 1282, p. 135150, 2023.

[37] A. Jesus, L. Romão, B. Araújo, A. Costa, and J. Marques, "Use of humin as an alternative material for adsorption/desorption of reactive dyes," *Desalination,* vol. 274, pp. 13-21, 2011.

[38] J. Park, S. Kim, Y. Park, T.-H. Kim, and Y. Hwang, "Aminated covalent organic polymers for anionic dye adsorption in aqueous systems," *Applied Sciences,* vol. 13, p. 2043, 2023.

[39] K. Vijayaraghavan, S. W. Won, and Y.-S. Yun, "Single-and dual-component biosorption of reactive black 5 and reactive orange 16 onto polysulfone-immobilized esterified Corynebacterium glutamicum," *Industrial & engineering chemistry research,* vol. 47, pp. 3179-3185, 2008.

[40] A. Umar, M. M. Sanagi, A. A. Naim, W. N. W. Ibrahim, A. S. A. Keyon, and W. A. W. Ibrahim, "Removal of orange G from aqueous solutions by

polystyrene-modified chitin," *Jurnal Teknologi (Sciences & Engineering)*, vol. 79, 2017.

[41] A. A. A. M, K. R. K, S. Selvan M, M. K. Rai, M. Priyadharshini, M. N, *et al.*, "Removal of Reactive Orange 16 by adsorption onto activated carbon prepared from rice husk ash: statistical modelling and adsorption kinetics," *Separation Science and Technology*, vol. 55, pp. 26-34, 2020.

[42] Z. Taibi, K. Bentaleb, Z. Bouberka, C. Pierlot, M. Vandewalle, C. Volkringer, *et al.*, "Adsorption of orange G dye on hydrophobic activated bentonite from aqueous solution," *Crystals*, vol. 13, p. 211, 2023.

[43] R. Muralikrishnan and C. Jodhi, "Experimental studies and mathematical modeling of decolorization of Reactive Orange 16 in packed column," *Desalination and Water Treatment*, vol. 217, pp. 422-430, 2021.

[44] A. K. Jain, V. K. Gupta, S. Jain, and Suhas, "Removal of chlorophenols using industrial wastes," *Environmental science & technology*, vol. 38, pp. 1195-1200, 2004.

[45] X. Wang and C. Chen, "Nanotechnology application in metal ion adsorption," in *Handbook of Advanced Industrial and Hazardous Wastes Management*, ed: CRC Press, 2017, pp. 997-1042.

[46] R. Bassam, M. El Alouani, J. Maissara, Y. Rachdi, N. Jarmouni, E. H. El Khattabi, *et al.*, "Enhanced removal of cadmium ions using Moroccan natural clays: characterization, kinetic, isotherm, thermodynamic, and regeneration investigations," *Materials Today: Proceedings*, vol. 62, pp. 6273-6280, 2022.

[47] G. Ebrahimzadeh-Rajaei, "Removal of reactive red-P2B from aqueous solutions by montmorillonite clay; Kinetics, thermodynamic and isotherm studies," *Inorganic Chemistry Communications*, vol. 149, p. 110386, 2023.

[48] N. N. Abd Malek, A. H. Jawad, A. S. Abdulhameed, K. Ismail, and B. Hameed, "New magnetic Schiff's base-chitosan-glyoxal/fly ash/Fe3O4 biocomposite for the removal of anionic azo dye: an optimized process," *International journal of biological macromolecules*, vol. 146, pp. 530-539, 2020.

[49] N. H. Abdullah, A. Borhan, and S. Z. A. H. Saadon, "Biosorption of wastewater pollutants by chitosan-based porous carbons: A sustainable approach for advanced wastewater treatment," *Bioresource Technology Reports*, vol. 25, p. 101705, 2024.

[50] J. Ghourbanpour, M. Sabzi, and N. Shafagh, "Effective dye adsorption behavior of poly (vinyl alcohol)/chitin nanofiber/Fe (III) complex," *International journal of biological macromolecules*, vol. 137, pp. 296-306, 2019.

[51] H. M. Agha, A. Allaq, A. H. Jawad, S. Aazmi, Z. A. ALOthman, and L. D. Wilson, "Immobilization of Bacillus subtilis bacteria into biohybrid crosslinked chitosan-glutaraldehyde for acid red 88 dye removal: Box–Behnken design optimization and mechanism study," *Journal of Inorganic and Organometallic Polymers and Materials*, vol. 35, pp. 216-230, 2025.

[52] N. S. Abdul Mubarak, T. Chuan, H. Khor, A. H. Jawad, L. Wilson, and S. Sabar, "Immobilized Fe-loaded chitosan film for methyl orange dye removal: competitive ions, reusability, and mechanism," *Journal of Polymers and the Environment*, vol. 29, pp. 1050-1062, 2021.

General Conclusion

The treatment of industrial wastewater, particularly that contaminated with synthetic dyes, remains one of the major environmental challenges facing the world today due to the harmful effects of these pollutants on human health and aquatic ecosystems. In light of the global shift toward sustainable and eco-friendly solutions, biobased materials have emerged as a promising option for water purification, owing to their abundance, biodegradability, and high adsorption efficiency.

In this context, the present work aims to develop a hybrid adsorbent material based on chitosan modified with illite-kaolinite clay, for the removal of the anionic dyes Orange G (OG) and Reactive Orange 16 (RO16) from aqueous solutions. The material was synthesized by crosslinking chitosan using epichlorohydrin (ECH) as the crosslinking agent. The adsorption conditions were optimized using the Box–Behnken Design (BBD) within the framework of Response Surface Methodology (RSM), by studying the influence of four main operational variables: adsorbent dosage, pH, temperature, and contact time.

The polymeric structure of the CTS-ECH/IKaol composite, composed of epichlorohydrin-modified chitosan and illite-kaolinite clay, contributed significantly to enhancing its adsorption capacity toward the Orange G dye. The results showed that the optimal conditions for removing OG, achieving a removal efficiency of 92.14%, were: 0.04 g of adsorbent, pH = 4, temperature of 60 °C, and a contact time of 25 minutes. These findings confirm the effectiveness of the prepared composite in dye removal from aqueous media under controlled conditions. As for RO16, the optimal removal conditions (96.52% efficiency) were obtained at a temperature of 45 °C, pH = 4, adsorbent dose of 0.06 g, and 25 minutes of contact time.

The adsorption data for Orange G (OG) were best fitted by the Freundlich isotherm model, with a high correlation coefficient (R^2 = 0.990), suggesting a multilayer adsorption on a heterogeneous surface. Furthermore, the maximum adsorption capacity (qmax) according to the Langmuir model was found to be 416.67 mg/g. In the case of Reactive Orange 16 (RO16), the Langmuir model provided the best fit (R^2 = 0.995), with a maximum adsorption capacity of 357.14 mg/g, indicating monolayer adsorption on a homogeneous surface.

Adsorption kinetics for both OG and RO16 under optimal conditions showed good agreement with the pseudo-second-order model, indicating that the adsorption process is mainly governed by chemical interactions between the active sites on the adsorbent surface and dye molecules.

In conclusion, the results of this work provide a strong foundation for the potential application of biopolymer-based adsorbents, such as the CTS-ECH/IKaol composite, in the efficient removal of industrial dyes from contaminated water.

Future recommendations:

In light of the findings of this study, we propose the following future directions that could contribute to advancing research in the field of pollutant removal using biobased materials:

- Valorization of chitosan extracted from waste sources for various applications, considering its biogenic origin and high adsorption capacity, which make it a promising option in environmental remediation.
- Surface modification of chitosan or the incorporation of auxiliary adsorbents such as clays or nanomaterials to enhance its physicochemical properties and improve adsorption performance.
- Expansion of chitosan applications to the treatment of various organic pollutants, particularly for the removal of cationic dyes, based on its demonstrated efficiency in the removal of ionic dyes in this work.
- Exploration of novel adsorbent materials derived from biomass and renewable sources, such as cellulose and starch, due to their abundance, low cost, and minimal environmental impact.
- Implementation of adsorption experiment modeling using design of experiment (DOE) software tools (e.g., Box-Behnken and RSM), which play a significant role in accelerating experimental processes, efficiently determining optimal conditions, and reducing costs and effort.

In this regard, we encourage our fellow students researchers to take advantage of statistical design tools, as they offer accuracy and effectiveness in analyzing influencing factors and improving experimental performance in a modern and systematic manner.

Appendix

1. **Reflux condenser**

2. **Analytical balance**

3. pH metr

4. Laboratory Oven

5. *Literature Review*

This work benefited from several research articles authored by Dr. Ali H. Jawad, which were accessed through his Google Scholar profile: https://scholar.google.fr/citations?user=_uMgRvcAAAAJ&hl=fr&oi=ao

Table 1. Some studies from the ALI H. JAWAD website

N°	Adsorbent	Adsorbate	Ads.Capasity	Kinetic Model	Isotherm Model
1	*CS/CAC*	*MV*	*88.9*	*PSO*	*Freundlich*
2	*CS-SL/CaO/Fe3O4*	*RBB*	*63.3*	*PFO*	*Langmuir*
3	*CHS-GLU/BCL*	*AR88*	*148*	*PFO*	*Langmuir*
4	*CHS-GTD/AL*	*MV 2B*	*123.2*	*PSO*	*Freundlich*
5	*CS-PEDGE*	*MV 2B*	*94.2*	*PSO*	*Freundlich*

6	*Chi-SL/CFA/Alg*	*MG*	*493.7*	*PSO*	*Freundlich*
7	*CH-AL-MK10/GL*	*MV 2B*	*98.3*	*PSO*	*Langmuir and Freundlich*
8	*Chit-SA/ALG*	*MV*	*115.6*	*PSO*	*Freundlich*
9	*CHS-GLA/n-Silica*	*AR88*	*115.9*	*PSO*	*Langmuir and Temkin*
10	*CS-PEDGE/FGA/MMT*	*MV 2B*	*94.2*	*PSO*	*Freundlich*
11	*chitosan – E. coli*	*MG*	*164.7*	*PSO*	*Langmuir*
12	*CS/Alg/FA*	*MV2B*	*63.4*	*PSO*	*Langmuir*
13	*CS-PVA/FGA/MMT*	*MV 2B*	*105.7*	*PSO*	*Langmuir*
14	*CS-BZ/Alg/FA*	*RBBR*	*259.9*	*PSO*	*Freundlich*
		THN	*69*	*PSO*	*Langmuir*
15	*CTS-GEN/AGA*	*MV*	*71.9*	*PSO*	*Temkin*
16	*Cn-Bn-FSH-Fe3O4*	*RB19*	*309.6*	*PSO*	*Freundlich*
17	*CS-BD/Alg/FA*	*BG*	*239.3*	*PSO*	*Langmuir*
18	*CS-TPP/FGA/MMT*	*MV 2B*	*165.9*	*PSO*	*Langmuir*
19	*CHS-GLU/BCL*	*AR88*	*148*	*PFO*	*Langmuir*
20	*CHI-BZI/OC/Fe3O4*	*RBBR*	*102.9*	*PSO*	*Langmuir*
21	*CsMaTk/S*	*BG*	*957*	*PSO*	*Freundlich and Langmuir*
22	*CTS/FGA*	*MV 2B*	*179.8*	*PSO*	*Langmuir*
23	*MCH-EGDE/ORNC*	*RBBR*	*168.4*	*PSO*	*Freundlich*
24	*MCTS-GOX/OMMT*	*RB19*	*122.3*	*PSO*	*Langmuir*
25	*CHI/n-SiO2*	*AR88*	*215.1*	*PFO*	*Langmuir*
26	*CHI-BEZ/n-SiO2*	*AR88*	*261.2*	*PFO*	*Langmuir*
27	*CTS-SA/SiO2*	*AR88*	*184.2*	*PSO*	*Langmuir*
28	*CHT-GLX/ALG*	*MV 2B*	*110.8*	*PSO*	*Freundlich*
29	*CHA-BA/FGA*	*MV 2B*	*126.51*	*PSO*	*Langmuir*
30	*MCH-SAL/NCLA*	*AR88*	*173.5*	*PFO*	*Temkin*
31	*CTA-BZA/SiO2*	*AR88*	*252.4*	*PFO*	*Langmuir and Freundlich*
32	*CS-SL/Fe3O4*	*AR88*	*137.3*	*PSO*	*Freundlich*
33	*CS-BD/Fe3O4*	*AR88*	*154.1*	*PFO*	*Temkin*
34	*CHI/MMT/ALG*	*BG1*	*509.5*	*PSO*	*Langmuir*
		RB19	*227.9*	*PSO*	*Temkin and Langmuir*
35	*MCH-EGDE/ORNC*	*RBBR*	*168.4*	*PSO*	*Freundlich*

36	***MCTS-GOX/OMMT***	***RB19***	***122.3***	***PSO***	***Langmuir***
37	***CHI/n-SiO2***	***AR88***	***215.1***	***PFO***	***Langmuir***
38	***CHI-BEZ/n-SiO2***	***AR88***	***261.2***	***PFO***	***Langmuir***
39	***CTS-SA/SiO2***	***AR88***	***184.2***	***PSO***	***Langmuir***
40	***CHT-GLX/ALG***	***MV 2B***	***110.8***	***PSO***	***Freundlich***
41	***CHA-BA/FGA***	***MV 2B***	***126.51***	***PSO***	***Langmuir***
42	***MCH-SAL/NCLA***	***AR88***	***173.5***	***PFO***	***Temkin***
43	***CTA-BZA/SiO2***	***AR88***	***252.4***	***PFO***	***Langmuir and Freundlich***
44	***CS-SL/Fe3O4***	***AR88***	***137.3***	***PSO***	***Freundlich***
45	***CS-BD/Fe3O4***	***AR88***	***154.1***	***PFO***	***Temkin***
46	***CHI/MMT/ALG***	***BG1***	***509.5***	***PSO***	***Langmuir***
		RB19	***227.9***	***PSO***	***Temkin and Langmuir***
47	***CS-SA/ALG/MTN***	***RBBR***	***148.1***	***PSO***	***Freundlich***
		BG	***440.3***	***PSO***	***Langmuir and Freundlich***
48	***CHS-BZ/MT/AL***	***RB19***	***213.6***	***PSO***	***Langmuir***
		BG	***899.5***	***PSO***	***Langmuir***
49	**Chi/Sep/Alg (pH 8)**	**MG**	**515.7**	**PSO**	**Freundlich**
	Chi/Sep/Alg (pH 4)	**RBBR**	**292.4**	**PSO**	**Freundlich**
50	***CTS-AC***	***TH***	***56.7***	***PSO***	***Freundlich***